The Thesis committee for Jared Brett Garrison

Certifies that this is the approved version of the following thesis:

An Integrated Energy Storage Scheme for a Dispatchable Wind and Solar Powered Energy System

Approved by
Supervising Committee:

Michael E. Webber, Supervisor

Philip Schmidt

An Integrated Energy Storage Scheme for a Dispatchable Wind and Solar Powered Energy System

by

Jared Brett Garrison, B.S.E.

Thesis

Presented to the Faculty of the Graduate School of

The University of Texas at Austin

in Partial Fulfillment

of the Requirements

for the Degree of

Master of Science in Engineering

The University of Texas at Austin

December 2009

Dedication

I would like to dedicate this thesis to my family who have given me love and support and to all the teachers who have helped guide and educate me. These people have helped me grow in vision, knowledge, aspiration, and thought, all of which have helped shape the person I am today, for which I am eternally grateful.

Acknowledgements

I would first like to thank my advisor, Dr. Michael Webber, for giving me the opportunity to pursue work that is not only interesting, but also meaningful to me. His guidance and encouragement have been a constant source of support and the example that his career and actions have set will continue to be inspirational to me in my future career.

Additionally, I would like to thank Dr. Philip Schmidt for providing me with invaluable resources as well as for helping guide me throughout my college career and Dr. Surya Santoso for helping me better understand and communicate the modeling of modern wind turbines. I would also like to acknowledge all the faculty of the Cockrell School of Engineering who I have had the privilege of interacting with and who have helped advance my intellectual abilities through classroom and personal discussions.

I must also thank my colleagues in the Webber Energy Group for all their support and interactive discussion. It has been my honor to be involved with such compassionate and genuine individuals. The insight gained from this group has helped me expand my education and be successful in my research endeavors.

I also want to acknowledge Austin Energy, the Department of Mechanical Engineering and Center for International Energy and Environmental Policy at the University of Texas at Austin, and the Cockrell School of Engineering for their financial support during the completion of this body of work. Also, thanks to the administrative staff of the Department of Mechanical Engineering, the Cockrell School of Engineering, and the Jackson School of Geosciences for their assistance throughout my graduate studies. Special thanks to Mark Kapner of Austin Energy for his dedication and selfless actions toward bringing fresh concepts for the incorporation and integration of renewable energy to the forefront of the energy industry.

Lastly, I would like to thank my family and close friends for their love and encouragement throughout this process and throughout the course of my life.

December 4, 2009

Abstract

An Integrated Energy Storage Scheme for a Dispatchable Wind and Solar Powered Energy System

by

Jared Brett Garrison, MSE

The University of Texas at Austin, 2009

Supervisors: Michael E. Webber

Wind and solar technologies have experienced rapid market growth recently as a result of the growing interest for implementation of renewable energy. However, the intermittency of wind and solar power is a major obstacle to their broader use. The additional risks of unexpected interruptions and mismatch with demand have hindered the expansion of these two primary renewable resources.

The goal of this research is to analyze an integrated energy system that includes a novel configuration of wind and solar coupled with two storage methods to make both wind and solar sources dispatchable during peak demand, thereby enabling their broader use. Named DSWiSS for Dispatchable Solar Wind Storage System, the proposed system utilizes compressed air energy storage (CAES) that is driven from wind energy and thermal storage supplied by concentrating solar thermal power in order to achieve this desired dispatchability. Although DSWiSS mimics the operation of a typical CAES

facility, the replacement of energy derived from fossil fuels with energy generated from renewable resources makes this system unique. While current CAES facilities use off peak electricity to power their compressors, this system uses power from wind turbines. Also, rather than using natural gas for heating of the compressed air before its expansion through a turbine, DSWiSS uses solar thermal energy and thermal storage.

For this research, two models were created; the first is a dynamic model of a 1.5 MW variable speed wind turbine, programmed in PSCAD/EMTDC, that utilizes rotor resistive control to maintain rated power output. This model simulates the dynamic response of the wind turbine to changing wind conditions as well as the nominal performance parameters at all wind speeds. The second model is a steady state thermodynamic simulation of the turbomachinery power unit in the DSWiSS facility. By assuming conditions similar to those of a currently operating CAES facility in McIntosh, Alabama, the model calculates the performance parameters of DSWiSS and estimates the relative energy input requirements. By combining these models with a levelized lifetime cost analysis estimates of the power system performance and the cost of energy for the DSWiSS facility were estimated. The combination of these components yielded an efficiency greater than 46% for the main power block and a nearly equal utilization of both renewable resources. It was also estimated that the overall system is only slightly more expensive per unit of electricity generated than the current technologies employed today, namely coal, nuclear, and natural gas, but is comparable to a stand-alone solar thermal facility. However, this economic analysis, though accurate with regard to the technologies chosen, will not be complete until cost values can be placed on some of the externalities associated with power generation such as fuel cost volatility, national security, and emissions.

Table of Contents

List of Tables

List of Figures

Nomenclature

A	rotor blade swept area
$AeroTorque$	aerodynamic torque applied to the rotor shaft
B_{eq}	equivalent damping for rotor and generator
B_{gen}	generator damping
B_{rot}	rotor damping
CF	capacity factor
C_p	coefficient of performance for wind turbine
C_p	specific heat at constant pressure
C_{p_i}	specific heat at constant pressure of component i
$C_{p_{mix}}$	mixture specific heat at constant pressure
C_v	specific heat at constant volume
$C_{v_{mix}}$	mixture specific heat at constant volume
d	discount rate
$e_{in,solar}$	heat energy requirement of DSWiSS supplied by the solar subsystem
$e_{in,wind}$	electrical energy requirement of DSWiSS supplied by the wind turbines
$e_{in,tot}$	total specific energy input requirement of DSWiSS
F_s	fraction of energy input to DSWiSS from solar heat
F_w	fraction of energy input to DSWiSS from wind electricity
G_I	integral gain of PI controller
G_P	proportional gain of PI controller
GR	gear ratio in wind turbine gear box

h_i	enthalpy of component *i*
$h_{i,ref}$	reference enthalpy of component *i*
h_{mix}	mixture enthalpy
h_{in}	inlet enthalpy
$h_{in,air}$	air-side inlet enthalpy
$h_{in,air@Tcoolant}$	air enthalpy at temperature of inlet coolant
h_{out}	exit enthalpy
$h_{out,air}$	air-side exit enthalpy
$h_{out,s}$	isentropic exit enthalpy
I	current
J_{gen}	generator inertia
J_{rot}	rotor inertia
k	specific heat ratio
K_{eq}	equivalent stiffness for rotor and generator
K_{gen}	generator stiffness
K_{rot}	rotor stiffness
$\dot{m}_{air}$	air mass flow rate
$\dot{m}_{t,air}$	air mass flow rate through turbine train
$\dot{m}_{c,air}$	air mass flow rate through compression train
$m_{air,tot}$	total air mass used in DSWISS per day
m_{in}	air mass input into air storage cavern during a filling process
$m_{initial}$	mass of air in storage cavern before filling process
m_{out}	air mass exiting air storage cavern during an emptying process

$m_{initail}$	air mass in the air storage cavern before a filling process
M_i	molecular weight of component *i*
M_{mix}	mixture molecular weight
N	technical lifetime of DSWiSS facility
N_1	number of teeth on rotor shaft gear
N_2	number of teeth on generator shaft gear
P	absolute pressure
P_{max}	maximum allowable pressure for air storage cavern
P_{min}	minimum allowable pressure for air storage cavern
P_{ref}	reference pressure
P_{gen}	wind turbine generator output
$\dot{P}_{t,rated}$	rated turbine train output power
$\dot{P}_{gen,rated}$	rated generator output power
$PitchAngle$	blade pitch angle for wind turbine
Q_{in}	heat input from the CSP subsystem
q_{added}	heat added in one of the heaters
$q_{added,tot}$	total heat added in both heaters
$q_{removed}$	heat remove in one of the cooler
$q_{removed,max}$	maximum amount of heat that could be removed in a cooler
$\dot{Q}_{added,daily}$	daily heat requirement of the heaters
$\dot{Q}_{added,ss}$	steady state heat requirement of the heaters
$\dot{Q}_{removed,ss}$	steady state cooling load of the compression train
$\bar{R}$	universal gas constant
R_i	gas constant for component *i*
R_{ext}	external rotor resistance

R_{mix}	mixture ideal gas constant
R_{rot}	rotor radius of wind turbine blade
s	entropy
$s°$	temperature dependent portion of entropy
$s°_i$	temperature dependent portion of entropy of component *i*
$s°_{i,ref}$	temperature dependent portion of reference entropy of component *i*
s_{mix}	mixture entropy
T	temperature
T_{ref}	reference temperature
t_{comp}	number of hours compression occurs per day
t_{gen}	number of hours generation occurs per day
T_{gen}	generator torque
T_{rot}	rotor torque
u_i	internal energy of component *i*
$u_{i,ref}$	reference internal energy of component *i*
$u_{initial}$	internal energy of air in storage cavern before a filling process
u_{final}	internal energy of air in storage cavern after a filling process
u_{mix}	mixture internal energy
v	free-stream wind velocity
v	specific volume
V_{cavern}	volume of air storage cavern required
w_c	single compressor's specific work requirement

$w_{c,tot}$	total compressor train specific work requirement
$w_{gen,tot}$	total generator specific work output
$w_{motor,tot}$	total motor specific work requirement
w_t	single turbine's specific work output
$w_{t,tot}$	total turbine train specific work output
$\dot{W}_{motor,daily}$	daily electrical requirement of the motor
$\dot{W}_{motor,ss}$	steady state electrical requirement of the motor
ω_{gen}	angular speed of wind turbine generator shaft
ω_{rot}	angular speed of wind turbine rotor shaft
x_i	mass fraction
y_i	molal fraction
$\Delta\Theta$	angular deflection of the rotor/generator shaft
λ	tip speed ratio for wind turbine
ρ	air density
Θ	turbine blade pitch angle
τ	integral time constant for PI controller
η_c	compressor thermal efficiency
η_{gen}	generator electrical efficiency
η_{motor}	motor electrical efficiency
η_t	turbine thermal efficiency
ε_{cooler}	cooler effectiveness
$\varepsilon_{recuperator}$	recuperator effectiveness

Superscripts

$'$	rotor quantity that is referred to the generator reference frame
1	includes the cost of thermal storage

Acronyms and Abbreviations

$/MWh – U.S. dollar per megawatt-hour

°C – degree Celsius

°F – degree Fahrenheit

AC – aftercooler

AEI – Alternative Energy Institute

AWEA – American Wind Energy Association

CAES – compressed air energy storage

CAPEX – capital expenditures

CO_2 – carbon dioxide

const – constant

CREZ – competitive renewable energy zone

CSP – concentrating solar power

DFIG – doubly-fed induction generator

DSWiSS – dispatchable solar wind storage system

EERE – office of Energy Efficiency and Renewable Energy

EIA – Energy Information Administration

EPRI – Electric Power Research Institute

ERCOT – Electric Reliability Council of Texas

ESA – Electricity Storage Association

ft – feet

GW – gigawatt

H_20 - water

HP – high pressure

HX – heat exchanger

Hz - hertz

IC – intercooler

IEA – International Energy Agency

IP – intermediate pressure

IPCC – Intergovernmental Panel on Climate Change

K – Kelvin

kg – kilogram

kJ – kilojoule

kmol – kilomole

kPa - kilopascal

kWh – kilowatt-hour

LCOE – levelized cost of electricity

LCRA – Lower Colorado River Authority

LP – low pressure

m – meter

m/s – meters per second

MCPEL – market clearing price of energy for load

MMBTU – million British thermal units

MVA – mega volt-ampere

MW – megawatt

MWh – megawatt-hour

N_2 - nitrogen

NREL – National Renewable Energy Laboratory

O_2 - oxygen

OPEX – operation and maintenance expenditures

per unit – unit-less, normalized based on rated value

PHS – pumped hydroelectric energy storage

PI – proportional and integral

PSCAD – power systems computer aided design

psia – pounds per square inch absolute

PTC – production tax credit

PUCT – Public Utilities Commission of Texas

P-v – pressure-volume

Quad – quadrillion British thermal units

rad/s – radians per second

Req - required

RPS – renewable portfolio standard

SECO – Texas State Energy Conservation Office

TIPS – Texas Interactive Power Simulator

T-s – temperature-entropy

TX – Texas

USCS – United States Customary System

UT – The University of Texas at Austin

V – volts

Chapter 1: Introduction

1.1. Motivations for Increasing Renewable Energy Generation

The rapid growth of the human population and the incredible advancement of our science and technology over the last one-hundred years can be attributed to many factors, but one major driving force was the abundance of cheap and easily accessible fossil fuels. Oil, natural gas, and coal fueled the industrial revolution and the more recent technology boom. And until recently, these fuels were burned without full comprehension of the possibly negative consequences. Over the last few decades scientists have confirmed with greater certainty that carbon dioxide levels in our atmosphere have been increasing at an accelerated rate compared to that of the last 650,000 years and that burning fossil fuels is a primary cause for this change [1].

In 1824, Joseph Fourier discovered the greenhouse effect, which is the heating of the surface of a planet as a result of the emission of infrared radiation from gases in the atmosphere. In short, gases like carbon dioxide absorb radiation that the earth emits and re-radiate some of it back to earth. The more of these gases there are in the atmosphere, the more radiation that the earth is forced to absorb. The science community has concluded with reasonable confidence that the emission of carbon dioxide and other greenhouse gases has begun to change the global climate change, which will be exacerbated if burning of fossil fuels continues [2].

In addition to their emissions, fossil fuels are also finite resources. As these fuels are produced, underground reservoirs become depleted. Even though new deposits of these fuels are discovered yearly, it is expected that fossil fuels will be increasingly more difficult and more expensive to extract [3].

Because of concerns about global climate change and the anticipation of rising fossil fuel prices, the last decade has witnessed the commercialization and market

penetration of many renewable and non-emitting energy generation technologies. In particular, wind and solar energy have vast potential and have been the focus of the renewable power industry. Both these resources provide a clean and non-depleting means of generating electricity. They are also both domestic resources and have no associated fuel costs. Over the last decade, wind energy development has outpaced solar development mainly because the costs of large-scale wind facilities are cheaper than solar. However, the development of newer processes and cheaper materials has already began to lower the costs of both photovoltaic and concentrating solar collectors. Together, the two technologies could account for a significant portion of a cleaner more sustainable future for humans. However, the growth of these two technologies is hindered by the inherent variability of the wind and solar resources, a key issue that this research attempts to address and overcome.

1.2. THE NEED FOR LARGE SCALE ENERGY STORAGE

Currently, wind and solar technologies only generate 0.77% and 0.014% of the U.S. electricity consumption, respectively [4]. Though only a small portion of total U.S. electricity production, both sources have seen significant growth recently. For instance, Texas has more than quintupled its installed wind capacity over the period from 2004-2008 with new installations totaling over 7100 MW [5, 6]. These two resources are globally available and have the potential to generate massive amounts of electricity.

Despite their advantages, in their current form, both wind and solar energy systems are variable. These sources are subject to diurnal variation, seasonal variation, and weather conditions, such that neither typically matches electricity demand. One example of problems arising from these issues occurred in February of 2007 when wind generation from West Texas dropped from 1700 MW to 300 MW in a matter of hours.

Even though this drop was predicted, the regional grid distributor, the Electric Reliability Council of Texas (ERCOT), had to act quickly to avoid major blackouts and electricity disruptions because ancillary service providers were not available [7]. This occurrence illustrates how even with the presence of backup facilities, the intermittency of wind and solar can still cause strain on the electricity grid.

One way to overcome this inherent variability with wind and solar is by using energy storage. If there existed an efficient and cheap method at a scale of hundreds of MWh to store the energy generated from these renewable sources, then this source could be used on a dispatchable basis much like natural gas plants, allowing generation to match demand. Incorporating such forms of energy storage with wind and solar technologies would enable the large-scale integration of renewable and non-emitting generation to the electricity grid.

1.3. SCOPE

The goal of this research is to analyze an integrated energy system that includes a novel configuration of wind and solar coupled with two storage methods to make both wind and solar sources dispatchable during peak demand, thereby enabling their broader use. Named DSWiSS for Dispatchable Solar Wind Storage System, the proposed system utilizes compressed air energy storage (CAES) that is driven from wind energy and thermal storage supplied by concentrating solar power (CSP) in order to achieve this desired dispatchability. While current CAES facilities use off peak electricity to power their compressors, this system uses power from wind turbines to compress air to high pressure for storage. Also, rather than using natural gas for heating of the compressed air before its expansion through a turbine, which is typical for conventional systems, the

system described in this paper replaces the use of natural gas with solar thermal energy and thermal storage.

The analysis detailed in this document is broken into three sections. The first of these is a dynamic simulation of a typical 1.5 MW wind turbine. Using the electronic programming language PSCAD/EMTDC the model estimates the performance and output under various wind conditions, as well as the dynamic response to changing wind conditions. The primary goal for this analysis is to estimate the power curve for a common wind turbine so that the power output can easily be calculated at any known wind speed. The second section is a steady state thermodynamic model of the DSWiSS turbomachinery power unit. The goal for this simulation is to calculate the required electricity and heat inputs for a specified electrical output, as well as estimate the sizes of the solar and energy storage facilities required. The final section is an economic analysis that uses capital and operation and maintenance cost estimates and information from the previous two sections to determine the levelized cost of electricity (LCOE) for DSWiSS. This cost is then compared to that of typical electricity generation technologies such as coal, nuclear, and natural gas.

Chapter 2: Background

2.1. Renewable Energy in Texas

As concerns about global warming, carbon costs, and energy security converge, the power sector is seeking to implement carbon-free, domestic, and renewable energy systems. The United States has vast resources available for various types of renewable energy including wind, solar, and biomass; however, these resources are not uniformly available across the country. Texas is uniquely positioned among all other states as an ideal test bed for the integration of renewable energy because it has a large solar and wind energy potential, as seen below in Figure 2.1, and its own grid system and operator, the Electric Reliability Council of Texas (ERCOT).

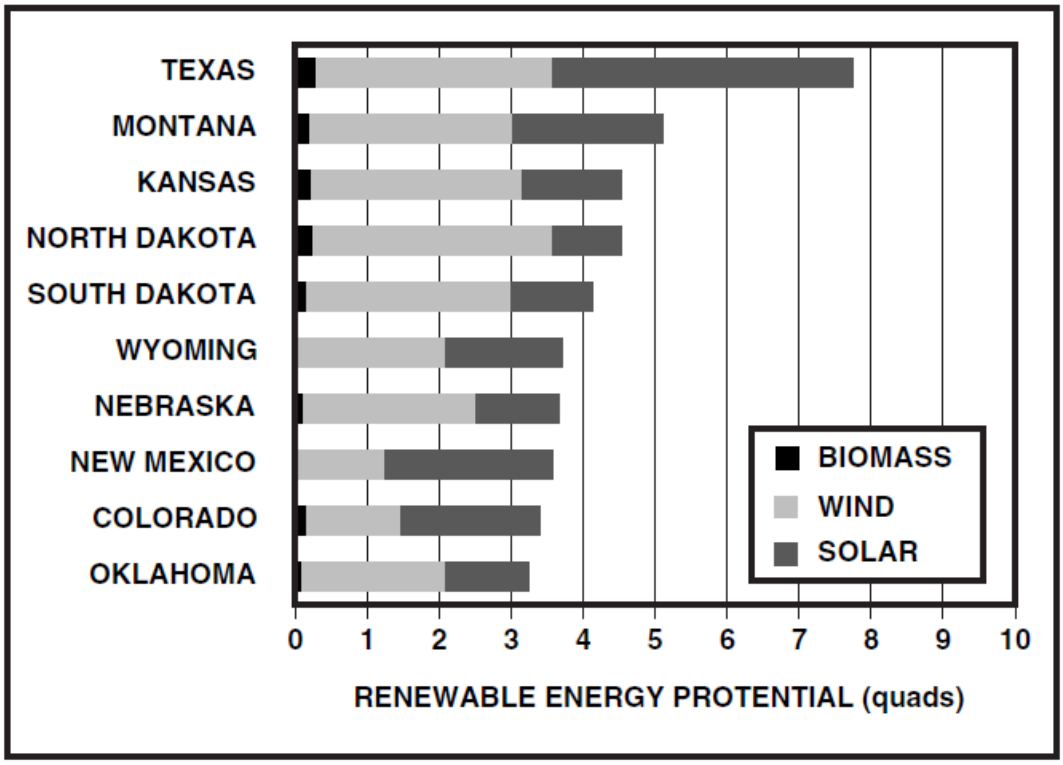

Figure 2.1: Texas has by far the largest renewable potential of any state in the U.S. [8]

2.1.1. Wind Energy Potential and Growth

Across the United States, wind energy has the greatest potential in the central plains and along the coastal regions. In the state of Texas, areas with consistently high wind speeds are the northern panhandle, western, and gulf coast regions. As seen in Figure 2.2 below, much of the panhandle region as well as a few spots in the west and coastal areas are characterized by a wind of class 3 or higher. Typically, class 3 wind is on the edge of what is considered to be profitable for generating energy with large wind turbines. Furthermore, if energy prices rise, or if costs for wind turbines fall, more and more of the marginal class 3 and class 2 areas of the state will become viable locations for installing large scale wind turbines.

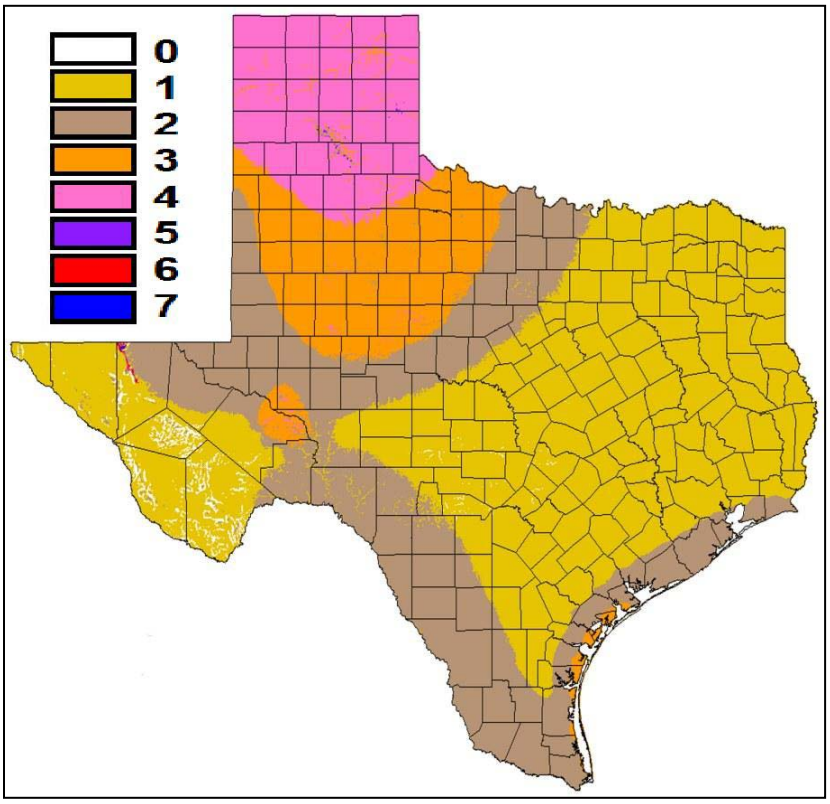

Figure 2.2: Wind class in Texas is highest in the panhandle, regions of the west, and along the coastline [9].

As was described earlier, Texas is already far outpacing every other state regarding the amount of installed wind capacity. Figure 2.3, seen below, illustrates the distribution of installed wind turbines around the U.S. at the end of 2008. Texas has more than double the installed capacity of the next highest state, Iowa, and has shown no signs of significantly slowing down the rate of installations it has achieved over the last few years.

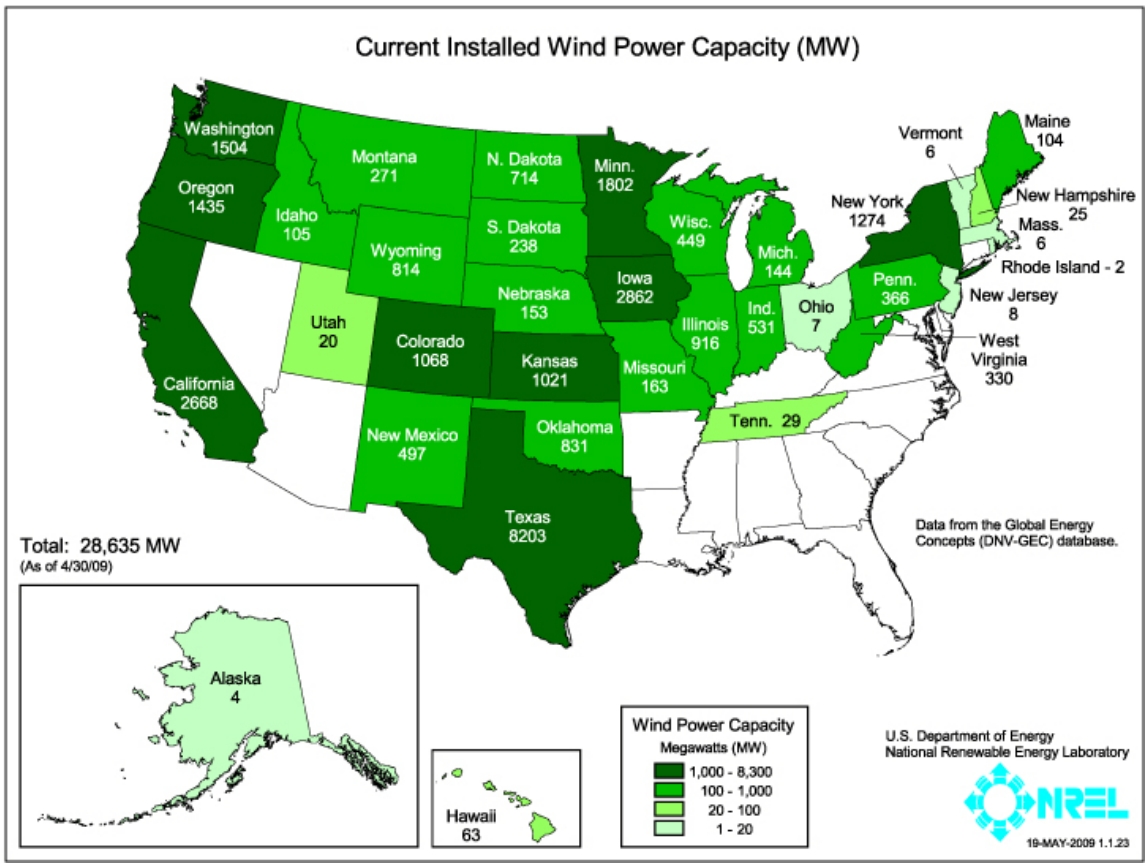

Figure 2.3: Texas leads the nation in renewable wind energy generation [10].

In fact, with the state government's creation of competitive renewable energy zones (CREZ) in the west and the beginning of construction of high voltage power lines

from these zones to the load centers in the east, Texas is preparing for continued rapid growth of its wind energy industry. Over the last five years, no state has matched the rate at which Texas has been installing wind turbines. Figure 2.4 shows the installation rate for the three states with the largest installed wind turbine capacity. This recent history illustrates the value of Texas as a test-bed for renewable energy technology and implementation.

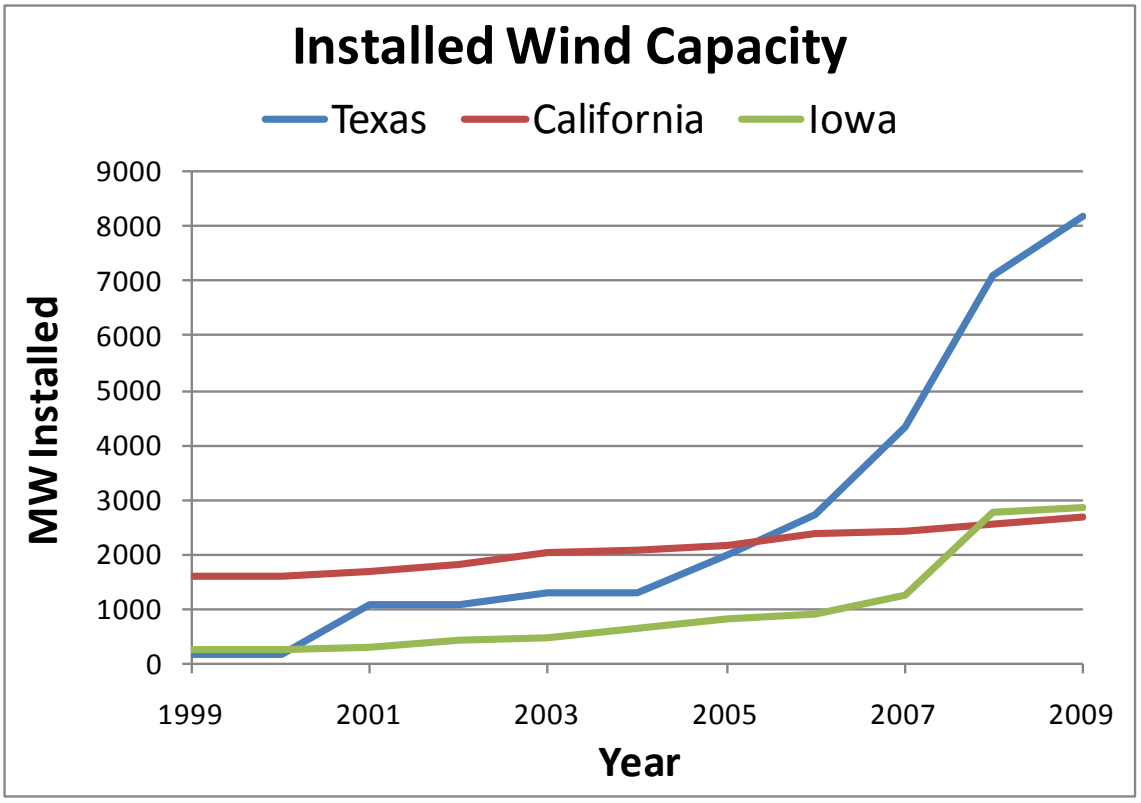

Figure 2.4: Over the last few years Texas has shown a sharp rise in wind turbine installations, helping it far outpace all states in total installed wind capacity [10].

2.1.2. Solar Energy Potential

Similar to the wind resources in Texas, solar resources are concentrated in the west and panhandle regions of the state. Texas' total potential to generate electricity in these hot, arid regions of the state is even higher than its total wind generation potential. As seen in Figure 2.5, the average solar irradiance over all daylight hours in one day in west Texas can reach up to 5.7 kWh/(m^2·day).

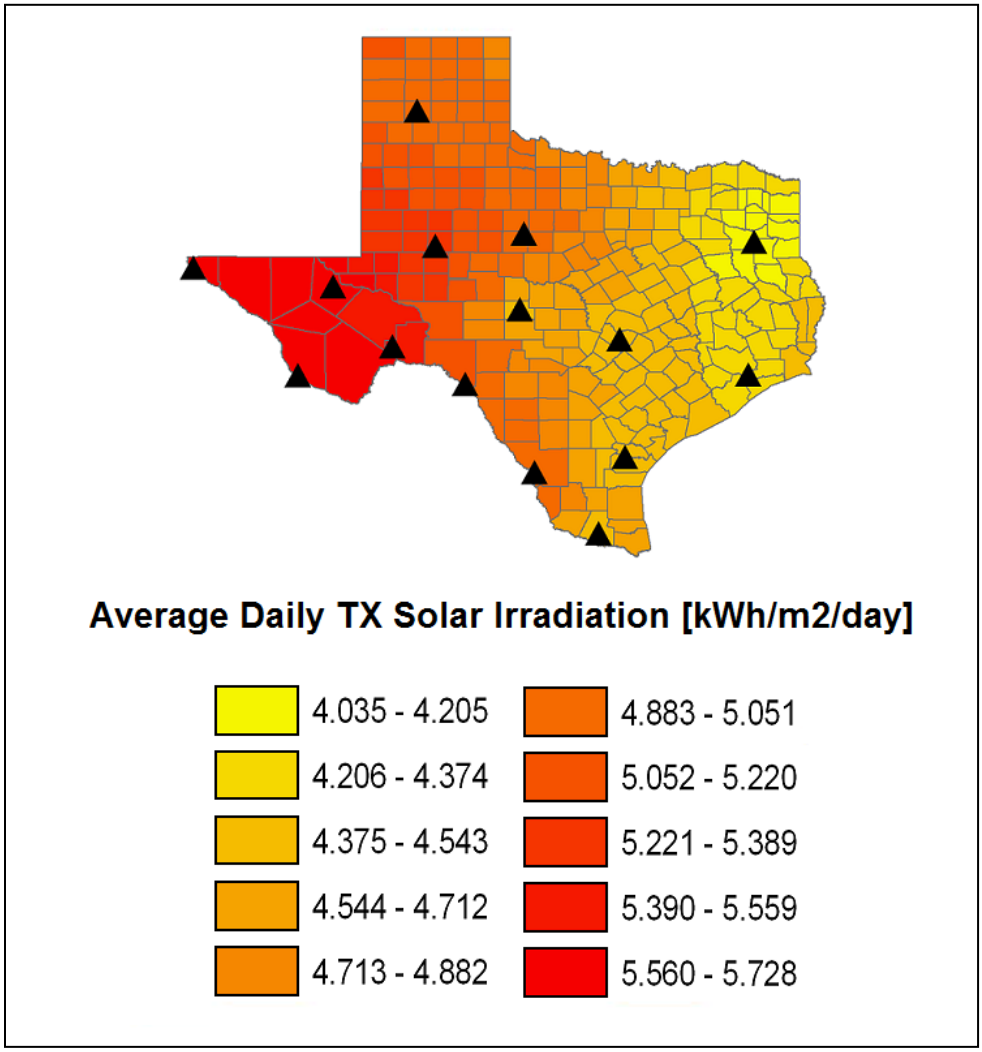

Figure 2.5: The west and panhandle regions of Texas have a high average solar irradiance [11]. The fifteen triangles represent the data collection sites.

However, the abundance of solar resources in Texas has not yielded record growth similar to that of the wind energy industry. High costs associated with both photovoltaic and concentrating solar technologies have kept them from being as attractive to energy utilities and venture capitalists.

2.2. INTEGRATION ISSUES WITH WIND AND SOLAR ENERGY

Wind and solar energy are both compelling sources of clean and renewable energy, but in their current form both are also difficult to effectively incorporate into the electric grid on a large scale. As the grid operates now, nuclear and coal electricity makes up the base-load while electricity from natural gas is used to fill in during the peaks. Wind and solar resources are not dispatchable like nuclear, coal and natural gas. Therefore, they add another level of difficulty to the operation and control of the electric grid.

2.2.1. Inherent Variability and Mismatch with Demand

Both wind and solar resources are inherently variable. These naturally occurring energy sources are subject to diurnal (daily) variation, seasonal variation, and local weather conditions such that neither matches electricity demand and therefore both require backup/reserve generation facilities as firming power in case of daily and seasonal outage. Figure 2.6 below illustrates these sources' natural mismatch with electricity demand.

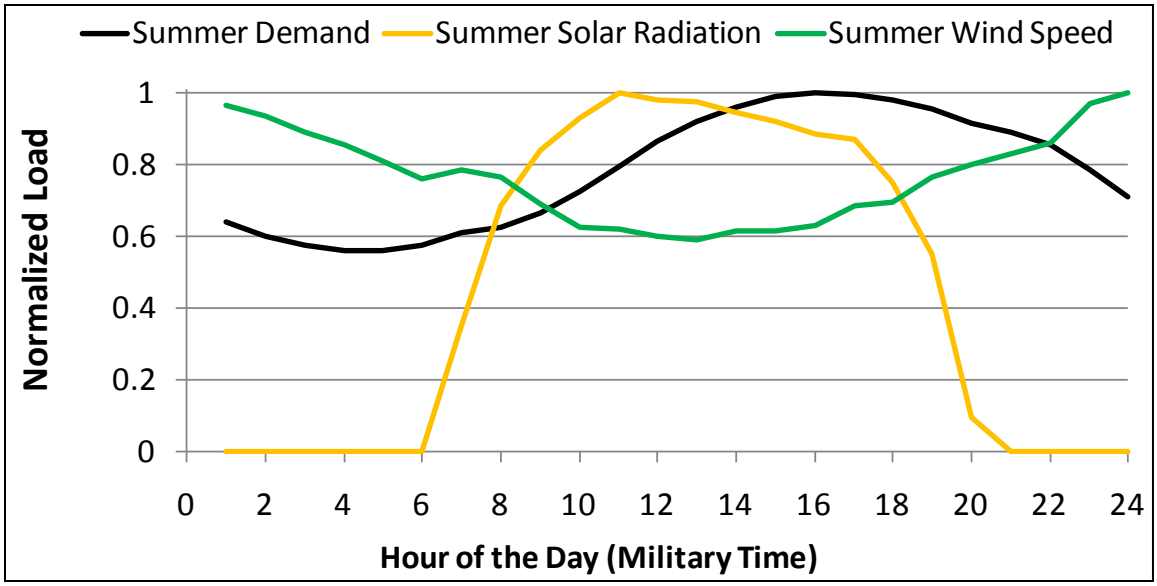

Figure 2.6: The intermittency of both wind and solar generation (shown here for a typical summer day in West Texas) hinder their large scale incorporation into the electricity market.

Shown in black is the normalized electricity demand in the ERCOT electric grid for the peak day in August of 2007 [12]. Demand rises during the morning and early afternoon, peaks at around 4pm, and then slowly drops off to a minimum at around 4am. Shown in yellow is the normalized average hourly direct-normal solar radiation for the month of July from 2000 to 2002 in Abilene, Texas [13]. Over the course of the day, solar radiation increases in the morning along with demand, but quickly drops off in the late afternoon when demand is still at its peak. Shown in green is the normalized average hourly wind speed for the month of July in 2007 at the Tall Tower South wind farm just west of Abilene [14]. This curve shows how wind speed and demand are almost completely out of phase with each other over a typical one-day period in the summer. When demand is highest in the afternoon, wind is at its weakest and when demand is lowest at night, wind energy reaches its peak.

2.2.2. The ERCOT Electricity Grid and Issues with Curtailment and Negative Pricing

The rapid increase in wind turbine installations in Texas has caused ERCOT, the electric grid controller, to make operational adjustments over the last few years. Done in order to maintain grid stability and reliability these adjustments include maintaining higher amounts of spinning reserve in order to compensate for unpredicted fluctuations in wind generation, and the curtailment of total wind generation to avoid overloading of electric lines running to load centers. As more wind turbines are installed, these issues might be exacerbated. In an effort to overcome curtailment issues, the Texas government and ERCOT are building a network of high voltage power lines to the CREZ zones mentioned earlier. These lines should minimize grid congestion and curtailment and allow for the future installation of over 10,000 MW of new wind turbine facilities [15].

Another phenomenon, spurred from the rapid growth of the wind industry in Texas, is negative pricing. Wind farms have relatively low marginal costs because the operational and maintenance costs are much lower than conventional coal or natural gas facilities and they have no fuel costs. As a result, since ERCOT is a competitive market, wind energy producers often issue a very low, if not zero bid price for their energy. However, in addition to the lower marginal cost of the wind farms, wind energy producers have also been receiving the national production tax credit (PTC) for generating renewable energy. This government subsidy is in effect an incentive for wind producers to continue generating even when their marginal costs are more than the price they are paid for their electricity. The result is that sometimes wind producers accept a negative price, meaning they actually pay ERCOT to take their electricity, as long as the negative price plus their marginal costs is less than the PTC. This phenomenon often happens in the west region of the ERCOT grid at night when electricity price is at its

lowest and wind generation is at its highest. Figure 2.7 illustrates this phenomenon's occurrence on March 3, 2009. During this day, in the West region of ERCOT, the market clearing price of energy for load (MCPEL) reached as low as negative thirty-four dollars per MWh and stayed negative much of the night and early morning hours. Such occurrences of negative prices are typical during low demand hours of mild seasons when heating and cooling loads are minimal. This negative price is also transmitted to the customer, meaning the consumers are being paid for using electricity, and the more power they use the more they are paid. [16]

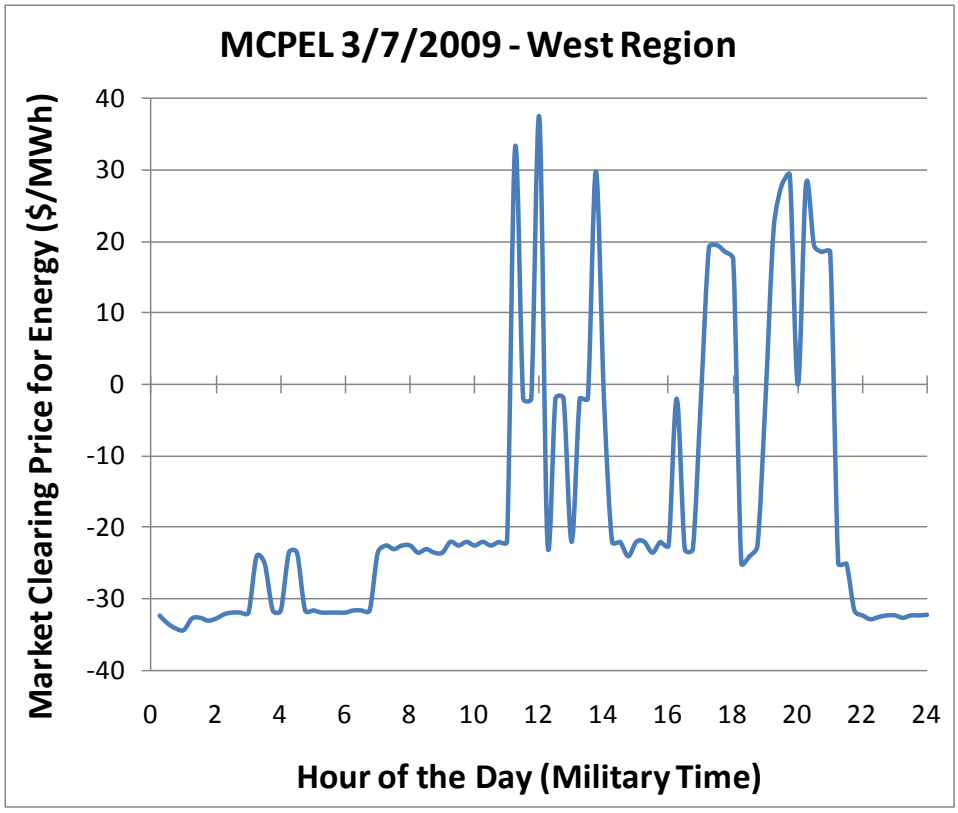

Figure 2.7: Grid congestion and availability of the PTC can cause negative prices as seen on March 7, 2009 when for much of the day the Market Clearing Price of Energy for load (MCPEL) was negative [17].

The wind producers' desire to continue operating and accept very low or even negative prices causes higher maintenance cost from extra hours of operation. Additionally, the conventional baseload generation facilities are forced offline more often than normal thereby facing additional maintenance cost because of wear and tear from ramping up and down of their machines.

2.3. LARGE SCALE ENERGY STORAGE SCHEMES

One way to overcome the issues of inherent variability and mismatch with demand of wind and solar resources is to incorporate large-scale energy storage so that the energy can then be used on a dispatchable, load-balancing basis much like natural gas plants, allowing generation to match demand. As of today, there are only three practical and deployable industrial scale energy storage methods: potential energy storage (pumped hydro), thermal storage, and compressed air energy storage, only the first of which is currently in wide use [18].

2.3.1. Pumped Hydroelectric Storage (PHS)

As its name implies, PHS involves using energy when available to pump water from a low elevation to a high elevation; then, whenever needed the water is allowed to flow back down to the lower elevation through hydroelectric turbines to generate electricity. Even though the energy requirement of the pumping process makes this type of facility a net energy consumer, the operators generate revenue by storing during times of reduced demand when prices are low and generating during times of peak demand when prices are high.

This type of energy storage is by far the most widely used around the world with over 100 operating facilities. The technology, similar to typical hydroelectric plants, is mature and can be rapidly switched on or off.

However, even though this technology is well understood, it is not without complications. Locating a good site for a PHS plant is very limited because of two critical terrain requirements. First, a PHS facility requires an immense amount of water in order to store a useful amount of energy. The reservoir for the Ludington PHS facility, seen in Figure 2.8 below, holds approximately 27 billion gallons of water. Water availability was not an issue in this case because the Ludington facility is located on the bank of Lake Michigan. Second, the site must contain a large natural terrain elevation change in order to build the lower and upper reservoirs. The Ludington facility was built on the top of a 363 ft plateau in order to achieve an adequate potential difference.

Figure 2.8: The Ludington PHS facility, commissioned in 1973, can generate over 1.8 GW of electricity [19].

The likelihood of finding a single location with both a large water resource and a high elevation change is slim in West Texas. However, PHS facilities around the world are providing load-leveling power and when fed by wind or solar electricity, are doing so in a clean and renewable way.

2.3.2. Thermal Storage

Thermal energy storage is usually associated with concentrating solar power (CSP) systems, but could be used in any situation where there is an available heat source. Many forms of thermal storage have been developed including high pressure steam and hot oil, but industry uses molten salt as the preferred storage medium. Companies such as Abengoa and Ausra and researchers at laboratories such as NREL have been experimenting with these technologies at industrial scales for nearly two decades [20]. In a typical system the salt mixture, kept in its liquid form at a low temperature in one tank, is heated by concentrating solar reflectors to a temperature of up to 550°C. Once heated, the salt is sent to a second 'hot' tank for storage, until when needed, the hot salt is used to produce superheated steam, which is then used to run a typical turbine-generator. This configuration, called a 'two tank' system, is only one of the designs that can be used with molten salt. Additionally, unlike PHS, thermal storage can be built almost anywhere and has no specific terrain requirements.

Recently, research is being done on modifications to the precise materials used in the molten salt in order to create a superior 'alloy'. The goal of this research is to push the upper temperature bound that the molten salt can reach or push the lower temperature bound with which the salt is still in a liquid phase. Also, much of the current research is focused on modifications to an indirect heating system that uses different heat transfer

fluid in the CSP system, system modeling in order to predict performance and material properties, and the use of more exotic thermal storage media like porous castable ceramics and solid media beds [21].

This technology, though less mature than PHS, is already under development in industrial applications. NREL demonstrated one of the first thermal storage systems in the Solar Two project in the mid 1990's. Seen below in Figure 2.9, Solar Two was a 10 MW central receiver facility that utilized sun-tracking mirrors to heat the molten salt up to 565°C. By using a thermal storage system, Solar Two was able to achieve a capacity factor of around 65%. This result is remarkable when compared to the typical 25% capacity factor of solar technologies that do not incorporate thermal storage [22].

Figure 2.9: Solar Two, built by NREL, used molten salt to store solar energy for up to three hours [22].

2.3.3. Compressed Air Energy Storage (CAES)

As its name suggests, CAES utilizes compressed air as an energy storage medium. Used similar to the PHS facility, a CAES plant will pull electricity from the grid during

periods of low demand and cheap prices to compress air to high pressures. This air is then stored, usually in an underground geologic formation like a salt cavern or depleted aquifer. Then, whenever desired, the air is allowed to exit the storage cavern for expansion through a gas-fired turbine. Currently, there are two CAES facilities in the world, the first in Huntorf, Germany and the second in McIntosh, Alabama, that operate by using off-peak electricity to compress air that is stored in an underground cavern. The McIntosh CAES plant, commissioned in 1991 and shown in Figure 2.10, is the newer of the two facilities and includes the addition of a recuperator to recover waste heat from the turbine exhaust and improve the power system efficiency.

Figure 2.10: 110 MW CAES plant in McIntosh Alabama is the newer of the two facilities of this type in the world.

Both CAES plants use natural gas-fired combustors to heat the compressed air before expansion in order to generate electricity during times of peak demand. It is convenient to think of these facilities as similar to a conventional gas turbine power plant but with one important difference: in a typical gas turbine plant nearly two-thirds of the turbine generated power is required to run the compressors, leaving only one-third

available to operate the electric generators. In the CAES facility the compressors are instead powered by cheap off-peak grid electricity so that all the power created by the turbines can be used to produce electricity in the generator [23]. In effect, this pre-compression step significantly increases the amount of produced electrical power per unit of heat required by the combustors. So, for a rated output level, the CAES facility will consume from half to one-third as much natural gas as a conventional gas-fired power plant (note: by standard convention, any natural gas that might have been used to compress the air is not included in this calculation, so no fuel use is associated with the consumed grid electricity). The simple schematic diagram, seen in Figure 2.11, illustrates the main components and basic operation of a CAES facility.

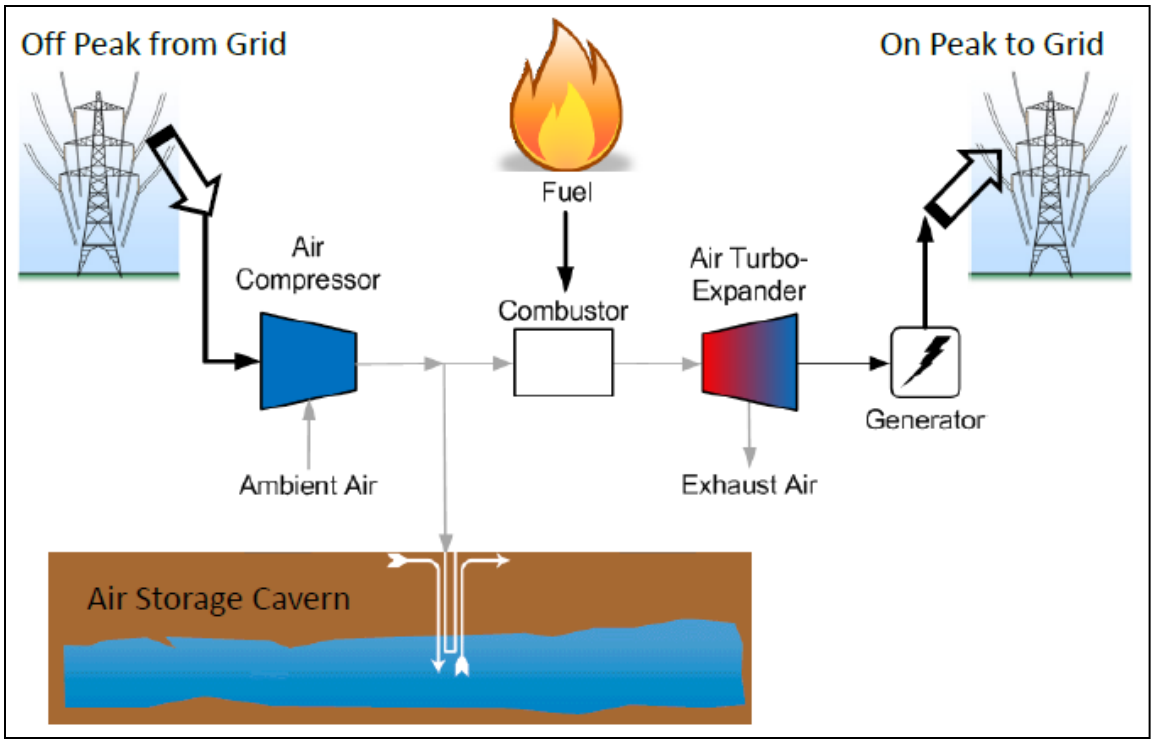

Figure 2.11: CAES mimics a typical natural gas power cycle with the addition of an air storage cavern and the decoupling of the compressor and turbine.

In the case of a typical natural gas plant, the compression ratios are in the range of 15:1, which is much less than the 70:1 ratio of a CAES facility. With much more energy input from the compressors to reach such a high compression ratio, it could be anticipated that the CAES plant may not need to heat the air before entering the expansion turbine. However, because the heat removed from the air during compression in a series of intercoolers is not recovered, the air exits the storage cavern at around 38°C. So, in order to increase the energy content and avoid freezing during the expansion process, the existing CAES facilities add heat by using a natural gas combustor [24].

It has been estimated that approximately 85% of the U.S. would be able to access underground geological formations suitable for compressed air storage and that most the West Texas areas of interest would actually have access to three different type of suitable formations [25]. Additionally, since this type of facility is so similar to a typical natural gas plant, it too can be quickly turned on and off. Again, like the PHS facility, this dispatchability is desirable and adds to the grids robustness to compensate for variability in other renewable energy sources.

2.4. DESCRIPTION OF THE PROPOSED SYSTEM

The purpose of the proposed system is to combine wind and solar energy with both compressed air and thermal storage techniques in a way that couples excess night-time wind capacity with peak solar output. In essence this design mimics the CAES plants previously described but replaces the natural gas combustor with concentrating solar power and thermal storage and will draw power to operate the compressors from excess wind energy instead of off-peak grid electricity. These key changes 1) eliminate all fossil fuel consumption of the CAES plant as well as the need to draw grid electricity

and 2) maintain the system's dispatchability. A schematic diagram of the proposed DSWiSS energy system can be seen below in Figure 2.12.

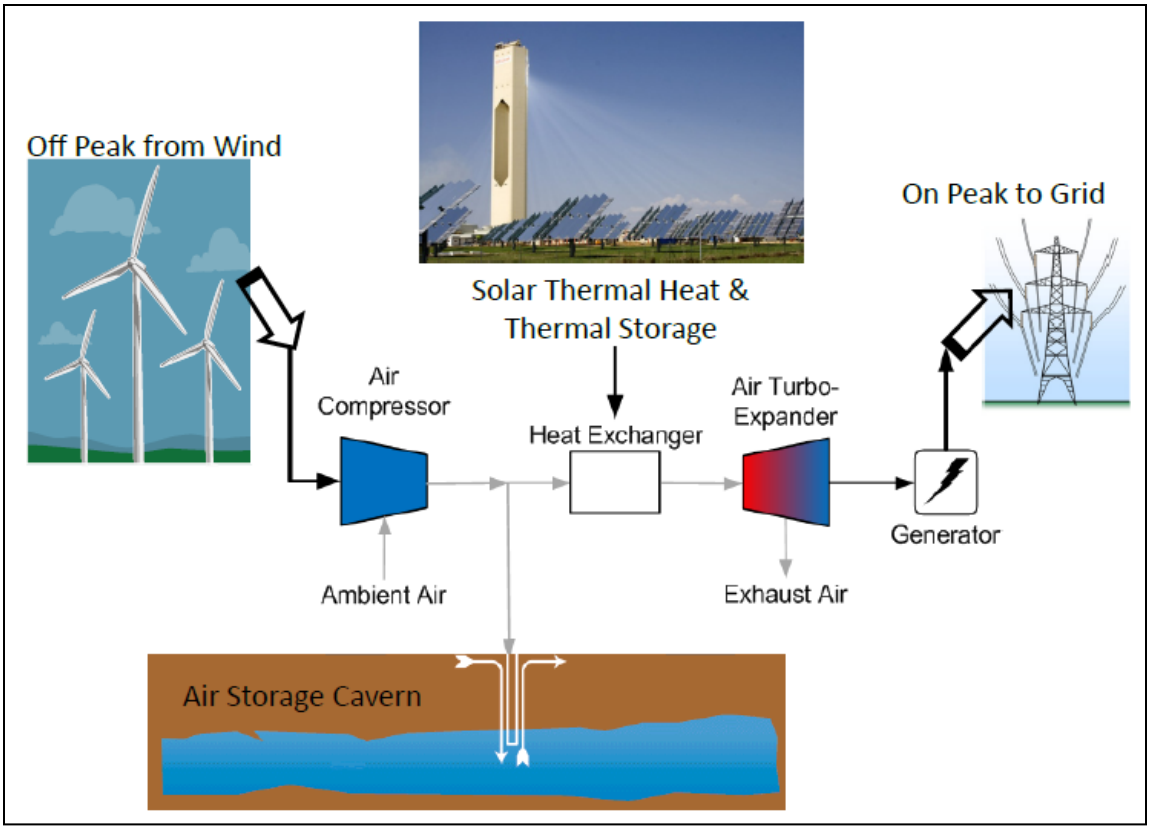

Figure 2.12: The DSWiSS facility replaces both energy sources from the typical CAES facility with renewable resources in the form of wind energy and solar thermal heat.

2.4.1. Integrating Wind-Solar-Storage for Dispatchability

In this system wind power drives the compression of air, which is then stored in underground caverns. Then, whenever the operator decides, the air is released from the cavern to be heated by the solar thermal system and expanded through the turbine-generator. Thermal storage is also incorporated here in order to ensure that the turbine-

generator system can operate into the evening hours when the price for electricity is still high, or continue to run during off peak hours as a form of firming power. Using this combination of technologies, the energy system should be able to operate on demand during all afternoon and early evening hours. The duration of the system's operation into the evening is dependent on the size of the solar thermal and thermal storage system. These two components could be sized large enough to ensure twenty-four hour operation if it is in fact cost-effective to do so. In addition, this design includes bypasses as shown on the solar thermal primary heat exchanger (HX) and thermal storage unit in Figure 2.13. This diagram simply shows how one or both of these devices will be used to heat the compressed air depending on the amount of available energy from the solar collector at any point during the day and evening.

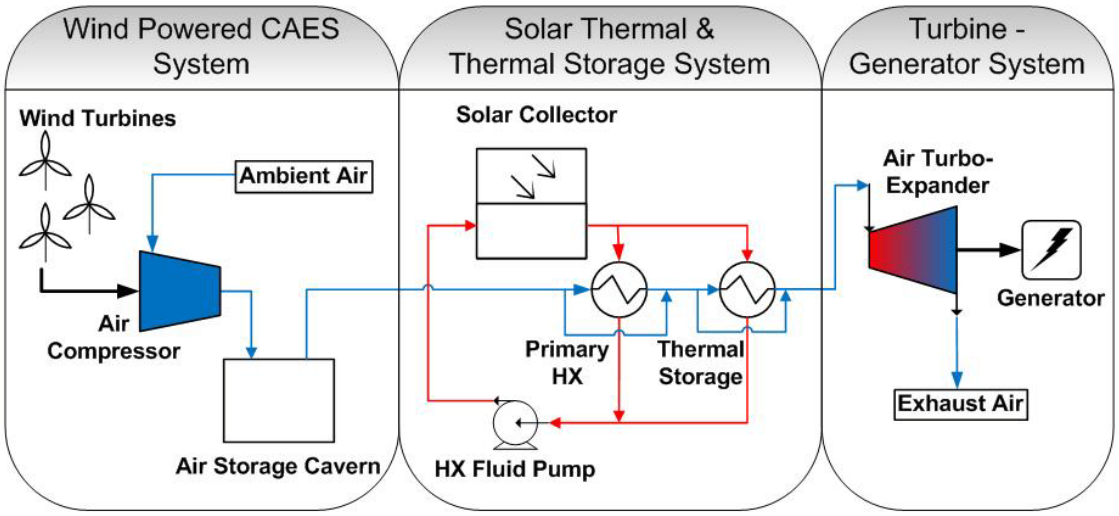

Figure 2.13: Air exiting the storage cavern can be heated directly by the solar thermal collector or by the thermal storage unit, thus allowing for generation into the evening hours.

What is not illustrated in this diagram is that the compression and expansion processes will actually be accomplished by multistage units that utilize intercooling and reheat, respectively, all of which are modeled in the subsequent thermodynamic analysis. The compressor train modeled herein consists of four stages of compressors with three intercoolers and an aftercooler in order to minimize the required compression work. The turbine system consists of a two-stage turbine with a reheater supplied by the solar thermal system. By utilizing reheat, the second stage turbine will operate at conditions identical to that of a typical gas turbine. Also not shown on the diagram is a recuperator to preheat the air exiting the cavern by using the hot exhaust air from the second stage turbine. This form of waste heat recovery will reduce the amount of energy the solar thermal system will need to provide. This turbomachinery system is identical to that located in the McIntosh CAES facility and was designed by Dresser Rand [26].

The operation of such a combination of technologies will not be restricted to a single method. Based on real time variables like energy price and solar availability, the operator will be able to choose the mode of operation in order to maximize profits or minimize total system costs. Figure 2.14 illustrates the different operational modes of DSWiSS. First, at any point in time, the operator may choose to sell the wind-generated electricity directly to the grid instead of using it to compress air. This scenario might occur in the middle of the day when the price for electricity is highest. Also, since the compression and generation operations are decoupled, generation can occur anytime given that there is available compressed air. Once these decisions have been optimized, it is expected that the generation operation will be run for a period of time when electricity price is high. For example, perhaps the system will generate for six hours when the price is highest, and the wind energy will be used for compression at all times except during the two hours when the price is highest and it is instead sold directly.

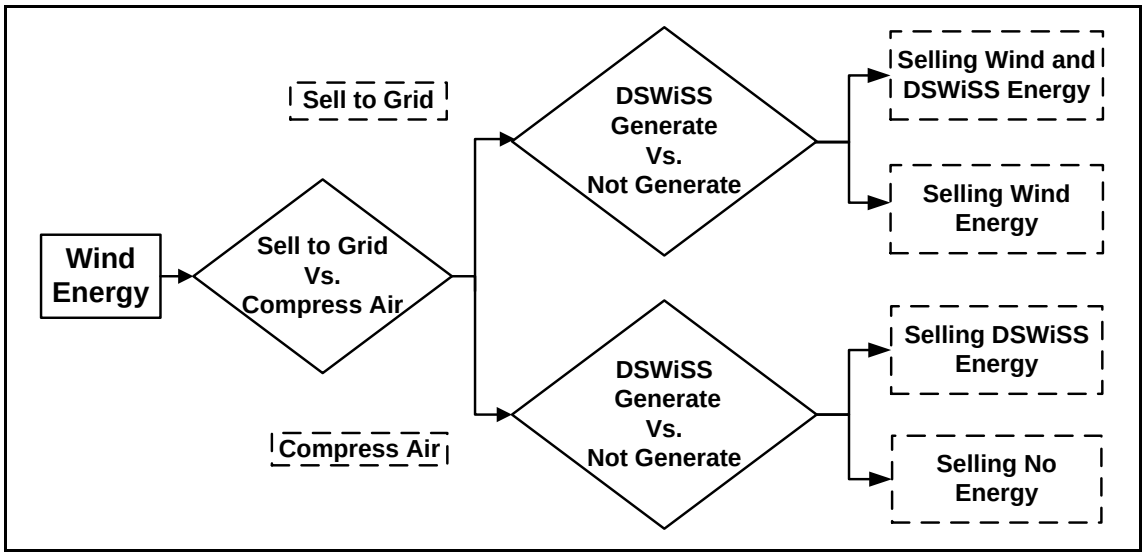

Figure 2.14: Different power system operating scenarios will affect the system's profitability.

2.5. RELEVANT POLICY ISSUES

Recently, the Texas and national governments have been developing policies that promote the implementation of renewable energy.

2.5.1. Texas State Policies and Incentives

Up until 2002, the electricity market in Texas was a 'regulated market'. This term means that the Public Utility Commission of Texas (PUCT) had the authority to ensure that only one electric energy provider exist to serve each area of the state. Starting in 2002, under Senate Bill 7, the electricity market in Texas was deregulated to encourage competition among electricity providers with the intent of providing lower prices to consumers. In addition deregulation, the bill also created a renewable portfolio standard

(RPS), which mandated that the state have at least 2000 MW of renewable power capacity by 2009 [27]. The RPS was so successful that in 2005 Texas already had 1140 MW of installed renewable capacity, and so the legislature expanded the RPS to 5000 MW by 2015 in Senate Bill 20. Once again, this quantity was easily surpassed when in 2008 Texas already had 7100 MW of installed wind capacity [6].

2.5.2. Federal Policies and Incentives

The U.S. government has been passing legislation aimed at increasing the domestic production of renewable energy since 1992. Created as part of the Energy Policy Act of 1992, a production tax credit (PTC) gives a credit based on kWh electricity production to numerous types of alternative energy facilities. This credit is one of the primary driving mechanisms behind the rapid growth of wind energy. Most recently, the American Recovery and Reinvestment Act, passed in February 2009, extended the PTC through 2012 at a rate of 2.1 cents per kWh for electricity from wind turbines [28].

One issue currently under debate in the U.S. Congress is the creation of a cap and trade system for carbon emissions in an effort to reduce atmospheric carbon dioxide levels. The American Clean Energy and Security Act of 2009 [29], a bill introduced by representatives Henry Waxman and Edward Markey, as well as the Clean Energy Jobs and American Power Act [30], a bill introduced by senators John Kerry and Barbara Boxer, both are intended to create a mechanism for carbon emissions reduction. Both propose to employ a cap and trade carbon market in which emitters would have to buy credits in order to release carbon emissions. This additional cost is expected to make renewable energy technologies more attractive for future development, and help bridge the cost gap between traditional and renewable energy generation facilities.

With both state and national governments creating incentives for renewable energy, issues with the intermittency of wind and solar energy might be exacerbated. As more and more wind and solar energy is incorporated into the electric grid, operators like ERCOT will continue to struggle to compensate for these variable resources.

Chapter 3: Modeling of a 1.5 MW Variable Speed Wind Turbine in PSCAD/EMTDC

3.1. Fixed Speed vs Variable Speed Wind Turbines

Utility-scale three-bladed, upwind, horizontal axis wind turbines dominate the modern wind turbine industry. This combination of design features allows for maximum power output while reducing maintenance needs and costs. Still, within this small set of possible wind turbine designs there is a range of available manufacturers with various designs and features that give a valuable range of choices based on site-specific details and the cost and power requirements.

One of the most important of these choices is the selection of either a fixed or variable speed wind turbine. A fixed speed wind turbine is simply a turbine with a fixed blade pitch angle and no active control mechanism to maintain peak power output. As seen in Figure 3.1 below, a fixed speed wind turbine only reaches its peak power output at a single wind speed (the rated wind speed), while a variable speed wind turbine is able to maintain maximum power output at all wind speeds between the rated speed and the cut-out wind speed [31].

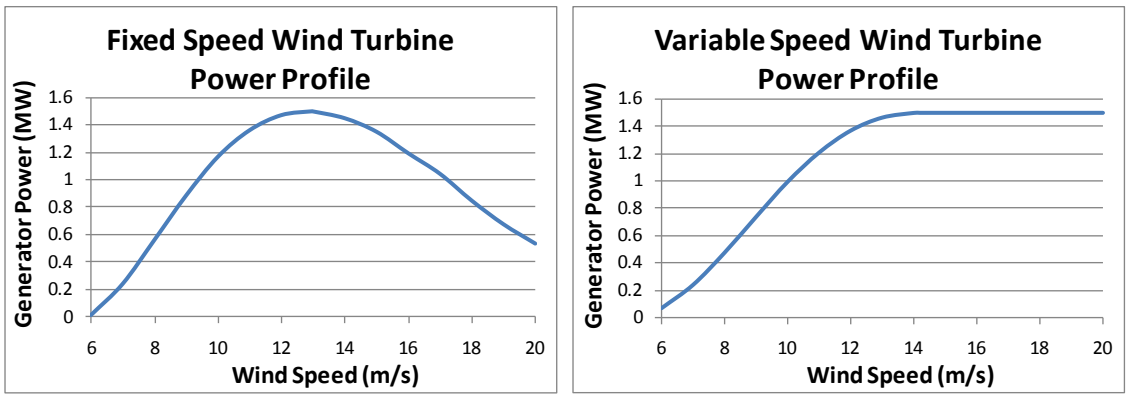

Figure 3.1: The power generation at high wind speeds will be significantly different for a fixed versus variable speed 1.5 MW wind turbine.

The major benefits of the variable speed wind turbine are that it will produce the rated power at wind speeds above the rated speed; however, the fixed speed turbine is a simpler design and therefore requires less maintenance and is less expensive. Recently, for land-based applications, a 1.5 to 2.5 MW variable speed wind turbine has been the preferred selection. As technology has progressed and costs have decreased, the benefits of the variable speed turbine including higher power output and improved safety have outweighed the higher costs [31].

3.2. Control Mechanisms for Variable Speed Wind Turbines

There are two methods for creating a variable speed wind turbine, both of which employ feedback control mechanisms. First, there are aerodynamic controls that utilize the aerodynamics of the blade to control the turbine blade speed. One such type of control, called pitch control, adjusts the pitch blade angle depending on the wind speed so that the rated power can be maintained through a range of wind speeds. This method is common among variable speed wind turbines, and though effective is relatively slow. In order to change the blade pitch during the occurrence of higher than rated wind speeds, hydraulic motors rotate each blade individually until they regain rated power output. This process can take multiple minutes and therefore is not an adequate control mechanism for continuously changing wind speeds; however, this method works well for smoothing out the daily highs and lows [31].

The second type of control method involves electronic manipulation of the generator inside the nacelle of the wind turbine. These electronic controls react almost instantaneously and require very little added machinery and weight. One such control mechanism, called slip control, utilizes an adjustable external rotor resistance that will

vary the generator slip by as much as 10%, which allows the generator to maintain maximum power output. However, increasing the external rotor resistance at wind speeds higher than the rated speed causes additional heating losses. Another electronic control mechanism uses a doubly-fed induction generator (DFIG) which can maintain maximum power by controlling the magnitude and phase of the alternating current in the rotor circuit. This generator also allows for the independent control of both real and reactive power. However, this system is much more complex and therefore adds cost and weight [31].

3.3. MODEL DESCRIPTION

This analysis consists of modeling various components of a 1.5 MW variable-speed wind turbine that uses the external rotor resistive control in the software package PSCAD/EMTDC. PSCAD was developed at the Manitoba HVDC Research Center and is robust power systems simulation software. EMTDC is the simulation engine or solver that operates behind the PSCAD graphical user interface. One of the primary uses for PSCAD is to simulate time domain instantaneous responses in electrical systems, also known as electromagnetic transients.

Two versions of the PSCAD model were created, both of which use the rotor resistive control; each employs a unique feedback controller in order to maintain constant stator power output above rated wind speeds. See Appendix A for more details of the wind turbine model code. The following components were included in the model: wind turbine blades (tip speed ratio calculation, coefficient of performance estimate, and low-speed shaft torque calculation), gear-box (2 mass shaft model), and generator (wound rotor induction machine, 3 phase breaker, and 3-phase voltage source). Figure 3.2

illustrates how these three components are connected by two shafts; the low-speed shaft (or rotor shaft) connects the blades and gear-box while the high-speed shaft (or generator shaft) connects the gear-box and the generator.

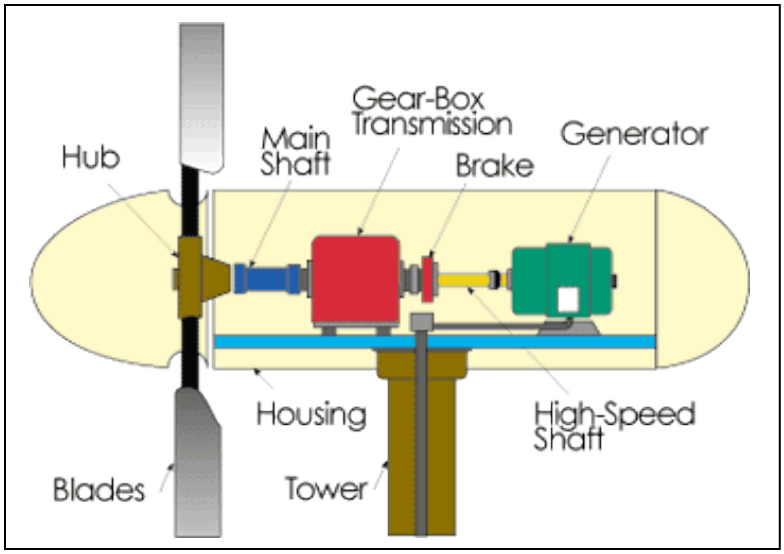

Figure 3.2: The basic wind turbine model consists of three main parts: blade model, gear-box model, and generator model [32].

The model solves in PSCAD iteratively, meaning that the program runs until the variables converged to a solution. Unknown values that the computer simulation solves for in this way include wind turbine rotor speed and torque, generator rotational speed, and generator torque. Table 3.1 lists the user defined variables needed in the simulation.

Table 3.1: User defined parameters for wind turbine model.

Parameter	Value	Unit
Rated Generator Output	1.5	MW
Turbine Rotor Diameter	72	m
Turbine Cut-In Speed	6	m/s
Turbine Cut-Out Speed	20	m/s
Gearbox Gear Ratio	70.2	
Generator Poles	6	
Generator Frequency	60	Hz
Generator Voltage	690	V
Generator Turns Ratio	0.379	

3.3.1. Turbine's Coefficient of Performance and Aerodynamic Torque Calculation

The first part of the model simulates the wind turbine blades and rotor shaft by calculating the blade tip-speed ratio (λ), the turbine's coefficient of performance (C_p), and the aerodynamic torque applied to the generator rotor shaft (*AeroTorque*), which is attached to the turbine blades. As shown in Figure 3.3, inputs to the system include rotor radius (R_{rot}), blade pitch angle (*PitchAngle*), and wind speed (v). It is also important to note that the input (ω_{rot}), which is the angular speed of the rotor shaft, is not known and hence this is why the simulation must solve iteratively. As will be discussed in detail later, once the design pitch angle is determined, it will remain constant throughout the simulation.

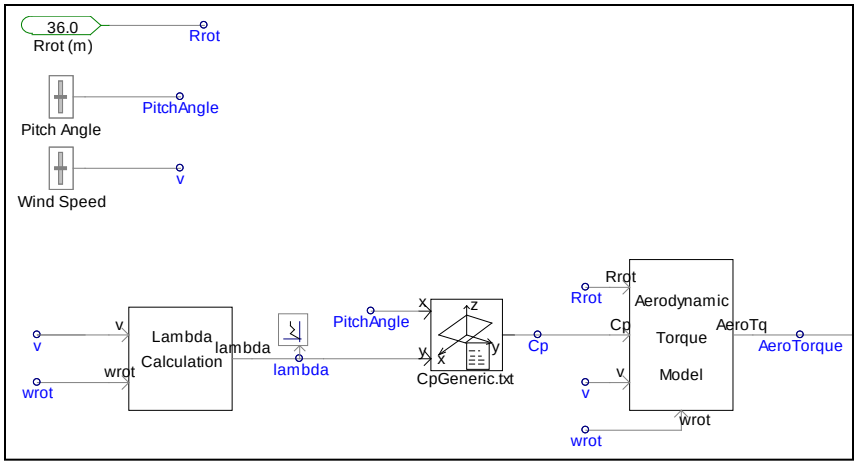

Figure 3.3: The wind turbine blade aerodynamic model as programmed in PSCAD.

The tip-speed ratio (λ) is the ratio of the linear turbine-blade tip speed to the free-stream wind speed. This calculation is very simple and can be seen in Equation 3.1.

$$\lambda = \frac{\omega_{rot} R_{rot}}{v} \tag{3.1}$$

In this equation, ω_{rot} is the rotational velocity of the rotor shaft, R_{rot} is the turbine-blade rotor radius, and v is the wind free-stream velocity.

Next, the model calculates the turbine's coefficient of performance (C_p), which is the ratio of the power extracted from the wind to the power available in the wind. Equation 3.2 illustrates this ratio.

$$C_p = \frac{P_{extracted}}{P_{available}} = \frac{P_{extracted}}{.5\rho A v^3} \tag{3.2}$$

where ρ is the air density and A is the rotor blades swept area.

According to Betz's Law, which uses an idealized analysis, the maximum possible power factor achievable is 59.3% [31]. The calculation used in this model is based on the analytical Equations 3.3 and 3.4 which are from the book *Wind Turbine Operation in Electric Power Systems* by Dr. Zbigniew Lubosny [31].

$$C_p = C_1 \left(C_2 \frac{1}{\Lambda} - C_3 \Theta - C_4 \Theta^x - C_5 \right) e^{-C_6 \frac{1}{\Lambda}} \quad (3.3)$$

$$\frac{1}{\Lambda} = \frac{1}{\lambda + 0.08\Theta} - \frac{0.035}{1+\Theta^3} \quad (3.4)$$

In this equation, λ is the tip speed ratio, Θ is the blade pitch angle, and the coefficients are defined based on an Enercon E-40 wind turbine as: C_1*=0.5,* C_2*=116,* C_3*=0.4,* C_4*=0,* C_5*=5,* C_6*=21* [31]. Since C_4 is zero, there is no need to specify the exponent *x*.

The last step needed for the turbine blade model is the calculation of the torque that the blades are extracting from the wind and turning into torque in the rotor shaft, which is below in Equation 3.5.

$$AeroTorque[\mathrm{J}] = \frac{\rho \pi R_{rot}^2 C_p v^3}{2\omega_{rot}} \quad (3.5)$$

3.3.2. Two-Mass Gear-Box Model (Shaft Model)

The next component in the wind turbine model is the gear-box. In order to model the gear-box, a two mass 'shaft model' was used where one mass represents the turbine blades, rotating with a torque and speed, and the other mass represents the generator rotor, spinning with a different torque and speed. In the model, a single shaft connects the two masses, so the original two shafts and gear-box are now represented by a single shaft. Figure 3.4 illustrates this simplification.

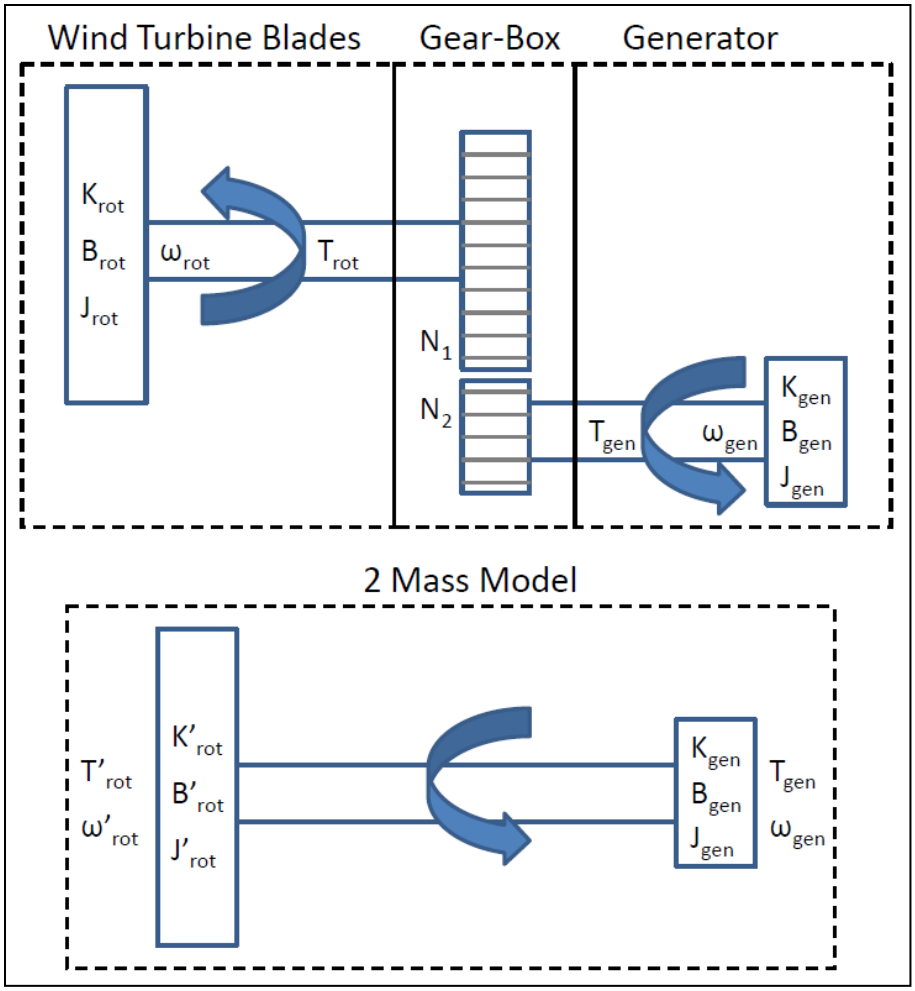

Figure 3.4: Gear-box two-mass shaft model is used to simulate the gear box coupling between the rotor and generator shafts.

Once the two mass model is selected, the first task is to calculate the equivalent shaft stiffness and damping values, both of which are a combination of the stiffness and damping values of the rotor and generator shafts. Care must be taken with this calculation because in reality two gears connect these shafts, so the torque, stiffness, damping, and inertia values from the reference frame on one side of the gear-box must be referred to the reference frame on the other side. This calculation is done by using the gear ratio. For this model, since the goal is to use the generator torque and speed to

calculate the generator power, we refer all the rotor values to the generator reference frame as shown in Equations 3.6, 3.7, 3.8, 3.9, and 3.10. In these equations T_{rot} is the rotor torque, ω_{rot} is the rotor speed, K_{rot} is the rotor stiffness (which is a measure of the resistance to deflection), B_{rot} is the rotor damping (which is a measure of the resistance to instability or oscillatory conditions), J_{rot} is the rotor inertia (which is a measure of the resistance to a change in state of motion), and GR is the gear ratio.

$$T_{rot}^{'} = \frac{T_{rot}}{GR} \tag{3.6}$$

$$\omega_{rot}^{'} = \frac{\omega_{rot}}{GR} \tag{3.7}$$

$$K_{rot}^{'} = \frac{K_{rot}}{GR^2} \tag{3.8}$$

$$B_{rot}^{'} = \frac{B_{rot}}{GR^2} \tag{3.9}$$

$$J_{rot}^{'} = \frac{J_{rot}}{GR^2} \tag{3.10}$$

The primes in the previous equations indicate that the values are referred to the generator reference frame; also note how the prime values are represented in the two mass model in Figure 3.4. Now that all values are in terms of the generator reference, the equivalent shaft stiffness and damping can be calculated using Equations 3.11 and 3.12.

$$B_{eq} = B_{rot}^{'} + B_{gen} \tag{3.11}$$

$$\frac{1}{K_{eq}} = \frac{1}{K_{rot}^{'}} + \frac{1}{K_{gen}} \tag{3.12}$$

In these equations, the subscripts (*eq*) indicate an equivalent value representative of the single shaft connecting the turbine rotor mass and the generator rotor mass.

Finally, the two-mass shaft can be modeled with a system of three differential equations. This set, seen below in Equations 3.13, 3.14 and 3.15, must be solved simultaneously and iteratively. Once these equations converge to a solution, the rotational speed and torque for both the turbine rotor shaft and generator shaft can be calculated.

$$\frac{d\omega_{rot}^{'}}{dt} = \frac{1}{J_{rot}^{'}}\left[T_{rot}^{'} - B_{eq}\left(\omega_{rot}^{'} - \omega_{gen}\right) - K_{eq}\Delta\theta\right] \tag{3.13}$$

$$\frac{d\omega_{gen}}{dt} = \frac{1}{J_{gen}}\left[-T_{gen} + B_{eq}\left(\omega_{rot}^{'} - \omega_{gen}\right) + K_{eq}\Delta\theta\right] \tag{3.14}$$

$$\frac{d\Delta\theta}{dt} = \omega_{rot}^{'} - \omega_{gen} \tag{3.15}$$

Figure 3.5 shows how this set of differential equations is programmed into PSCAD. The three graphs on the right are for $\Delta\theta$, ω_{rot}, and ω_{gen}, respectively; note that they converge to a solution in less than three seconds. The ease with which this type of iterative system of equations is solved is one of the benefits of using PSCAD.

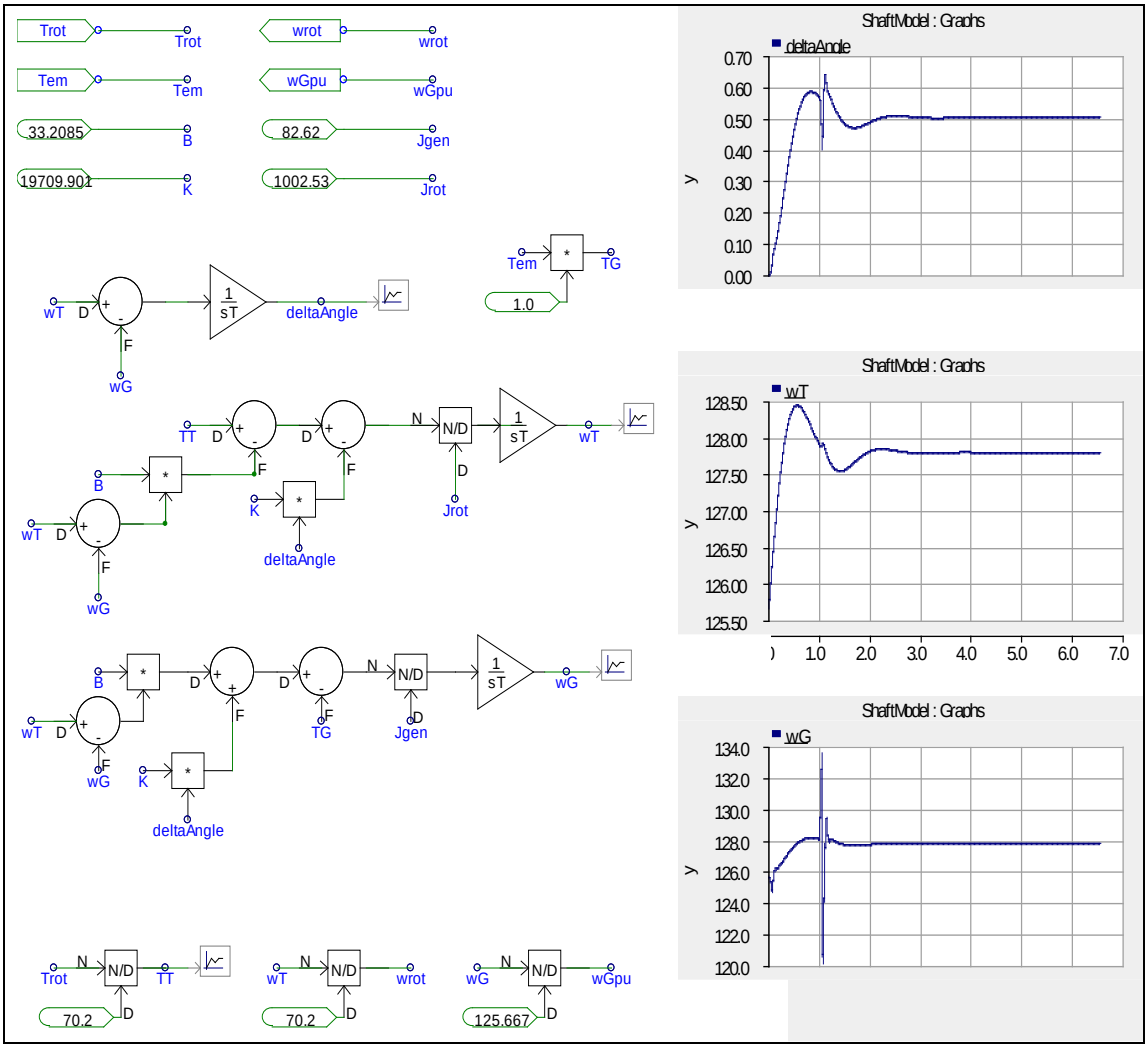

Figure 3.5: Gear-box two-mass shaft model is made up of three interlinked differential equations that PSCAD solves for iteratively.

3.3.3. Wound Rotor Induction Machine Model and Controller

The last components that are incorporated into the wind turbine model are the electric generator and controller. For the electric generator, PSCAD already has a built-in model of a squirrel-cage wound-rotor induction machine that will work well. By using this built-in function, the difficult physics and mathematics are able to be bypassed that

would be required for creating a new model of the generator. All that is needed for the induction machine model to work properly are a few user-defined parameters. Table 3.2 lists these necessary inputs.

Table 3.2: User defined parameters for wound rotor induction machine [33].

Parameter	Value	Unit
Rated Power	1.8	MVA
Rated Voltage	690	V
Base Angular Frequency	376.99	rad/s
Stator/Rotor Turns Ratio	0.379	
Angular Moment of Inertia	0.578	s
Mechanical Damping	0.01	per unit
Stator Resistance	0.00472	per unit
Wound Rotor Resistance	1.0e-006	per unit
Magnetizing Inductance	6.83309	per unit
Stator Leakage Inductance	0.08	per unit
Wound Rotor Leakage Inductance	0.04782	per unit

The completed induction machine model, seen in Figure 3.6, calculates the generator's output electrical power in megawatts. In the upper part of the figure there are three resistances labeled R_{ext}. These variables are the rotor external resistance that will be adjusted in order to maintain constant power output, and there are three because the induction machine is a three phase device.

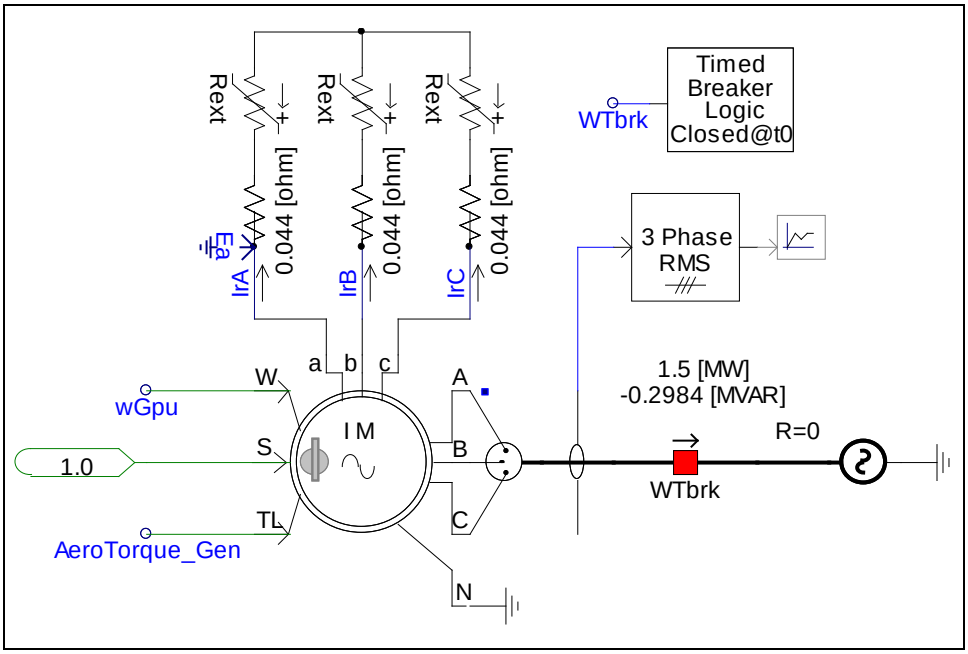

Figure 3.6: Induction machine model uses the built-in squirrel cage induction motor in PSCAD

The last step is to implement a controller that compares the actual generator output with the desired 1.5 MW output and adjusts R_{ext} accordingly. For this task, two separate controllers were made, one that utilized a built-in PI controller from PSCAD and one that uses a user-defined PI controller built by piecing together multiplier and integrator functions. Both controllers take in the generator output from the squirrel-cage induction machine (P_{gen}) and compare it with the user defined desired value, in this case 1.5 MW. Once the relative error of these two values, defined as their difference divided by the desired value, has been calculated, the PI controller adjusts R_{ext} and loops back through the model resulting in a new P_{gen} value. This process repeats until the generator output is sufficiently close to the desired 1.5 MW. Figure 3.7 shows the first controller using the built-in PI function.

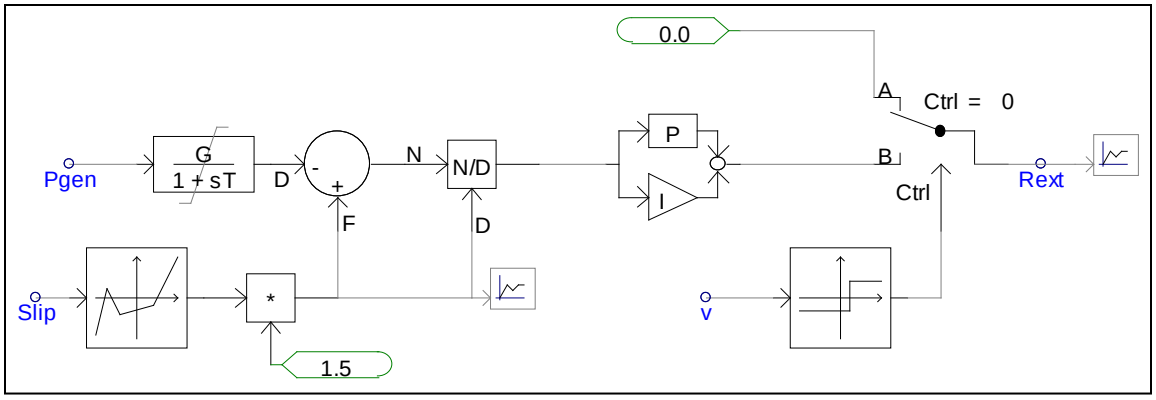

Figure 3.7: The first feedback mechanism model for rotor external resistance (R_{ext}) uses a built-in PI controller.

A switch on the right hand side is controlled by the wind speed. This component is added so that the controller does not engage until the current wind speed has gone above the rated wind speed, thereby leaving R_{ext} equal to zero at all slower speeds. Also, some tuning of the PI controller's proportional gain and integral time step is necessary in order to minimize the convergence time.

The second controller, seen in Figure 3.8, is identical to the first except for the use of the built-in PI function. In this controller, the PI function is created using the multiplier and integrator functions. The benefit to using the user-defined controller is the increased flexibility to define the parameters of the proportional and integral controls.

As was discussed earlier, both controllers operate on the external rotor resistance concept. So, once the wind speed goes above the rated speed, the controllers increase R_{ext} until the generator power output converges back to 1.5 MW. As the wind speed continues to increase, R_{ext} also will continue to increase thereby increasing the slip in the generator and maintaining the 1.5 MW power output.

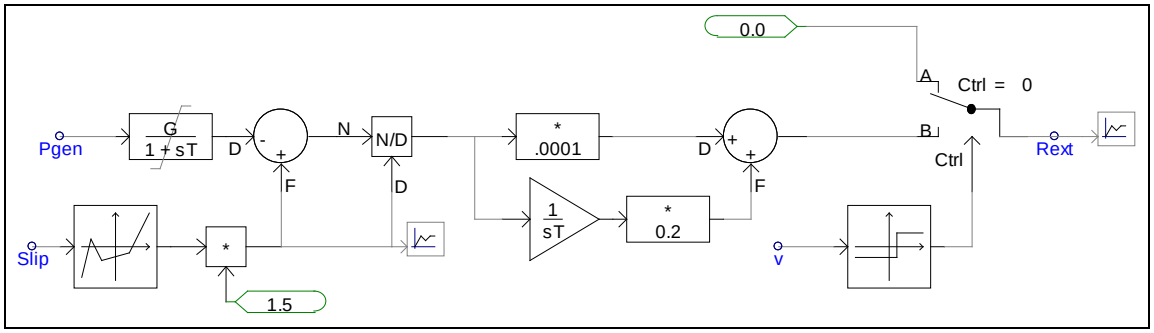

Figure 3.8: The second feedback mechanism model for rotor external resistance (R_{ext}) uses a user-defined PI controller.

3.4. DETERMINATION OF RATED WIND SPEED AND BLADE PITCH ANGLE

The first task of the model is a calibration experiment that will not use the rotor resistive control. As is seen from the fixed speed power curve of Figure 3.1, for every blade pitch value (β), there is one wind speed that results in a maximum generator output power (P_{gen}). In Figure 3.1, the design blade pitch resulted in a maximum power output of 1.5 MW at a wind speed of 12.95 m/s. If the blades of this fixed speed turbine had been designed at a different pitch angle, the power curve would have been shifted toward regions of lower wind speed and lower power output or regions of higher wind speed and higher power output, resulting in a different maximum power at a different wind speed. To clarify, the wind speed and blade pitch that result in the desired maximum power output are referred to as the rated wind speed and design pitch, respectively.

The calibration task for this simulation is to determine which blade pitch angle, for the specific C_p calculation, seen before in Equations 3.3 and 3.4, yields a maximum power output of 1.5 MW. In order to determine the wind turbine model's rated wind speed and design pitch a sweep was done. For a selected pitch angle, the simulation ran over the entire range of wind speeds to find which wind speed resulted in maximum

power output. This experiment was done for numerous blade pitch angles until the particular combination of wind speed and pitch angle resulted in a maximum power of 1.5 MW. Using the analytical C_p function from Equations 3.3 and 3.4, the rated wind speed and design pitch angle were found to be 14.4 m/s and -0.663°, respectively. Figure 3.9 shows the results of the sweep test at three different pitch angles.

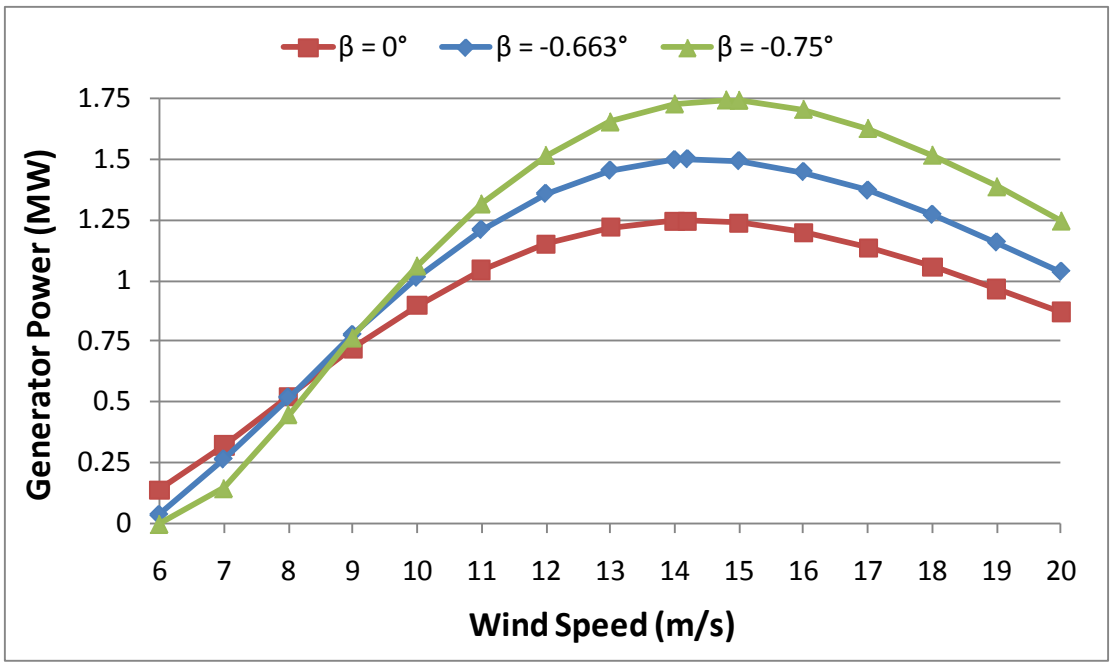

Figure 3.9: The power curves for these three pitch angles illustrate the importance of selecting the design blade pitch based on a desired power output.

This figure shows that even a small change in the blade pitch angle can have a large effect on the performance of the wind turbine. Changing the pitch angle by only 0.75°, the generator power output can be increased by half a megawatt. For this model, the blade pitch angle that results in a maximum power of 1.5 MW is selected. Now that this value has been established, the rest of the simulation efforts will be attempting to maintain the 1.5 MW power output at all wind speeds greater than the rated wind speed

of 14.4 m/s. For wind speeds below the rated speed, the wind turbine will function like a fixed speed wind turbine, meaning that no control mechanism will be active.

3.5. Rotor Resistive Control Results and Discussion

The remaining simulations all incorporate the external rotor resistive controllers previously described. The first simulation involves the transient response of the wind turbine to changing wind conditions, while the second simulation is concerned with the steady state performance at all wind speeds.

3.5.1. Dynamic Response to Changing Wind Conditions

Dynamic response to an increase or decrease in wind speed is very important to the safety and life expectancy of a wind turbine. Sudden wind speed changes can result in unwanted spikes and dips in the rotor and generator shaft torque and speed as well as in the power output. These spikes can increase stresses in the wind turbine components and lead to failure. So, in an effort to minimize these transient effects, two controllers were implemented, one using the built-in PI function and one using a user-defined PI function. It is expected that by using a user-defined PI controller, which has more adjustability, the gains and time constants can be tuned more accurately in order to achieve better transient responses.

Once the controllers were coded the last step was to tune the proportional gain and integral time step for the PI functions; an improperly tuned controller can result in an unstable system. By properly tuning the controllers the transient oscillations, spikes, and response time can be minimized. For the first controller, using the built-in PI function, two variables were adjusted until an optimum response was reached that worked well

over all wind speeds. This controller can be seen in Figure 3.6 above. The final values of these parameters are:

Proportional Gain (G_P) = 0.3

Integral Time Constant (τ) = 15.0

For the second controller, which uses the user-defined PI function, three variables could be adjusted. The additional variable is an integral gain that is simply a multiplying factor to the integrator. This controller can be seen in Figure 3.7 above, and the final values for the three parameters are:

Proportional Gain (G_P) = 0.0001

Integral Time Constant (τ) = 15.0

Integral Gain (G_I) = 0.2

The combination of parameters that worked best for the low wind speeds (15-16 m/s) did not work well for the high wind speeds (19-20 m/s) and vice versa. So, an intermediate combination was chosen that was not necessarily optimum for a single wind speed but that worked well for all wind speeds. It seems that a more complex controller could use different values of the parameters for different wind speeds in an effort to get quicker and smoother transient responses. Even using two sets of the parameters, one for low wind speeds and one for high wind speeds, would result in a more optimized controller.

In order to test the hypothesis of an improved transient response when using the user-defined PI controller, both controllers underwent an identical simulation. Once each PI controller has been properly tuned, each model ran with increasing wind speeds starting at 14.4 m/s (which is the rated wind speed), followed by 15 m/s, and finally 16 m/s. Figure 3.10 shows the dynamic response of the generator power output to this increasing wind speed for both PI controllers.

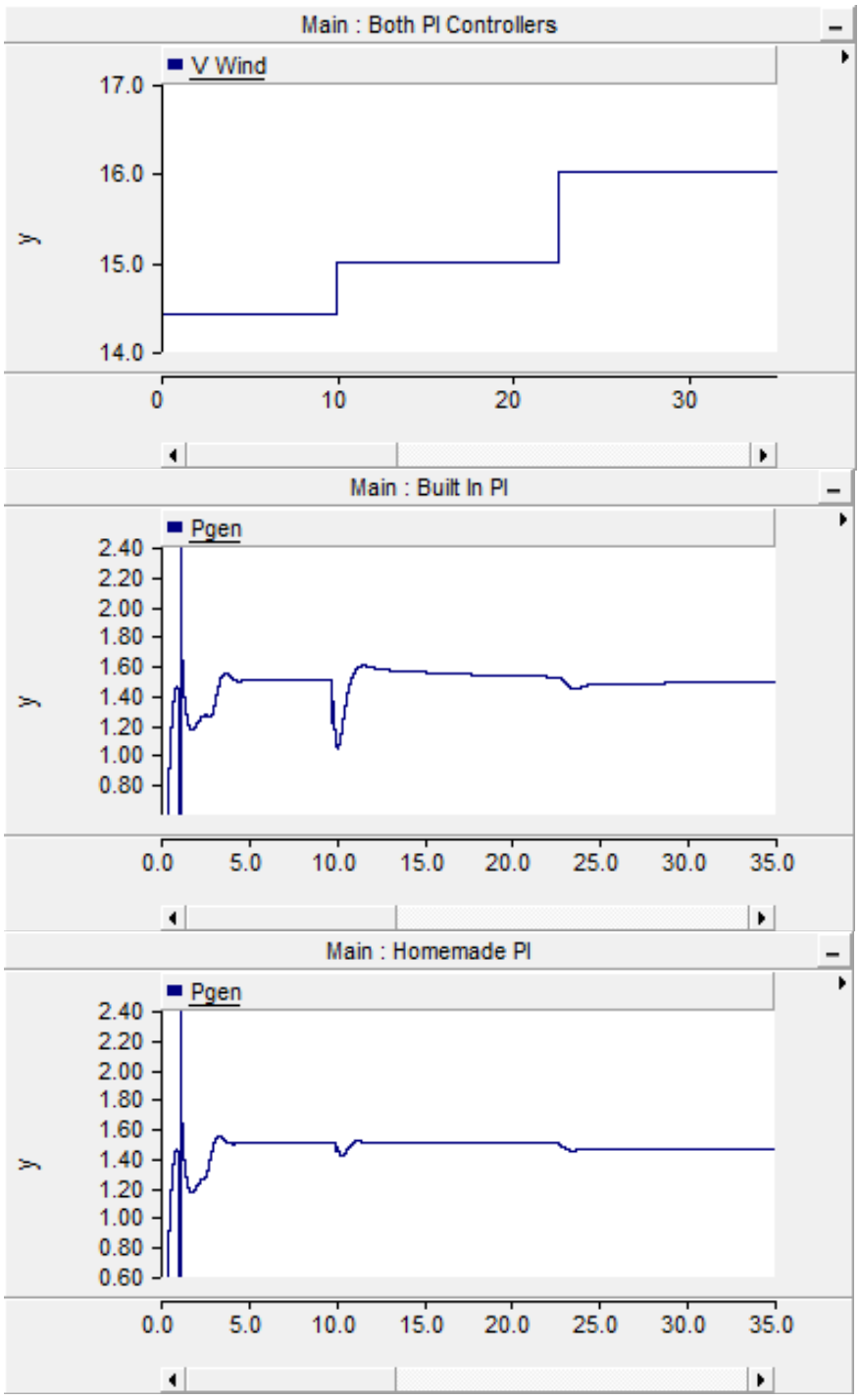

Figure 3.10: The user-defined PI controller shows much better dynamic response than the built-in PI controller to increasing wind speeds.

The top graph, plotting the wind speed in meters per second, illustrates exactly when the wind speed increases. The other plots show the generator power output for the built-in PI function and the user-defined PI function, respectively. The first wind speed jump, from 14.4 to 15 m/s, produced more of a transient spike in both controllers than the second jump, from 15 to 16 m/s. During this transient period, the built-in PI function reached as low as 1.0414 MW and as high as 1.5964 MW before converging back to 1.5 MW, while the user-defined PI reached a low of only 1.4111 MW and a high of 1.5102 MW. Also, note that the user-defined PI function had a reduced convergence time. The user-defined PI function clearly performed better than the built-in PI function and would result in reduced transient stresses, maintenance requirements, and safety concerns.

3.5.2. Steady State Performance Results at all Wind Speeds

Now that the dynamic response of the wind turbine has been characterized, the next task is to look at the steady state performance at all wind speeds from cut-in (6 m/s) to cut-out (20 m/s). For this simulation, the same model is run as before, but this time it is allowed to converge until all output values have reached a steady state. By allowing this convergence, the wind turbine's performance at various wind speeds can be quantified on a macroscopic level. So, the model runs at each wind speed until convergence so the operational parameters can be recorded. Figure 3.11 shows the generator's external rotor resistance at each wind speed. Once the wind speed increases above the rated speed, the controller increases the resistance in order to maintain maximum power output and as the wind speed continues to increase, the resistance also continues to increase.

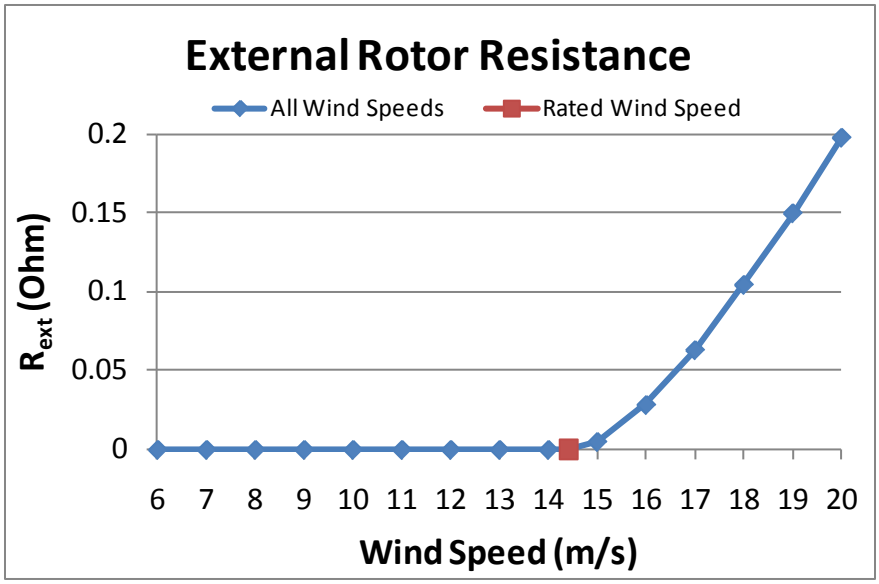

Figure 3.11: At wind speeds above the rated speed the external rotor resistance increases in order to maintain a constant 1.5 MW power output.

As was mentioned before, the effect of increasing the external rotor resistance is an increase in the generator slip, which simply means that the generator rotational speed is accelerating more rapidly away from the generator's synchronous speed. For a 6-pole generator with a rated frequency of 60 Hz, like the one modeled, the synchronous speed is 125.66 rad/s. Figures 3.12 and 3.13 illustrate the direct relationship between the generator slip and rotational speed. Up until the rated wind speed, the slip only increases moderately, while at the high wind speeds the slip increases much more rapidly.

The moderate increases in generator slip at low wind velocities correspond to moderate increases in the generator rotational speed. However, as seen in Figure 3.13, at wind speeds above the rated speed, the generator rotational velocity increases significantly, hence the name variable speed wind turbine.

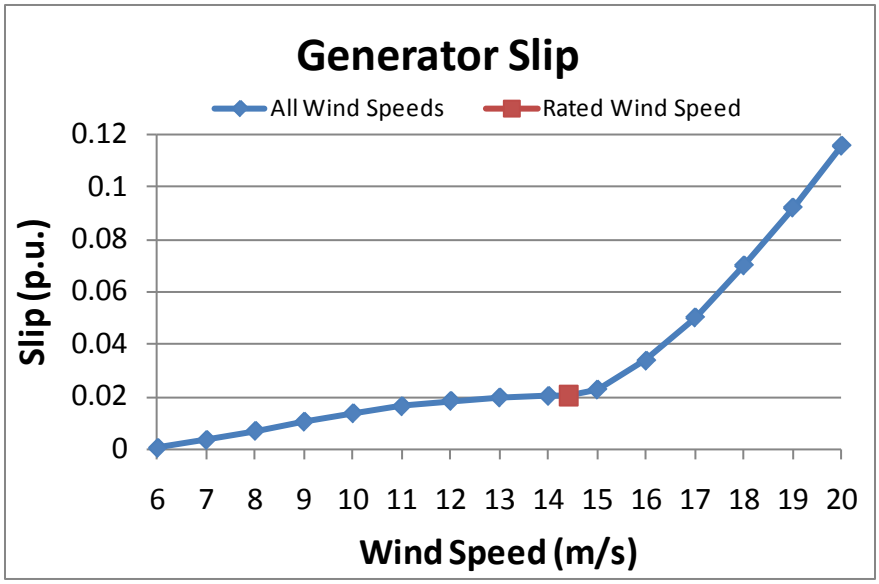

Figure 3.12: Generator slip increases much more significantly as R_{ext} increases.

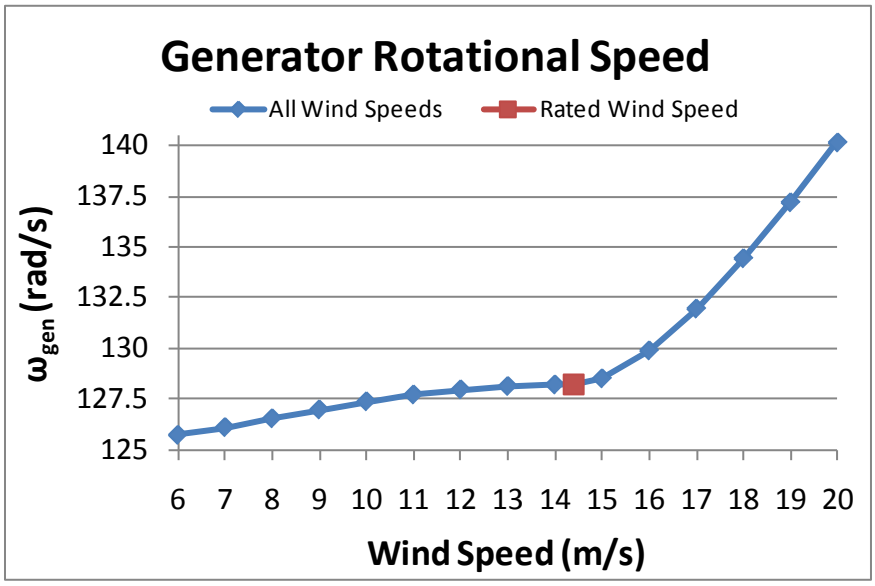

Figure 3.13: The generator rotational speed also increases as R_{ext} increases.

The goal of the resistive control mechanism that allows for the variable generator speed is to maintain maximum power output at all wind speeds above the rated wind

speed. Figure 3.14 shows how this control scheme does in fact maintain a 1.5 MW power output at all wind speeds above 14.4 m/s. At low wind speeds, the power profile acts like that of a fixed speed wind turbine, but after the rated wind speed the generated power is maintained at 1.5 MW. This type of variable speed wind turbine would therefore be better suited than a fixed speed wind turbine for locations where wind speed is consistently above 14 m/s.

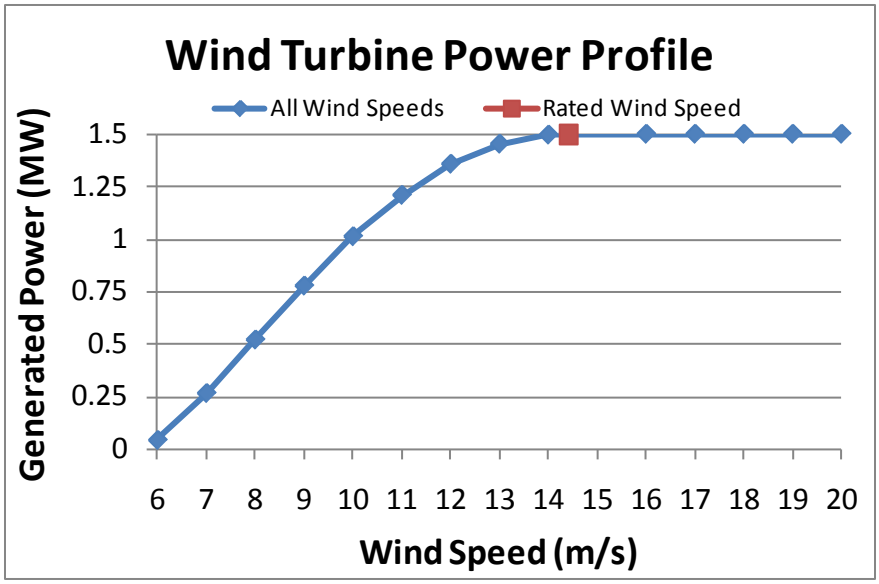

Figure 3.14: The resulting wind turbine power profile shows constant 1.5MW output at all wind speeds greater than the rated wind speed.

However, this control mechanism is not without drawbacks. By increasing the external rotor resistance, the amount of resistive heat losses in the generator circuitry also increases. Figure 3.15 shows the resistive heat losses that are incurred by the resistive control mechanism. Though only fractions of a MW, these losses reach up to 10% of the wind turbine generator output.

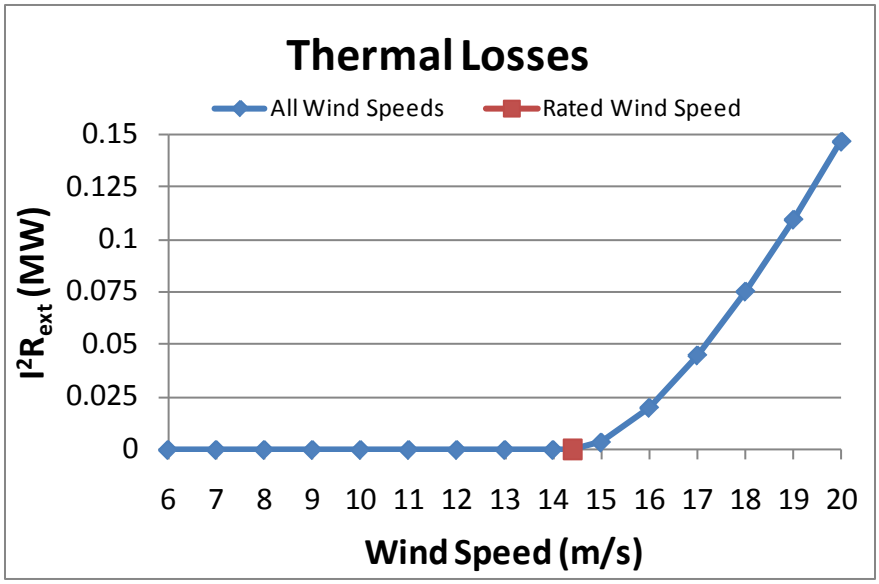

Figure 3.15: Increasing R_{ext} also leads to additional resistive heat energy losses in the wind turbine.

One practical method to reduce the resistive heat losses and avoid any unnecessary maintenance requirements due to build up of heat in the generator circuitry would be to use a dual control scheme that incorporates rotor resistive control with blade pitch control. Since the rotor resistive control reacts quickly, as seen in the dynamic simulation, it can be used to smooth out the short-term wind speed changes. By then incorporating the adjustable blade pitch, which is a much slower process, the rotor resistance can be reduced over the long-term while still maintaining maximum power output. However, the incorporation of the blade pitch control would increase the amount of equipment in the wind turbine nacelle as well as the cost.

Overall, these simulations were able to model the characteristics of a variable-speed wind turbine with constant power rotor resistive control. Through first calibrating the model, by varying the blade pitch angle, the design specifications of blade pitch and wind speed were found that result in a peak desired output of 1.5 MW. Then using the

method of controlling the external rotor resistance, the model was able to maintain the 1.5 MW power generation for all wind speeds between the rated and cut-out speeds. Also, by building a user-defined PI controller, the dynamic response of the control scheme was improved by reducing the magnitude of the initial response and convergence time resulting from changes in wind speed and by reducing fluctuations in the control of the power output.

Chapter 4: Thermodynamic Analysis of the DSWiSS Power System

4.1. Modeling Methodology

A thermodynamic model was created for analyzing the performance of the DSWiSS power generation equipment and for establishing the design specifications of the wind, CAES, CSP, and thermal storage components. This detailed thermodynamic simulation uses first and second law concepts in order to estimate the required energy inputs per unit energy output. Figure 4.1 illustrates that the turbomachinery system is included in this model. The wind and solar components are not yet included in the model, rather, they are considered inputs. From this analysis the power system efficiency and required cooling loads will be calculated.

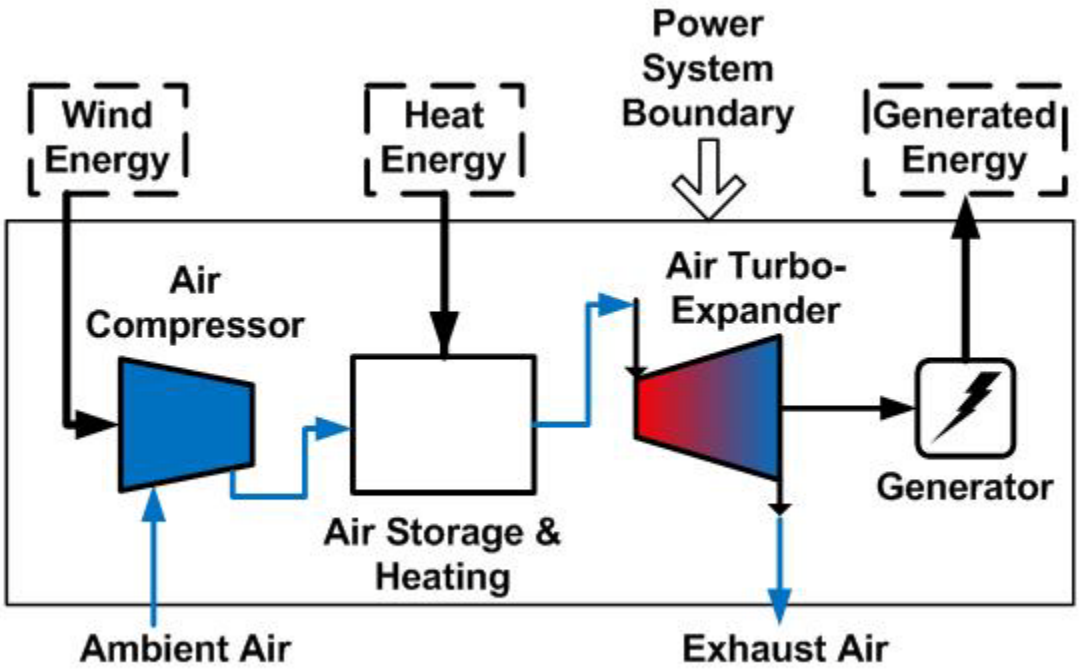

Figure 4.1: The power system energy inflows and outflows are needed to calculate the power generation efficiency.

Please note that the compression and expansion components are actually multistage equipment that is much more complex than shown in this figure. The component details of the McIntosh CAES facility, which are similar to those in DSWiSS, can be seen in Figure 4.2.

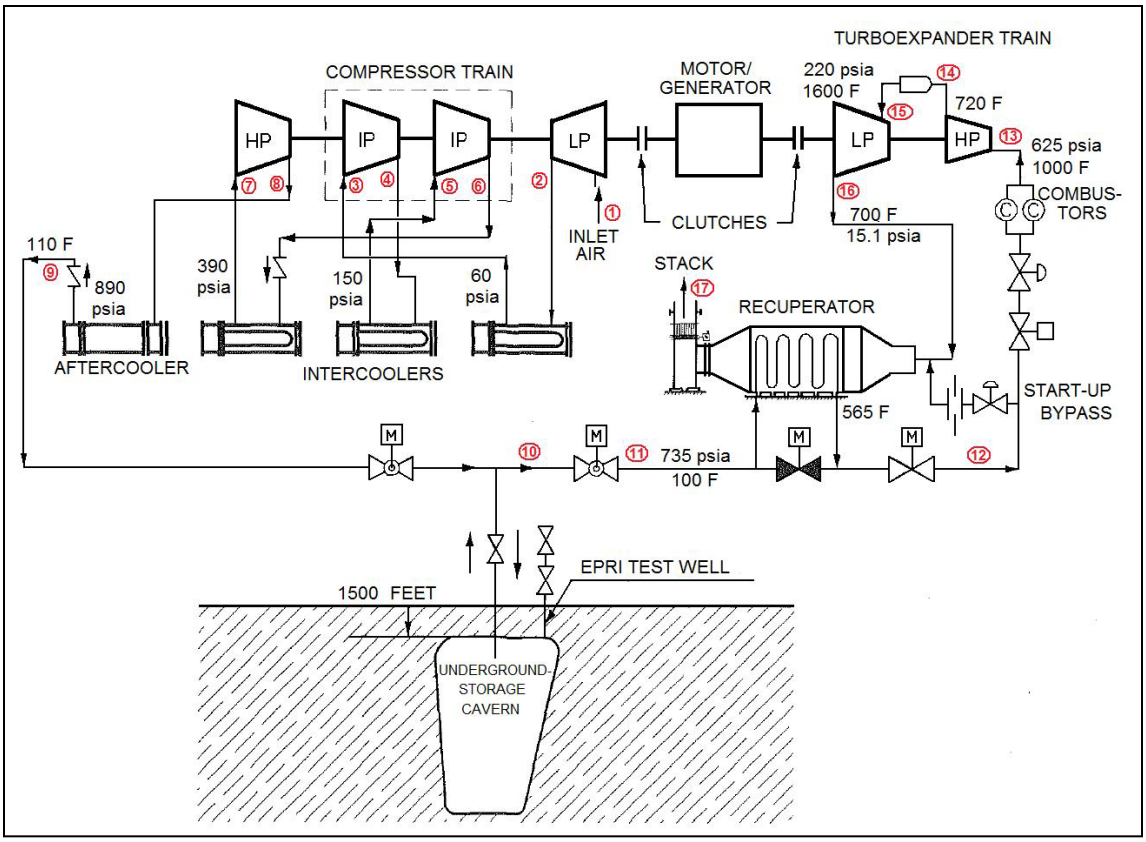

Figure 4.2: The only difference between the component details of the McIntosh CAES facility and the DSWiSS facility is the use of heat exchangers instead of combustors to supply the necessary heat to the air before expansion [26].

The remainder of the model will use the estimated energy inputs to calculate the sizes of the wind, solar, and energy storage components. In order to be consistent, all calculations will be done in SI units. Therefore, even though some of the data gathered are in USCS units, they will be converted into SI units for subsequent use.

4.1.1. McIntosh CAES Facility Data and Assumptions

Since the DSWiSS facility will operate similarly to a typical CAES facility, it was decided that the power generation equipment in the DSWiSS plant would be modeled directly after the turbomachinery at the McIntosh CAES plant. The benefit to using identical turbomachinery for the DSWiSS is that important temperature and pressure data will be available to use in the model, and the number of assumptions made regarding the specific components will be reduced, both of which increase the validity of the model. Tables 4.1 and 4.2 list the basic data available from the McIntosh CAES plant. These data are broken up into two sections: data used directly in the model in Table 4.1, and data used indirectly in Table 4.2 [26].

Table 4.1: These data from the McIntosh CAES facility are used directly in the DSWiSS model.

Parameter	Value	Unit
Inlet Temperature to Cavern	110	°F
Inlet Temperature to Recuperator	100	°F
Inlet Temperature to Turbine 1	1000	°F
Inlet Temperature to Turbine 2	1600	°F
Installed Generator Capacity	100	MW
Air Storage Cavern Maximum Pressure	1150	psia
Air Storage Cavern Minimum Pressure	750	psia

Table 4.2: These data from the McIntosh CAES facility are used indirectly in the DSWiSS model.

Parameter	Value	Unit
Inlet Pressure to Compressor 2	60	psia
Inlet Pressure to Compressor 3	150	psia
Inlet Pressure to Compressor 4	390	psia
Inlet Pressure to Air Storage Cavern	890	psia
Inlet Pressure to Recuperator	735	psia
Inlet Pressure to Turbine 1	625	psia
Inlet Pressure to Turbine 2	220	psia
Outlet Pressure from Turbine 2	15.1	psia

In addition to these data, some basic and detailed assumptions had to be made in order to complete the thermodynamic model. First, the four basic assumptions are: ① kinetic and potential energy effects are negligible, ② all components are well insulated (Adiabatic), ③ air behaves as an ideal gas, and ④ inlet air molal composition is made up of oxygen, nitrogen, carbon dioxide, water vapor, argon, and helium in quantities according to Table 4.3. In addition to these, some specific assumptions are made regarding particular components of the power generation equipment. Table 4.4 lists these assumptions.

Table 4.3: The molal composition of molecular constituents of air by percentage [34].

Constituent	Mole Fraction
Oxygen	20.95
Nitrogen	78.08
Carbon Dioxide	0.03
Water Vapor	0.0
Argon	0.93
Helium	0.01

Table 4.4: These specific assumptions are necessary for the simulation of the power system and were not available from McIntosh data.

Parameter	Value	Unit
Ambient Air Temperature	72	°F
Ambient Air Pressure	14.7	psia
Compressor Isentropic Efficiencies	80	%
Intercooler & Aftercooler Pressure Losses	2	%
Intercooler and Aftercooler Effectiveness	85	%
Heat Exchanger Effectiveness	85	%
Generator Electrical Efficiency	90	%
Motor Electrical Efficiency	90	%
Water Coolant Inlet Temperature	72	°F

Finally, by using the assumptions from Table 4.4 along with the McIntosh pressure data from Table 4.2 the remaining required parameters can be calculated that

will allow the completion of the thermodynamic model. Table 4.5 lists these calculated data.

Table 4.5: The parameters were calculated from the combination of the McIntosh data and assumptions.

Parameter	Value	Unit
Pressure Ratio – Compressor 1	4.16	--
Pressure Ratio – Compressor 2	2.55	--
Pressure Ratio – Compressor 3	2.65	--
Pressure Ratio – Compressor 4	2.33	--
Pressure Ratio – Turbine 1	2.48	--
Pressure Ratio – Turbine 2	14.57	--
Turbine 1 Isentropic Efficiency	89.1	%
Turbine 2 Isentropic Efficiency	87.39	%
Recuperator Effectiveness	76.99	%
Recuperator Pressure Losses	2.65	%
Heat Exchanger Pressure Losses	12.65	%

These parameters make up all the user specified data required to run a complete thermodynamic simulation of the power generation system.

4.1.2. Creation of a Thermodynamic Property Calculator

A thermodynamic property calculator was created for air. The calculator, for any specified temperature, pressure, and molal composition (y_i's) of oxygen, nitrogen, carbon

dioxide, water vapor, argon, and helium, will determine the following properties: mixture molecular weight (M_{mix}), mixture ideal gas constant (R_{mix}), mass fraction of air mixture components (x_i's), specific heats (C_p, C_v, k), mixture enthalpy (h_{mix}), mixture internal energy (u_{mix}), and mixture entropy (s_{mix}).

At the heart of this property calculator is a 7th order polynomial function that calculates the specific heat at constant pressure (C_p) for oxygen, nitrogen, carbon dioxide, and water vapor based on temperature [35]. Equations 4.1 and 4.2 combined with Table 4.6 allow for this calculation.

$$C_{p_i} = A_0 + A_1 \times T_Z + A_2 \times {T_Z}^2 + A_3 \times {T_Z}^3 + A_4 \times {T_Z}^4 + A_5 \times {T_Z}^5 + A_6 \times {T_Z}^6 \tag{4.1}$$

$$T_Z = \frac{T}{1000} \tag{4.2}$$

where C_{p_i} is the specific heat for component i and has units of kJ/(kg·K), T is the temperature in Kelvin and all coefficients A_0 through A_6 for oxygen, nitrogen, carbon dioxide, and water vapor are from Table 4.6.

For the remaining two constituents of air, argon and helium, C_p can be calculated directly using Equation 4.3 since both these gases are monotonic and have a constant specific heat that does not change with temperature.

$$C_{p_i} = \frac{5\bar{R}}{2M_i} \tag{4.3}$$

where $\bar{R}$ is the universal gas constant in kJ/(kmol·K), and M_i is the molecular weight of component i in kg/kmol.

Table 4.6: The coefficients for the polynomial expression of specific heat at constant pressure for selected gases [35].

	O_2	N_2	CO_2	H_2O
A_0	1.006450	1.075132	0.408089	1.937043
A_1	-1.047869	-0.252297	2.027201	-0.967916
A_2	3.729558	0.341859	-2.405549	3.338905
A_3	-4.934172	0.523944	2.039166	-3.652122
A_4	3.284147	-0.888984	-1.163088	2.332470
A_5	-1.095203	0.442621	0.381364	-0.819451
A_6	0.145737	-0.074788	-0.052763	0.118783

Even though these equations only allow for the calculation of C_p for each component individually, a single C_p value can be calculated for any gas mixture of the components by incorporating the mass fractions as is shown in Equation 4.4.

$$C_{p_{mix}} = \sum_i x_i C_{p_i} \tag{4.4}$$

where $C_{p_{mix}}$ is the specific heat of the mixture of gasses and x_i is the mass fraction of component i. However, since the user specified data includes molal fractions and not mass fractions, some initial calculations must be done first in order to determine the given mixture's specific heat. Seen in Equations 4.5, 4.6, and 4.7 are the calculation for the mixture molecular weight (M_{mix}), mixture ideal gas constant (R_{mix}), and mass fractions of gas mixture components (x_i's).

$$M_{mix} = \sum_i y_i M_i \tag{4.5}$$

$$R_{mix} = \frac{\bar{R}}{M_{mix}} \tag{4.6}$$

$$x_i = \frac{y_i M_i}{M_{mix}} \tag{4.7}$$

As noted previously, the gas mixture is air with molal fractions (y_i's) corresponding to Table 4.3. Once these equations are applied the mixture specific heat $C_{p_{mix}}$ can be calculated from Equation 4.4 as well as the specific heat at constant volume (C_v) and the specific heat ratio k as seen in Equations 4.8 and 4.9, respectively.

$$C_{v_{mix}} = C_{p_{mix}} - R_{mix} \tag{4.8}$$

$$k_{mix} = \frac{C_{p_{mix}}}{C_{v_{mix}}} \tag{4.9}$$

The next step in the thermodynamic property calculator is to use the polynomial expression for C_p to calculate enthalpy. Since C_p is a function of temperature only for ideal gases, the enthalpy can be calculated for each constituent (h_i) according to Equation 4.10 then combined for the mixture according to Equation 4.11 [36].

$$h_i = h_{i,ref} + \int_{T_{ref}}^{T} C_{p_i} dT \tag{4.10}$$

$$h_{mix} = \sum_i x_i h_i \tag{4.11}$$

where $h_{i,ref}$ is the reference enthalpy taken at the reference temperature T_{ref}. Reference data will also be required for the calculation of internal energy and enthalpy, all of which will be taken from standard tables. Table 4.7 lists the reference data selected at a reference temperature (T_{ref}) of 0 °C and a reference pressure (P_{ref}) of 1 atm.

Table 4.7: Reference properties for selected gases at T_{ref} = 0 °C and P_{ref} = 1 atm [36].

	Reference Enthalpy (h) [kJ/kg]	**Reference Internal Energy (u) [kJ/kg]**	**Reference Entropy (s°) [kJ/(kg·K)]**
O_2	248.80	177.78	6.3303
N_2	283.99	202.86	6.7494
CO_2	192.15	140.51	4.7857
H_2O	503.22	377.07	10.310

Again, since argon and helium are monotonic gases, their reference values can be calculated directly using Equations 4.12, 4.13, and 4.14.

$$h_{i,ref} = \left(\frac{5}{2}\right)\left(\frac{\bar{R}}{M_i}\right)T_{ref} \tag{4.12}$$

$$u_{i,ref} = \left(\frac{3}{2}\right)\left(\frac{\bar{R}}{M_i}\right)T_{ref} \tag{4.13}$$

$$s^{\circ}_{i,ref} = \left(\frac{5}{2}\right)\left(\frac{\bar{R}}{M_i}\right)ln\left(T_{ref}\right) \tag{4.14}$$

It is important to note that the reference entropy (*s*°) is not a true value of entropy; it is instead defined as only the portion of the entropy that is purely temperature dependent. Unlike enthalpy and internal energy, entropy also depends on the pressure, so an additional term is required. This calculation will be discussed in more detail later in this section when describing how to calculate the entropy for the gas mixture.

The next thermodynamic property to calculate is the internal energy, which is shown in Equation 4.15. Using the definition of enthalpy and the ideal gas law, Equation

4.15 can be used along with Equation 4.16 to calculate the internal energy of the gas mixture in kJ/kg.

$$\left(u_i - u_{i,ref}\right) = \left(h_i - h_{i,ref}\right) - R_i\left(T - T_{ref}\right) \tag{4.15}$$

$$u_{mix} = \sum_i x_i u_i \tag{4.16}$$

where R_i is the gas constant for component i.

The final calculation of the thermodynamic property calculator is for the value of entropy of the gas mixture. The entropy, in kJ/(kg·K), is made up of three terms: the temperature dependent term, $s°$; the pressure dependent term where P is the absolute pressure in kPa; and the mixing term as seen in Equation 4.17.

$$s_{mix} = s° - R_i \times ln\left(\frac{P}{P_{ref}}\right) - R_i \times \sum_i\left(y_i ln(y_i)\right) \tag{4.17}$$

where $s°$ is calculated according to Equations 4.18 and 4.19.

$$s°_i = s°_{i,ref} + \int_{T_{ref}}^{T} C_{p_i} \frac{dT}{T} \tag{4.18}$$

$$s° = \sum_i x_i s°_i \tag{4.19}$$

With this thermodynamic property calculator the critical properties of any gas mixture of oxygen, nitrogen, carbon dioxide, water vapor, argon, and helium given only temperature, pressure, and molal composition can be calculated. All these calculations were programmed using a custom Matlab script that could be used at any point along the power system model to determine specific thermodynamic properties at that particular state. See Appendix B for the detailed Matlab code.

4.1.3. Component Details

As was mentioned earlier, the actual equipment in the power generation system is much more complex than a single compressor and single turbine as was shown in Figure 4.1. The following sections describe in detail the multistage configuration that is modeled in the thermodynamic simulation. Note that all enthalpies expressed in the following sections are in units of kJ/kg.

Compression Subsystem

This subsystem consists of a four-stage train of compressors that utilize intercooling and aftercooling between stages, as seen in Figure 4.3, in order to minimize the required compression work. Through this sequence, outside ambient air is compressed and cooled before being sent to an underground air storage cavern. States 1 through 9 are noted on the Figure.

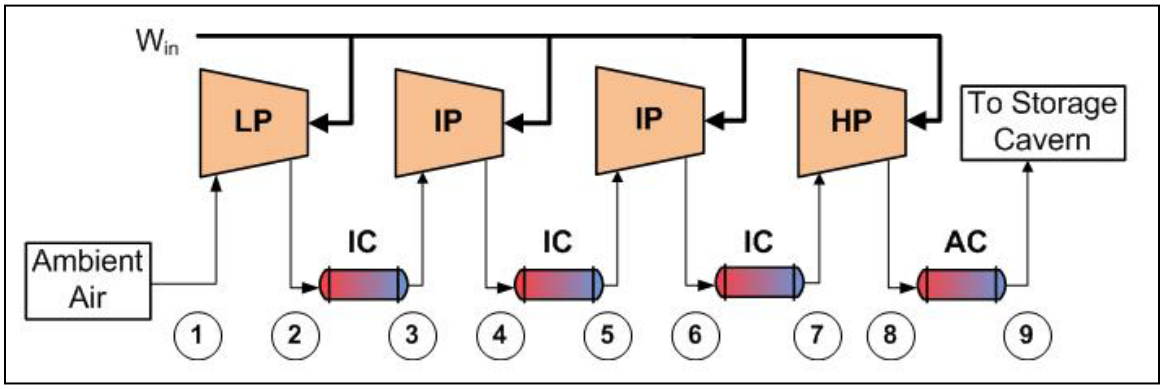

Figure 4.3: The compressor system consists of four stages of compression with three intercoolers and one aftercooler (LP = low pressure, IP = intermediate pressure, HP = high pressure, IC = intercooler, AC = aftercooler). States 1 through 9 are indicated.

Using First Law analysis and the previously listed data, the compression system can be analyzed, beginning at state 1. For each compressor, the exit enthalpy can be determined from Equation 4.20 based on the inlet enthalpy and compressor efficiency.

$$h_{out} = h_{in} + \frac{h_{out,s} - h_{in}}{\eta_c} \tag{4.20}$$

where h_{out} is the actual air exit enthalpy, h_{in} is the air inlet enthalpy, $h_{out,s}$ is the isentropic air exit enthalpy, and η_c is the compressor efficiency. For each cooler the air-side exit enthalpy can be determined with Equation 4.21 based on the air and coolant side inlet enthalpies and the cooler effectiveness.

$$h_{out,air} = h_{in,air} + \varepsilon_{cooler}\left(h_{in,air} - h_{in,air@Tcoolant}\right) \tag{4.21}$$

For Equation 4.21, $h_{out,air}$ is the air-side exit enthalpy, $h_{in,air}$ is the air-side inlet enthalpy, $h_{in,air@Tcoolant}$ is the enthalpy of air at the temperature of the inlet coolant, and ε_{cooler} is the cooler effectiveness, which is defined as the ratio of the actual amount of heat removed versus the maximum amount of heat that could be removed. Equation 4.22 illustrates this ratio.

$$\varepsilon_{cooler} = \frac{q_{removed}}{q_{removed,max}} = \frac{h_{in,air} - h_{out,air}}{h_{in,air} - h_{in,air@Tcoolant}} \tag{4.22}$$

Since all four coolers use water drawn at ambient conditions as the coolant fluid, the property calculator is used at the ambient temperature to calculate $h_{in,air@Tcoolant}$ [36].

Using these calculations, in addition to the compression ratios and pressure losses through the coolers, the temperature and pressure at each state can be determined thereby setting all thermodynamic states 1 through 9. Once all temperatures and pressures have

been found, the required energy per unit mass flow for each compressor can be found according to Equation 4.23.

$$w_c = \frac{\dot{W}_c}{\dot{m}_{air}} = h_{out} - h_{in} \tag{4.23}$$

where w_c is the compressor's specific work, h_{out} is the air exit enthalpy, and h_{in} is the air inlet enthalpy. Each enthalpy value can be calculated using the property calculator, and the compressor train's total specific work can be calculated by simply summing the specific work of all four compressors. Additionally, the cooling load can be found by summing the cooling load of all four coolers, which can each be calculated according to Equation 4.24.

$$q_{removed} = \frac{\dot{Q}_{removed}}{\dot{m}_{air}} = h_{in,air} - h_{out,air} \tag{4.24}$$

where $q_{removed}$ is the cooling load of a particular cooler in kJ/kg, and $h_{in,air}$ and $h_{out,air}$ are the inlet and exit air enthalpies of the particular cooler [36].

Turbine Generator Subsystem

This subsystem consists of a two-stage turbine, primary heater, reheater, recuperator, and generator (not shown). Figure 4.4 illustrates the schematic of the turbo-generator system. As air first exits the cavern it passes through a throttling valve, is heated first by the turbine exhaust in the recuperator and then by the primary heater. Next, after the first turbine stage a reheater increases the air temperature before the second stage turbine. Both the primary heater and reheater are supplied by the solar thermal system. For this model it is assumes that all necessary heat is available in order

for the turbine inlet temperatures to be met. All temperature values in this subsystem were taken from the available McIntosh plant data [26].

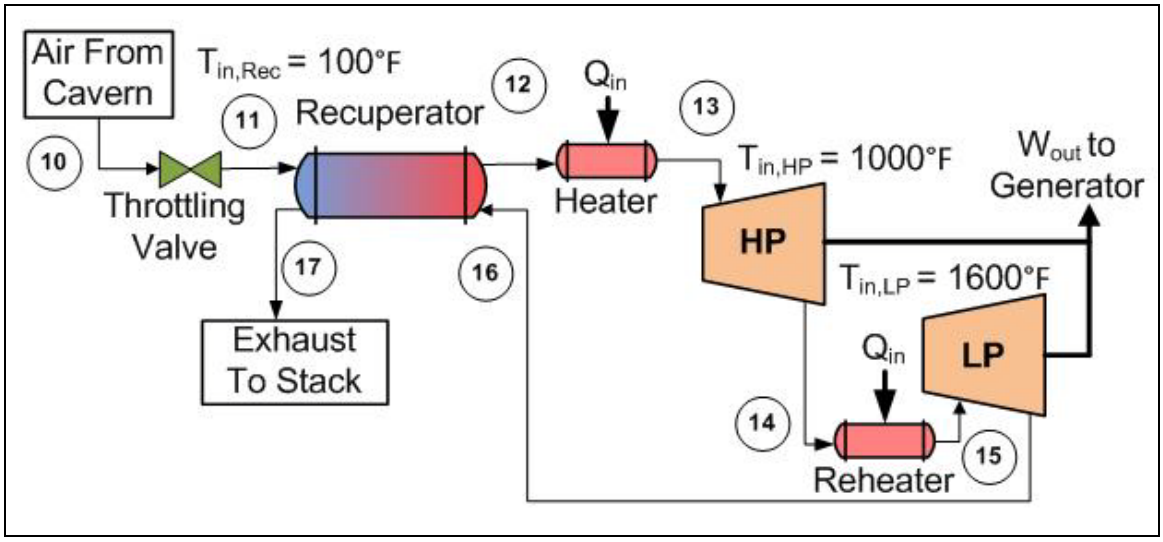

Figure 4.4: The turbine system consists of a two stage turbine with recuperator and reheater (HP = high pressure, LP = low pressure). States 10 through 17 are indicated.

The throttling valve is used in order to ensure a constant pressure into the recuperator. That is why the inlet pressure to the recuperator was listed as a given from the McIntosh CAES plant and will be back-calculated from the given air exit pressure at state 17 using the equipment pressure losses and expansion ratios.

Based on actual performance data from the McIntosh CAES plant, temperature values at the inlet of both turbine stages are known as well as the isentropic efficiencies for both turbines [26]. Note that the inlet to the first stage turbine is 1000°F while the inlet to the second stage turbine is 1600°F. This difference is based on the desire to operate turbine 2 at conditions consistent with a typical gas-fired turbine. Turbine 1 cannot be operated similarly because the inlet pressure is much higher than any typical

gas-fired turbines. In order to work through this system and set all thermodynamic states each turbine is analyzed. The exit enthalpy of the air for each turbine can be calculated with Equation 4.25 based on the inlet enthalpy and turbine isentropic efficiency.

$$h_{out} = h_{in} - \eta_t \left(h_{in} - h_{out,s} \right) \tag{4.25}$$

where h_{out} is the actual air exit enthalpy, h_{in} is the air inlet enthalpy, $h_{out,s}$ is the isentropic air exit enthalpy, and η_t is the turbine isentropic efficiency. By applying this equation to both turbines states 13 through 16 can be set. Next, using the known inlet temperature to the recuperator, Equations 4.26 and 4.27 can be used to calculate the cold-side and hot-side exit enthalpies, respectively.

$$h_{12} = h_{11} + \varepsilon_{recuperator} \ (h_{16} - h_{11}) \tag{4.26}$$

$$h_{17} = h_{16} + (h_{11} - h_{12}) \tag{4.27}$$

For Equations 4.26 and 4.27, each enthalpy refers to the particular state in Figure 4.3 and $\varepsilon_{recuperator}$ is the recuperator effectiveness, which is defined as the ratio of the actual amount of heat transferred from the hot-side to the cold-side versus the maximum amount that could be transferred [36].

Based on these calculations as well as using the turbine pressure ratios and pressure losses through the recuperator, heater, and reheater, the temperature and pressure for each state can be determined, thereby setting the thermodynamic states 11 through 17. Next, the specific energy output for each turbine can be calculated using Equation 4.29.

$$w_t = \frac{\dot{W}_t}{\dot{m}_{air}} = h_{in} - h_{out} \tag{4.29}$$

where w_t is the turbine's specific work output, h_{in} is the inlet air enthalpy, and h_{out} is the exit air enthalpy. Once again, the total specific electrical power output from the turbine-generator system can be calculated by summing the specific work of each turbine and multiplying by the generator's electrical efficiency. Additionally, the total required heat load for the solar thermal and thermal storage subsystem can be calculated from the combination of the heat loads of the heater and reheater, each which can each be found using Equation 4.30.

$$q_{added} = \frac{\dot{Q}_{added}}{\dot{m}_{air}} = h_{out,air} - h_{in,air} \tag{4.30}$$

where q_{added} is the specific heat load of the heater or reheater and $h_{out,air}$ and $h_{in,air}$ are the exit and inlet air enthalpies of the heater or reheater. Knowing this heat load will help when determining the size of the solar thermal and thermal storage subsystems [36].

Air Storage Cavern

The air storage cavern is inherently an unsteady device that requires a separate model to accurately determine thermodynamic conditions during the filling and emptying processes. A few key factors and assumptions are used to simplify the model.

First, the air cavern is assumed to be an infinite heat sink, meaning that any excess heat will be quickly removed from the air stored in the cavern and dispelled to the earth. Additionally, the cavern can also be viewed as an infinite heat source such that anytime the air in the cavern goes below the ground temperature the earth will heat the air until it once again is in equilibrium with the surrounding ground temperature. These two simplifications allow the air stored in the cavern to be considered at a constant temperature; whether filling or emptying, the air in the cavern will be at a constant

temperature equal to that of the ground temperature. For this model, in order to remain consistent with the operation of the McIntosh CAES facility, the ground temperature is assumed to be 100°F, which is equal to the temperature of the air as it exits the cavern [26].

It is also assumed that during the filling and emptying processes, the air storage cavern is a uniform state and uniform flow device. These terms simply means that during filling and emptying the properties are uniform throughout the open system at any instant in time and that the properties at the inlet and exit streams are uniform across their respective streams [36]. This assumption simplifies an otherwise differential form of the energy equation for the filling and emptying processes to those shown in Equations 4.31 and 4.32.

$$m_{in}\,h_{in} = (m_{in} - m_{initial})u_{final} - m_{initial}\,u_{initial} \tag{4.31}$$

$$m_{out}\,h_{out} = m_{initial}\,u_{initial} - (m_{initial} - m_{out})u_{final} \tag{4.32}$$

where m_{in} and m_{out} are the mass flows of air in kg into and out of the cavern during the filling and emptying processes, respectively, h_{in} is the inlet enthalpy during filling, h_{out} is the exit enthalpy during emptying, $m_{initial}$ is the initial mass in the cavern in kg, $u_{initial}$ is the internal energy of the initial mass in the cavern in kJ/kg, and u_{final} is the internal energy of the final mass in the cavern in kJ/kg.

Since the data and assumptions mentioned previously will be used to set the thermodynamic state at the inlet to the air storage cavern as well as the state at the inlet to the recuperator, and since those states will be constant during the compression and expansion operations, respectively, the transient filling and emptying processes will not need to be simulated in order to calculate system performance parameters. What is of

interest is the sizing of the air storage cavern to accommodate the appropriate amount of air needed during the expansion process. For this calculation, the ideal gas law at the charged and discharged states when the cavern pressure is at its maximum and minimum allowable limits can be used. Combining these two applications of the ideal gas law yields a single expression for the cavern volume as shown in Equation 4.33.

$$V_{cavern} = \frac{m_{air,tot} RT}{(P_{max} - P_{min})} \tag{4.33}$$

where V_{cavern} is the required volume of the cavern in m^3, $m_{air,tot}$ is the total mass of air that will be extracted and sent through the turbines when the cavern starts at the maximum level and ends at the minimum level in kg, R is the gas constant for air in kPa·m^3/(kg·K), T is the equilibrium temperature of the air in the cavern in Kelvin, and P_{max} and P_{min} are the maximum and minimum allowable pressures in the air storage cavern in kPa.

Solar Thermal and Thermal Storage Subsystem

This analysis assumes that all the necessary heat input needed from the CSP and thermal storage system is adequately supplied. This assumption means that the CSP system is large enough to supply all necessary heat input as needed to the heaters as well as supply enough additional heat to the thermal storage unit to maintain power generation into any evening hours as may be desired. Additionally, it means that the thermal storage unit will be large enough to store the additional heat necessary for generation after sunset. Future analysis will be done to optimize the time period for generation based on real time data and determine the required sizes of both the CSP and thermal storage units. At this time, the analysis focuses on calculating the amount of heat required per unit air mass

flow as well as estimating the sizes of the CSP and thermal storage units based on an assumed generation time window, which will be discussed more in the following sections.

The calculation for the amount of heat needed to raise the air to the appropriate temperature before going into each turbine was given above in Equation 4.29. By using this calculation for each required turbine inlet temperature then summing the two values, the total required heat input per unit air mass flow can be estimated.

Other parameters that are useful for estimating the sizes of the CSP and thermal storage components are the steady state heat requirement and total daily heat requirement. These values will be discussed in detail and calculated in the following sections.

Component Details Summary and State Table

Table 4.8 below gives a summary of the equipment in the power system and the thermodynamic states associated with the inlet and outlet of each piece of equipment. Additionally, the 1st Law equation that governs each component is also shown.

Table 4.8: Summary of power system components inlet and outlet states and associated equations.

System Component	State		Equation
	Inlet	Outlet	
Compressor 1	1	2	$\omega_{C1} = h_2 - h_1$
Compressor 2	3	4	$\omega_{C2} = h_4 - h_3$
Compressor 3	5	6	$\omega_{C3} = h_6 - h_5$
Compressor 4	7	8	$\omega_{C4} = h_8 - h_7$
Intercooler 1	2	3	$q_{removed1} = h_2 - h_3$
Intercooler 2	4	5	$q_{removed2} = h_4 - h_5$
Intercooler 3	6	7	$q_{removed3} = h_6 - h_7$
Aftercooler	8	9	$q_{removed4} = h_8 - h_9$
Turbine 1	13	14	$\omega_{T1} = h_{13} - h_{14}$
Turbine 2	15	16	$\omega_{T2} = h_{15} - h_{16}$
Heater	12	13	$q_{added1} = h_{13} - h_{12}$
Reheater	14	15	$q_{added2} = h_{15} - h_{14}$
Recuperator (hot side)	11	12	$q_{exchange} = h_{12} - h_{11}$
Recuperator (cold side)	16	17	$q_{exchange} = h_{16} - h_{17}$

4.2. CYCLE ANALYSIS

By following the methodology and calculations detailed in the previous section, performance parameters that will be used to evaluate the DSWiSS concept, such as thermal efficiency, can be estimated. All calculations done to this point are on a per unit air mass flow basis, which is useful, but will be expanded upon in section 4.3 with the addition of a few final assumptions.

4.2.1. Estimating the Power System's Thermodynamic Efficiency

Every thermodynamic state of the power system in DSWiSS has been set based on the compression train and turbine train analysis already described. Now, using the calculated values for total specific compression work $(w_{c,tot})$, total specific turbine work

$(w_{t,tot})$, and total specific heat input requirement of the heater and reheater $(q_{added\ ,tot})$, the thermodynamic efficiency of the DSWiSS power system can be calculated. First, the motor and generator efficiencies must be included to calculate the specific electrical power requirement of the motor to run the compressors and the specific electrical power output of the generator, respectively. Both values will be in kJ/kg as calculated below in Equations 4.34 and 4.35.

$$w_{motor\ ,tot} = \frac{w_{c,tot}}{\eta_{motor}} \tag{4.34}$$

$$w_{gen\ ,tot} = w_{t,tot} \times \eta_{gen} \tag{4.35}$$

For Equations 4.34 and 4.35, η_{motor} and η_{gen} are the efficiencies of the motor and generator, respectively. Once this conversion efficiency is incorporated, the total specific energy input required for DSWiSS $(e_{in,tot})$ in kJ/kg can be calculated, as seen in Equation 4.36.

$$e_{in,tot} = \frac{\dot{E}_{in\ ,tot}}{\dot{m}_{air}} = w_{motor\ ,tot} + q_{added\ ,tot} \tag{4.36}$$

Once this total energy input is known, the fraction of energy that comes from the wind (F_w) and solar (F_s) subsystems can be calculated as well as the thermodynamic efficiency of the entire power system, as seen below in Equations 4.37, 4.38, and 4.39, respectively.

$$F_w = \frac{e_{in\ ,wind}}{e_{in\ ,tot}} = \frac{w_{motor\ \ ,tot}}{e_{in\ ,tot}} \tag{4.37}$$

$$F_s = \frac{e_{in\ ,solar}}{e_{in\ ,tot}} = \frac{q_{added\ \ ,tot}}{e_{in\ ,tot}} \tag{4.38}$$

$$\eta_{PS} = \frac{w_{gen,tot}}{e_{in,tot}} \tag{4.39}$$

4.2.2. Results and Discussion

With the results from the compression train, seen in Table 4.9, the model calculates that the total specific energy requirement for the compressor train's motor is 605.6 kJ per kg of air mass flow through the compressor train. This value is the required electrical load that the wind turbines must supply in order to compress one kg of air to the appropriate pressure.

Next, the output parameters from the turbine train, seen in Table 4.10, are highlighted by the calculation of the total specific heat input requirement of 803.4 kJ per kg of air mass flow through the turbine train and the generator specific power output of 651.6 kJ per kg of air mass flow. The first value, the heater's input requirement, is the amount of heat that the solar thermal and thermal storage system must supply to the air before expansion in order to increase the air temperature to the appropriate inlet condition for each turbine. The second value, the generator's output, is the amount of energy that the turbine train's generator will produce per kg of air flow through the turbine train.

Table 4.9: Results from the compression train quantify the electrical energy input and cooling load required by the DSWiSS turbomachinery.

Compressor Train Output Parameters	
Compressor 1 Specific Work Req (kJ/kg)	185.3
Compressor 2 Specific Work Req (kJ/kg)	123.7
Compressor 3 Specific Work Req (kJ/kg)	127.5
Compressor 4 Specific Work Req (kJ/kg)	108.5
Compressor Total Specific Work Req (kJ/kg)	545.0
Motor Specific Work Req (kJ/kg)	605.6
Intercooler 1 Specific heat removed (kJ/kg)	157.6
Intercooler 2 Specific heat removed (kJ/kg)	128.6
Intercooler 3 Specific heat removed (kJ/kg)	127.7
Intercooler 4 Specific heat removed (kJ/kg)	111.5
Coolers total Specific heat removed (kJ/kg)	525.4

Table 4.10: Results from the turbine train components illustrate the relative quantities of heat energy input and power output.

Turbine Train Output Parameters	
Turbine 1 Specific Work output (kJ/kg)	167.2
Turbine 2 Specific Work output (kJ/kg)	556.8
Turbine Total Specific Work output (kJ/kg)	724.0
Generator Specific Work output (kJ/kg)	651.6
Heater 1 Specific heat Input Req (kJ/kg)	257.6
Heater 2 Specific heat Input Req (kJ/kg)	545.8
Heater Total Specific heat Input Req (kJ/kg)	803.4

Before continuing, it is important to realize that the air flows through the compression train and turbine train are not necessarily equal. Since the compression and expansion processes cannot occur simultaneously, the air flow rates through each will only be the same if they both operate for the same amount of time; for instance if they

each operate 12 hours every day. Although this scenario is a possibility, as will be discussed in the next section, it is unlikely that both processes operate over equal time intervals. The remaining performance parameters that are calculated, seen in Table 4.11, include the overall efficiency of the turbomachinery power system

Table 4.11: The remaining output parameters include the total energy input and power system efficiency.

Other Output Parameters	
Energy Input Total (kJ/kg)	1409
Energy Input % Wind	0.4298
Energy Input % Solar	0.5702
Power System Efficiency	0.4625
Electricity Input per unit Energy Output	0.9294
Heat Input per unit Energy Output	1.2329

The split between the amount of electrical energy and heat energy required is found to be 43% and 57%, respectively. From this result, it is evident that the DSWiSS system utilizes both renewable resources to create dispatchable energy. Also shown in the results are the required quantities of these two energy inputs relative to the amount of energy output from the generator. These values illustrate that the wind turbines must supply just under one unit of energy input per unit of energy generated and the CSP system must supply over 1.2 units of energy input per unit of energy generated, which is consistent with existing CAES systems. Lastly, the model calculates the overall power system's thermal efficiency by taking the ratio of the total power input and total power output, yielding 46.25%. This value is the efficiency of the power system only and does not include the efficiency of the wind turbines or solar thermal system.

In addition to these power and efficiency calculations, the power system process was sketched on *T*-*s* and *P*-*v* diagrams. These diagrams are typical for Brayton and Rankine power systems and provide visual insights to the physical process and performance. Seen below in Figure 4.5 is a *T*-*s* and *P*-*v* diagram for an ideal natural gas Brayton power cycle. In both graphs, the power output can be visualized as the enclosed area. For this ideal cycle, both compression and expansion processes are isentropic and the combustion process occurs at a constant pressure. Real power cycles will not be able to achieve these ideal process results. For the DSWiSS cycle, both compression and expansion will incur an increase in the entropy due to irreversibilities and the heating will incur a pressure drop due to friction as the air passes through the heaters. One other interesting aspect of the ideal cycle diagram is that states 4 and 1 are connected by a solid line, even though the cooling takes place exterior to the physical equipment.

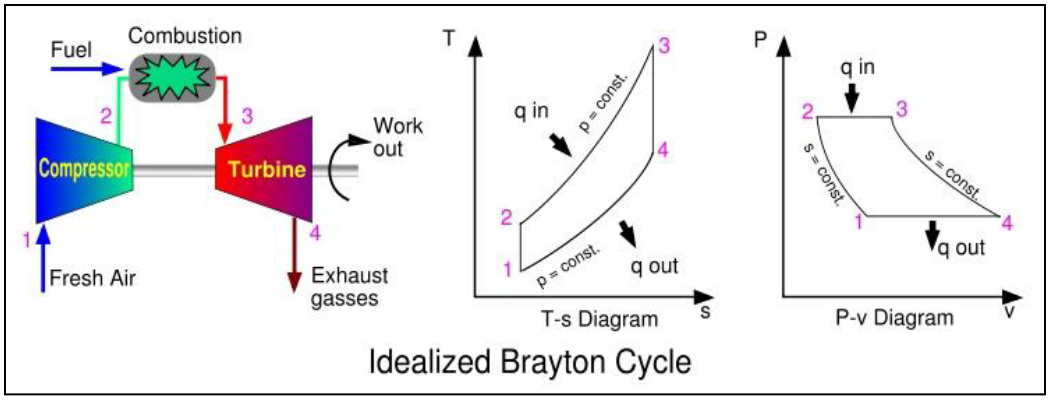

Figure 4.5: For the simple idealized Brayton cycle, the *P*-*v* and *T*-*s* diagrams help to visualize the heat and work transfer taking place during compression, combustion, expansion, and exhaust stages [37].

Using the known thermodynamic properties for states 1 through 17, *T*-*s* and *P*-*v* diagrams were drawn, as seen in Figures 4.6 and 4.7, for the DSWiSS power cycle.

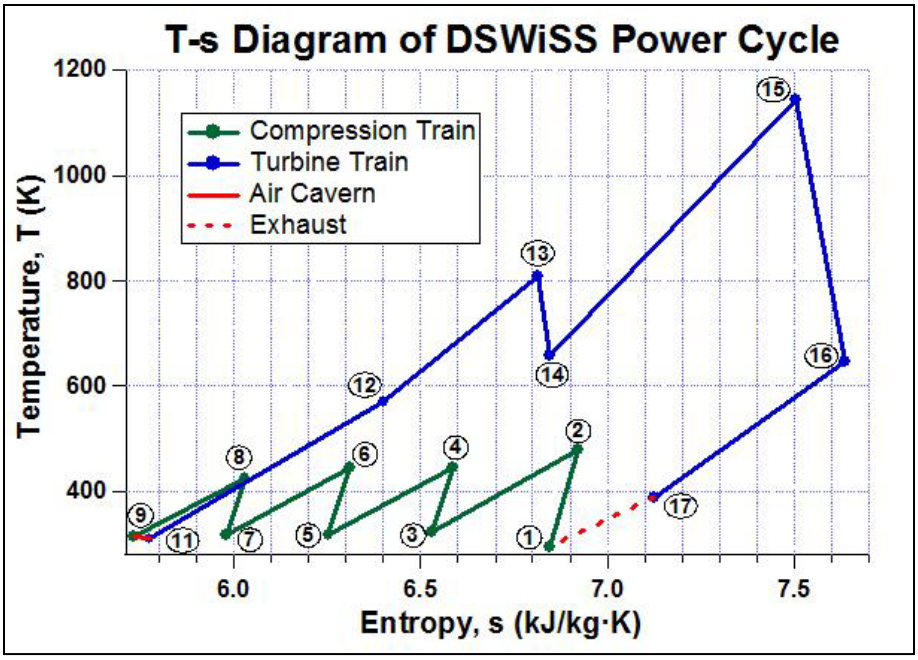

Figure 4.6: Conceptual *T-s* diagram of the DSWiSS cycle illustrates heat transfer.

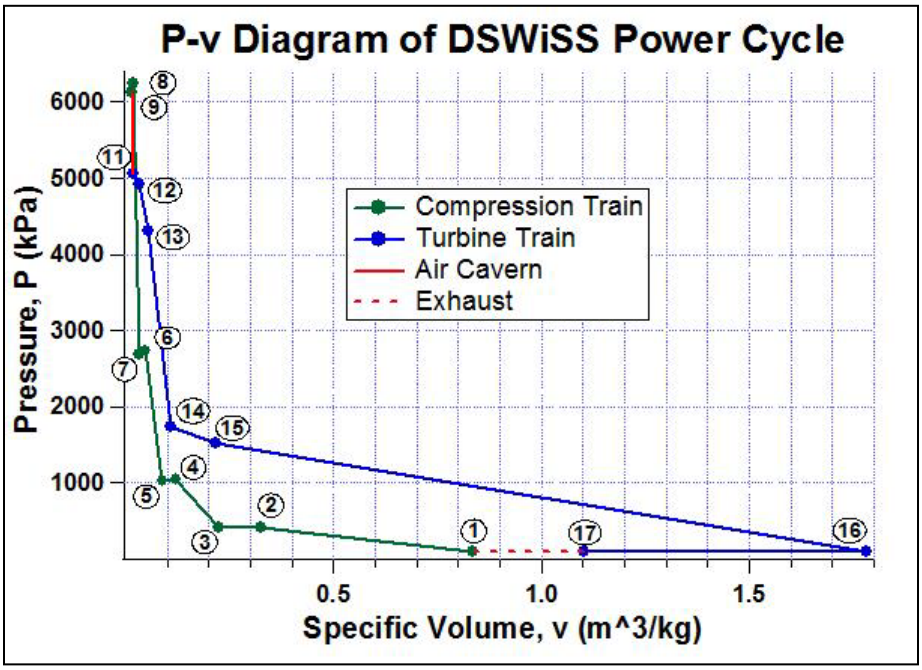

Figure 4.7: Conceptual *P-v* diagram of the DSWiSS cycle illustrates work transfer.

Clearly, the power cycle of DSWiSS is much more complex than that of an ideal Brayton cycle, but there are a few important features noticeable on this graph. First, the separation between the compression and expansion stages is visible by the line connecting states 9 and 11. Since the filling and emptying of the cavern is not a steady process, there is no single path that the air takes to get from state 9 to state 10, and only the presence of the variable throttling valve allows state 11 to be constant. Additionally, the exhaust process, which takes place in the outside atmosphere. is shown as a dashed line connecting states 17 and 1. Unlike the ideal graph, the output power of the turbine cannot be visualized as the enclosed area because the compression work is not supplied by the turbine output, as was the case for Figure 4.5, rather it was supplied by an external source. Instead, the output power can be visualized as the area under the line connecting states 11 through 16 in Figure 4.7, and the area under the line connecting states 11 through 17 in Figure 4.6 can be visualized as the heat exchanged in the heaters and recuperator. The net electrical output to the grid is represented in Figure 4.7 by the area between the line that connects states 1 through 9, which accounts for the grid supplied electricity used during compression, and the line that connects states 11 through 17, which accounts for the electricity supplied to the grid during generation. Also, note in Figure 4.6 that the heating from state 11 to state 12 is from recovered heat in the recuperator, which reduces the amount of heat the solar thermal collector is required to supply.

4.3. Assuming a Rated Output Capacity and Generation Time Window

All calculations done to this point are on a per unit air mass flow basis, which means that no information about the scale of the system and the size of the components

has been incorporated. This section discusses the calculation of various performance parameters including values such as steady state generator power output in MW and total air mass flow per day.

Ideally, determining how the DSWiSS plant will operate over a typical day is one of the goals. Therefore, calculating values such as the steady state air flow rate through the turbine or compressor trains, the steady state electrical energy and heat energy input required to run the compressors and increase the air temperature in the heaters, the total daily air mass flow, and the air storage cavern size is useful. However, in order to calculate these values, two important assumptions must be made:

- The rated output capacity of the generator must be set in order to calculate the steady state air mass flow through the turbine train. For this simulation, this rated capacity is assumed to be 100 MW, which is consistent with the McIntosh CAES facility.
- To calculate daily values, the time period when generation and compression takes place must be set. The turbomachinery at the McIntosh plant uses a common generator/motor so that generation and compression cannot take place simultaneously. To be consistent, it is assumed that generation and compression cannot operate at the same time; in the future, once more specific component selection is done this assumption could be relaxed if it is decided to operate an independent motor and generator. This simulation uses a generation time window of four hours during the peak time period of the day when electricity price is highest. During the generation time period, since compression cannot be occurring, the electricity generated from the wind turbines could also be sold to the grid to increase profits.

4.3.1. Steady State and Daily Parameter Calculations

Based on the specified rated power output, the air mass flow rate through the turbine train can be calculated using Equation 4.40 and 4.41 below.

$$\dot{P}_{t,rated} = \frac{\dot{P}_{gen,rated}}{\eta_{gen}} \tag{4.40}$$

$$\dot{m}_{t,air} = \frac{\dot{P}_{t,rated} \times 1000}{w_{t,tot}} \tag{4.41}$$

where $\dot{m}_{t,air}$ is the turbine air flow rate in kg/s, $\dot{P}_{t,rated}$ is the rated turbine power output in MW, $\dot{P}_{gen,rated}$ is the rated generator power output in MW, η_{gen} is the generator efficiency, and $w_{t,tot}$ is the specific work output of the turbine train in kJ/kg. Next, using the four-hour generation time window a number of important parameters including the total daily air mass flow through the turbine and compressor train, the steady state and daily heat requirement of the heaters, the air flow rate in the compression train, and the steady state and daily electricity requirements of the compression train can be calculated. Equation 4.42 below shows the calculation for the total daily air mass that is compressed, stored underground, and expanded through the turbines.

$$m_{air,tot} = \dot{m}_{t,air} \times t_{gen} \times 3600 \tag{4.42}$$

For Equation 4.42, $m_{air,tot}$ is the daily air mass in kg, t_{gen} is the number of hours generation occurs, and 3600 is the number of seconds per hour. Once the total air mass is calculated, Equation 4.33 can be used to estimate the air storage cavern volume. Additionally, since the total mass that goes through both the compression and turbine trains is the same, and the time window for compression is set as all hours when

generation is not occurring, the air mass flow rate through the compression train required can be calculated, as seen in Equation 4.43.

$$\dot{m}_{c,air} = \frac{m_{air\ ,tot}}{t_{comp} \times 3600} \tag{4.43}$$

where $\dot{m}_{c,air}$ is the air flow rate through the compression train in kg/s, t_{comp} is the time window for compression, in this case 20 hours, and again 3600 is the number of seconds per hour.

The next set of calculations involves the energy inputs of the system. It is important to know what the electrical and heat energy input requirements are as the compression train and turbine train are each operating at their steady state. Now that the air flow rates through both sets of components are known, these two instantaneous power values can be calculated. Equations 4.44 and 4.45 are for the steady state electrical power requirement of the motor that runs the compressors ($\dot{W}_{motor\ ,ss}$) and the steady state heat power requirement of the heaters that increase the air temperature during generation ($\dot{Q}_{added\ ,ss}$), respectively.

$$\dot{W}_{motor\ ,ss} = \frac{w_{motor\ ,tot} \times \dot{m}_{c,air}}{1000} \tag{4.44}$$

$$\dot{Q}_{added\ ,ss} = \frac{q_{added\ ,tot} \times \dot{m}_{t,air}}{1000} \tag{4.45}$$

where both $w_{motor\ ,tot}$ and $q_{added\ ,tot}$ are in kJ/kg and the division by 1000 is simply a unit conversion from kW to MW. Similarly, in order to get a better understanding of scale, the daily electrical power requirement of the motor that runs the compressors ($\dot{W}_{motor\ ,daily}$) and the daily heat power requirement of the heaters ($\dot{Q}_{added\ ,daily}$) are calculated, as seen in Equations 4.46 and 4.47.

$$\dot{W}_{motor\ ,daily} = \dot{W}_{motor\ ,ss} \times t_{gen} \tag{4.46}$$

$$\dot{Q}_{added\ ,daily} = \dot{Q}_{added\ ,ss} \times t_{comp} \tag{4.47}$$

where both values are in MWh. Lastly, as it was noted in the compressor details section, it is important that the amount of cooling needed during the multiple stages of the compression train be estimated. Since the air flow rate through the compressors is now known, the steady state cooling load that reduces the air temperature in the intercoolers and aftercooler can be calculated, as seen in Equation 4.48.

$$\dot{Q}_{removed\ ,ss} = \frac{q_{removed\ ,tot} \times \dot{m}_{c,air}}{1000} \tag{4.48}$$

where $\dot{Q}_{removed\ ,ss}$ is the steady state cooling load in MW, $q_{removed\ ,tot}$ is the specific cooling load of the three intercoolers and aftercooler combined in kJ/kg, and the division by 1000 is again a unit conversion factor.

4.3.2. Results and Discussion

The output from these equations will give a better idea of component sizes and daily operation. Seen in Table 4.12 are the results for the compressor train.

Table 4.12: Steady state and daily results for the compression train.

Compressor Train Output Parameters	
Compressor Air Flow Rate (kg/s)	30.7
Compressor Steady State Work Req (MW)	16.7
Motor Steady State Work Req (MW)	18.6
Motor Daily Work Req (MWh)	371.7

First, the steady state motor work requirement is found to be 18.6 MW. This value represents the electrical capacity that is required from the wind turbines at every instant that compression is operating. Interestingly enough, most wind farms are much larger than 18.6 MW, and it would seem that this value may indicate that the rated output capacity of the DSWiSS could be increased. Also note that the air flow rate through the compression train is just over 30 kg per second and that the total daily electrical requirement from the wind turbines is 371.7 MWh.

Similar results for the turbine train are shown in Table 4.13. The air flow rate through this section is 153.5 kg per second, much higher than that of the compression train. This difference is a result of the distinctive operational times for each set of components. Both systems must compress and expand the same amount of air each day but the compression operates over 20 hours while the expansion must occur over only 4 hours. Hence, the turbine train air flow rate and steady state power output are much higher than those of the compressor train.

Table 4.13: Steady state and daily results for the turbine train.

Turbine Train Output Parameters	
Turbine Air Flow Rate (kg/s)	153.5
Turbines Steady State Work output (MW)	111.1
Generator Steady State Work output (MW)	100.0
Heaters Steady State heat Input Req (MW)	123.3
Heaters Daily heat Input Req (MWh)	493.2

The steady state heat requirement is calculated to be 123.3 MW, also much higher than the steady state electrical requirement. This result is important because it means that

the CSP and thermal storage system will need to be sized and designed to provide a larger amount of power during generation operation than that of the wind turbines during compression. That doesn't mean the CSP and thermal storage system will need to be much larger than the wind turbine system, but because the generation process occurs over a short period, the CSP system will have to store heat during periods when generation is not occurring. Overall the daily heat requirement is found to be just under 500 MWh, not much more than the 371 MWh from the wind turbines, which again illustrates that both wind and solar resource are being almost evenly utilized in the DSWiSS power system to create dispatchable power.

The last few output parameters from the model, seen in Table 4.14, are the total daily air mass flow and cavern size. Based on the assumptions of a generation capacity of 100 MW and a generation time of four hours, the total daily air mass is calculated to be over 2.2 million kilograms, or 2436 short tons; in order to store this much air a cavern approximately 500,000 cubic meters, or 17.6 million cubic feet, would be required.

Table 4.14: Total daily air flow and cavern size results.

Other Output Parameters	
Total Daily Air Flow (kg)	2,209,900
Total Daily Air Flow (short tons)	2,436
Cavern Volume (m^3)	499,420
Cavern Volume (ft^3)	17,637,000

4.4. CONCLUSIONS

The use of a thermodynamic model of the DSWiSS power cycle has allowed the calculation of important performance information. The power system thermal efficiency

was found to be a little less than 50%, which is comparable to other power generation technologies. A better understanding of the size of the wind and solar components has been gained through the assumption of a rated generation capacity and generation time period. The selection of a four hour generation period results in higher steady state requirements of air flow and power input for the turbine train than that of the compressor train. Additionally, the system has been shown to use both wind and solar resources fairly equally in order to generate dispatchable power.

Detail of the various Matlab files used to develop the thermodynamic model can be seen in Appendix C. The primary program, named DREEM for dispatchable renewable electrical energy model, contains many subprograms such as the turbine model that calculated the exit enthalpy of either of the turbines. In total nine m-files were needed to complete the simulation including the property calculator.

Chapter 5: Economic Analysis of the DSWiSS Power System

5.1. Modeling Methodology

In order to be utilized in today's electricity market, this renewable energy system will have to compete from an economic standpoint with coal, nuclear, and natural gas power plants. In other words, the electricity price required by this system in order to cover all expenses needs to be on the same order as that of the current generation technologies.

In order to make this economic comparison a levelized lifetime cost approach was adopted. This method takes into account all capital, operation and maintenance, and fuel costs. The result is a busbar cost that does not include transmission or distribution costs. To start, all costs must be estimated and adjusted to a common year basis; in this case costs are calculated at the 2008 price level. In order to adjust the capital costs, the Construction Cost Trends of the United States Bureau of Reclamation was used to update the capital costs of various power generation options to a common date [38].

To adjust any other cost values, a discount rate must be chosen. For this report a 5% discount rate was selected. This value is consistent with the International Energy Agency's (IEA) Energy Technologies Perspectives 2006 report [39]. This discount rate takes into account the time value of money and will be used to convert any capital cost listed in a year after 2008 and all operation and maintenance costs to 2008 dollars, as well as to annualize the overnight capital costs in order to calculate the plants' levelized cost of electricity (*LCOE*).

However, calculating the *LCOE* for this integrated energy system will not be as easy as it would be for a typical wind only or CSP only system. In the latter cases, all that is needed is an estimate of the capital expenditures (*CAPEX*) and the operational and

maintenance expenditures (*OPEX*), along with appropriate values for the discount rate (d), technical lifetime (N), and plant capacity factor (CF). With these values a per MWh generated amount can be calculated for both the *CAPEX* and *OPEX* by using Equations 5.1 and 5.2. Once calculated, these costs would simply be added together to equal the *LCOE*, as seen in Equation 5.3. For DSWiSS, these calculations, as well as others will have to be done for each individual subsystem. Additionally, since the fuel for wind and solar technologies comes from a free renewable resource, there is no fuel cost.

$$CAPEX\left[\frac{\$}{MWh}\right] = \left\{\frac{CAPEX\left[\frac{\$}{kW}\right] \times d \times (1+d)^N}{((1+d)^N - 1)}\right\} \times \left\{\frac{\left(1000\left[\frac{kW}{MW}\right]\right)}{8760\left[\frac{hr}{yr}\right] \times (CF)}\right\} \quad (5.1)$$

$$OPEX\left[\frac{\$}{MWh}\right] = Usually\ quoted\ in\ \frac{\$}{MWh} \quad (5.2)$$

$$LCOE\left[\frac{\$}{MWh}\right] = CAPEX\left[\frac{\$}{MWh}\right] + OPEX\left[\frac{\$}{MWh}\right] \quad (5.3)$$

In most references, the *OPEX* is already listed in dollar per MWh form, which is what is desired. Just to be clear, this unit is dollars per MWh generated. However, the *CAPEX* is nearly always given in the form dollar per kW, which is dollars per kW installed capacity. In Equation 5.1 the first factor in $\{brackets\}$ annualizes this initial investment over the technical lifetime of the plant (N) using the already specified discount rate (d). Then the second factor converts from a per kW installed capacity value to a per MWh generated annually value by using two conversion factors (kW per MW and hr per yr) and the plant's capacity factor (CF).

In the case of DSWiSS, these types of calculations can be used independently for the wind and solar thermal sections, but costs of the CAES system and thermal storage system will need to be incorporated. Furthermore, since both the wind and solar thermal

sections provide a unique amount of energy, in MWh, per unit of output energy from the DSWiSS generator, the energy requirement ratios for the wind and solar thermal subsystems that were found in the thermodynamic analysis must also be included. Using these values will allow the calculation of each subsystem's cost per MWh of generator production and the combination of these costs into an overall *LCOE* for DSWiSS.

5.2. Evaluation of Each Subsystem's CAPEX and OPEX Costs

The following section details the literature search and evaluation for accurate values of the *CAPEX* and *OPEX* costs for each of the major subsystems.

5.2.1. Determining Costs for Wind and Solar Thermal Systems

Table 5.1 and Table 5.2 list the values that were found for *CAPEX* and *OPEX* costs for various wind and solar plants. Notice that any solar plant type listed with a superscript 1 includes the cost of thermal storage. The fact that some of the references estimate the cost of thermal storage along with the solar thermal system will be very helpful.

Table 5.1: *CAPEX* costs for wind and solar in 2008 dollars [39-44][1].

Plant Type	CAPEX [$/kw installed]	Capacity Factor [%]	Ref
Wind Onshore	929	32	[40]
Wind	1604	33	[41]
Wind	1223		[39]
Wind	1223		[42]
Solar Thermal	2517	15	[40]
Solar Parabolic Trough	2722	32.6	[43]
Solar Power Tower[1]	3804	35.6	[43]
Concentrating Solar	2327		[39]
Solar Parabolic Trough[1]	4013	56.2	[44]
Solar Power Tower[1]	4180	73	[44]

Table 5.2: *OPEX* costs for wind and solar in 2008 dollars [40, 41, 43, 44].

Plant Type	OPEX [$/MWh generated]	Capacity Factor [%]	Ref
Wind Onshore	8.7	32	[40]
Wind	10.5	33	[41]
Solar Thermal	34.5	15	[40]
Solar Parabolic Trough	14.6	32.6	[43]
Solar Power Tower[1]	18.6	35.6	[43]
Solar Parabolic Trough[1]	16.3	56.2	[44]
Solar Power Tower[1]	13.9	73	[44]

Comparing all the costs associated with wind facilities, the values from the Energy Efficiency and Renewable Energy (EERE) report are based on a broad yet specific data set. The average capital expenditures of 14 different wind projects installed in Texas between 2004 and 2007 is $1604 per kW, and the average operation and maintenance costs for 19 wind farms with a capacity of over 50 MW is $1604 per kW [41]. Since these costs apply to specific regions and are averages over many wind farms,

[1] Includes the costs of thermal storage

these values are selected as representative of what the wind component of the DSWiSS system will cost.

For the solar thermal components, three of the listed values for both the *CAPEX* and *OPEX* include the cost of a molten salt thermal storage system. This addition is very helpful, even though the specific type of thermal storage that will be used for DSWiSS has not been chosen yet. As a first estimate, it is assumed that these costs are of the same magnitude. At this point, it is also undecided whether a parabolic trough or a power tower design will be used for the CSP system. However, all three of the *CAPEX* costs for the solar thermal systems that include thermal storage are in a close range. Their average is approximately $4000 /kW, so that is selected as a representative *CAPEX* for all solar thermal systems. Unfortunately the estimated *OPEX* costs for these three systems are not as uniform. Because the report by Sargent and Lundy is more recent and is very detailed in its explanation of how it estimated costs, these data are selected as representative costs for the two solar thermal technologies [44]. Seen in Table 5.3 are the final values selected for *CAPEX* and *OPEX* costs for a wind power plant and both solar thermal plants including thermal storage. Capacity factors have also been included thus far along with the estimated cost values from every source that gave an estimate of the capacity factor.

Table 5.3: Selected *CAPEX* and *OPEX* costs for wind and solar thermal plants [41, 44].

Plant Type	CAPEX [$/kw installed]	OPEX [$/MWh generated]	Capacity Factor [%]	Ref
Wind	1604	10.5	33	[41]
Solar Parabolic Trough[1]	4000	16.3	56	[44]
Solar Power Tower[1]	4000	13.9	73	[44]

Lastly, a technical lifetime of 20 years is selected for all three technologies. This value is consistent with the Sargent and Lundy report on solar [44] and with the IEA report with respect to wind [40]. Again, it is important to note that all costs for the solar thermal technologies include the costs for thermal storage.

Now, by adding the *CAPEX* and *OPEX* (both in $/MWh) based on Equation 5.3, the *LCOE* for all these plant types can be estimated. Table 5.4 shows that the wind plant is overall the least expensive, and that a power tower design is more economical than a parabolic trough design. These values represent the price that would need to be charged for the electricity coming from such a plant in order for the plant owners to cover all expenses.

Table 5.4: Estimated *LCOE* for wind and solar thermal facilities.

Plant Type	LCOE [$/MWh]
Wind	55.0
Solar Parabolic Trough[1]	81.5
Solar Power Tower[1]	64.1

5.2.2. Determining Costs for CAES System

Even though costs for the wind, solar thermal, and thermal storage systems have been estimated, there has been no incorporation of the cost for the air compression system, air storage cavern, or the turbine-generator system. These components are integral to the operation and integration of the various subsystems in DSWiSS, and could compose a significant portion of the overall cost of the plant.

The cost estimates that were found next are for an entire CAES system, including all compressors, turbines, generators, recuperators, and storage caverns. So, these cost

estimates cover all remaining components of DSWiSS. Table 5.5 lists these *LCOE* values. Since the report by the RIDGE Energy Storage consultant group [25] was more recent and more thorough than the Lower Colorado River Authority's (LCRA) report [45] there was more confidence given to the $9.09 /MWh value. As a result, a final value of $10.5 /MWh was selected.

Table 5.5: Estimated *LCOE* for CAES [25, 45].

Component	LCOE [$/MWh]	Ref
CAES System 1	9.1	[25]
CAES System 2	14.5	[45]
Selected CAES System	10.5	

5.3. CALCULATION OF SYSTEM *LCOE* FOR VARIOUS SCENARIOS

The values used previously for calculating the *LCOE* for both solar thermal systems were based on per MWh of electricity output. So, in essence these values accounted for the conversion of the solar heat energy to electrical energy. In order to get an accurate cost estimate of the thermal system per MWh of heat energy this conversion will need to be reversed since it is heat that the solar thermal components are providing. In order to do this reversal, the turbine cycle efficiency was found for both designs from the Sargent and Lundy report [44]. These efficiencies represent the ratio of the amount of electrical energy generated per amount of heat energy supplied for each solar thermal system. Using these values, 40% and 41.4% for the parabolic trough and power tower, respectively, a finalized list of *LCOE* values for each subsystem is generated, as seen in Table 5.6.

Table 5.6: Finalized *LCOE* for all systems

System	LCOE [$/MWh]
Wind	55.0
Solar Parabolic Trough with Thermal Storage	32.6
Solar Power Tower with Thermal Storage	26.3
CAES System	10.5

Each *LCOE* is given in dollars per MWh, but these do not refer to the same MWh. The wind system is in dollars per MWh of electricity supplied from the wind turbines to the motor that drives the compressors. The solar thermal systems are in dollars per MWh of heat supplied to the air before entering the turbine. And the CAES system is in dollars per MWh of electricity sent to the grid from the entire integrated DSWiSS facility.

The last step before calculating the entire system's *LCOE* is to incorporate the energy requirement ratios for the wind and solar subsystems. Shown previously in Table 4.11, these values, incorporated in Equation 5.4, allow the conversion of each subsystems cost to a basis of dollars per MWh of generator output; note that the *LCOE* for the CAES system is already in terms of dollars per MWh of generator output.

$$LCOE = LCOE_{Wind} \times \left(\frac{MWh_{req}}{MWh_{gen}}\right)_{Wind} + LCOE_{Solar} \times \left(\frac{MWh_{req}}{MWh_{gen}}\right)_{Solar} + LCOE_{CAES} \quad (5.4)$$

Seen in Table 5.7 are two complete system *LCOE* values based on the different solar thermal technologies. Not only is the power tower design less expensive, it also allows for higher turbine inlet temperatures and has been successfully demonstrated with thermal storage. So, from this point on, only the power tower design is considered.

Table 5.7: Estimated *LCOE* for the DSWiSS using two different solar thermal technologies.

Plant Design	LCOE [$/MWh]
DSWiSS with Power Tower	94.1
DSWiSS with Parabolic Trough	101.8

5.4. Comparison to Other Generation Methods

In the U.S., coal, natural gas and nuclear plants are the majority providers of electricity. In 2006 these three combined to generate over 88% of all electricity consumed in the U.S. [4]. Based on data from the Electric Power Research Institute (EPRI), Figure 5.1 illustrates the relationship of the *LCOE* for all these types of facilities as well as a stand-alone wind farm and solar thermal trough facility to that of DSWiSS [46].

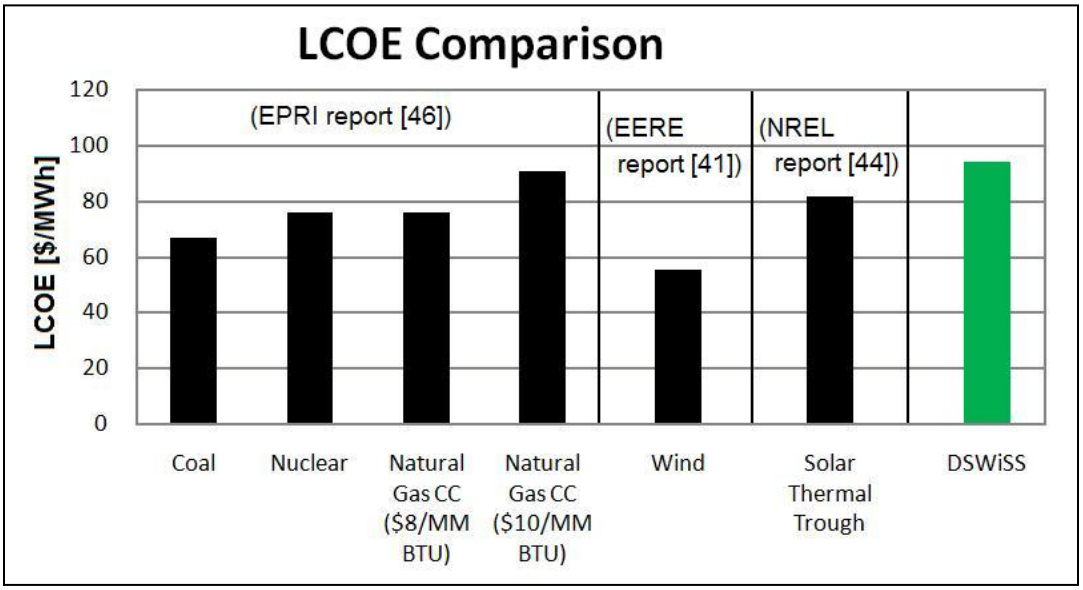

Figure 5.1: LCOE for DSWiSS is competitive with that of current generation technologies [41, 44, 46].

All of these plant types have a *LCOE* less than that of DSWiSS, but not much less. When looking trough reports that estimate the *LCOE* for various generation technologies, results were surprisingly variable. It was difficult to determine what a reasonable *LCOE* for a given technology should be. Therefore, in the previous figure, the *LCOE* values for the fossil fuel plants were selected from the EPRI report because it estimated all four values in a similar manner. However, comparison to the stand-alone wind and solar is not straightforward because it is unknown where all these values were arrived at through equivalent methods. Looking at the fossil fuel plants, two of the typical generation types, coal and nuclear are the least expensive at around 67 and 76 dollars per MWh, respectively. Two *LCOE* values for a natural gas power plant are represented based on two different fuel prices, which are both actually higher than the current cost of natural gas which is around 4.5 dollars per MMBTU. The *LCOE* for a stand-alone wind turbine facility with no energy storage method is actually fairly inexpensive, and the *LCOE* for a stand-alone solar thermal trough plant is in the higher ranges. Additionally, based on personal correspondence with eSolar, a company working to produce utility-scale power tower type solar thermal plants, the *LCOE* for their power tower design is around 120-160 dollars per MWh, which is also much higher than any of the *LCOE*'s listed so far. Furthermore, there are other additional benefits that have not been incorporated into this cost comparison that will favor the DSWiSS facility. First, the fuel price for a coal or natural gas plant makes up a significant portion of the overall costs. These fuel prices are subject to change, particularly the price of natural gas. Based on data used from the Texas Interactive Power Simulator (TIPS), an analytical tool developed by a UT graduate student, the cost of fuel for a natural gas plant can account for up to 70% of the total overall cost of the plant [47], and as can be seen from Figure

5.2, the historical price paid for natural gas by the electric power sector has been rising and falling significantly in recent history [48].

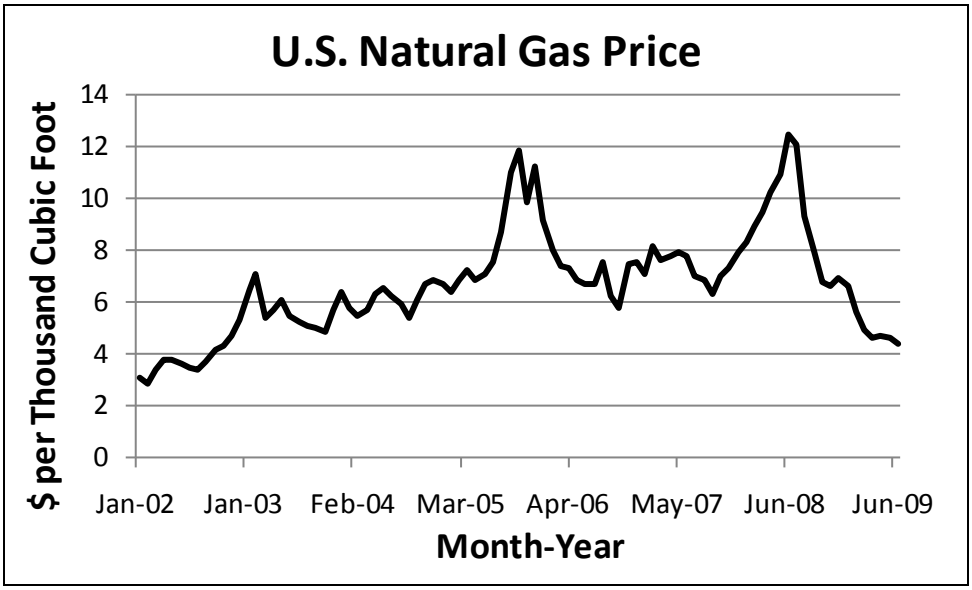

Figure 5.2: Historical U.S. natural gas price for the electric power sector shows significant fluctuations [48].

In addition to this fuel cost variability, it is widely anticipated that the U.S. government will adopt a carbon cap and trade system in order to create market incentives for the reduction of carbon emissions. It is unknown exactly what will be implemented, but it is expected that whatever legislation is passed will increase the cost of coal and natural gas power plants.

5.5. CONCLUSIONS

The final *LCOE* value calculated for DSWiSS is very encouraging. Even though this system is projected to be slightly more expensive than typical generation facilities, it is within a competitive range. Additionally, the DSWiSS facility will be dispatchable

and able to quickly ramp up or down to provide valuable load-balancing power, a claim that only natural gas and hydroelectric power plants can currently make.

Chapter 6: Summary of Conclusions and Recommendations

Through this analysis, the thermodynamic performance and cost of energy production from an integrated system consisting of wind and solar energy systems coupled to compressed air and thermal energy storage have been estimated. The combination of these components resulted in a power system efficiency of over 46% and energy requirements equivalent to those of current CAES facilities. The integrated system is also found to be slightly more expensive on a dollar per MWh generated basis than some of the current technologies employed around the world today, namely coal, nuclear, and natural gas at a low fuel price, but competitive with others such as stand-alone solar facilities and natural gas facilities at a high fuel price.

Even though the DSWiSS system was found to have higher expenses, there are many cost externalities that were not taken into account. These include rising fuel costs, fuel cost volatility, global warming, energy independence, national security, resource depletion, and the uncertainty over the future cost of emissions. In addition to these issues, the government has sought to encourage the development of wind and solar energy systems by providing among others a renewable electricity production tax credit, clean renewable energy bonds, and renewable energy production incentives, which were not included in this analysis. These government programs have been vital to the swift increase in wind development, and will continue to aid by improving the profitability of renewable energy technologies. Overall, this economic analysis will not be complete until cost values can be placed on some of these externalities associated with power generation.

Recently, much success has been made in the wind energy industry, particularly in Texas. This proposed wind-solar-storage system would be another step toward

meeting our increasing energy needs. And by providing this energy from systems that receive all necessary energy inputs through renewable sources with no fuel costs, it would also be a step toward a more environmentally friendly future. Such a facility would be able to store and generate energy when needed, overcoming current issues with intermittency and providing energy supplier like ERCOT with another form of reliable energy that they can count on during peak load periods.

This analysis is the beginning of a much more detailed thermo-economic investigation of this energy system's performance and profitability. Soon, real time data will be incorporated including area specific wind velocity along with wind turbine power profiles, local solar insolation, real time electricity pricing, and local daily temperature variation. It is evident that system optimization will be needed in order to determine the operation scenario of maximum profit. Optimization parameters such as time interval of energy production, wind turbine energy split between compression versus direct selling, and time duration of thermal storage heating will all need to be considered to in order to determine the most profitable design. More in depth analysis will also be done to determine optimum operating parameters that in this report were assumed equal to those of the McIntosh CAES facility. Sensitivity analysis will also be needed to discover the effect these parameters have on system performance and cost. Finally, specific selection of components will be done including design of the solar thermal and thermal storage subsystems.

Appendix A: Wind Turbine Model Code in PSCAD/EMTDC

A.1. Wind Turbine Model with Built-In PI Controller

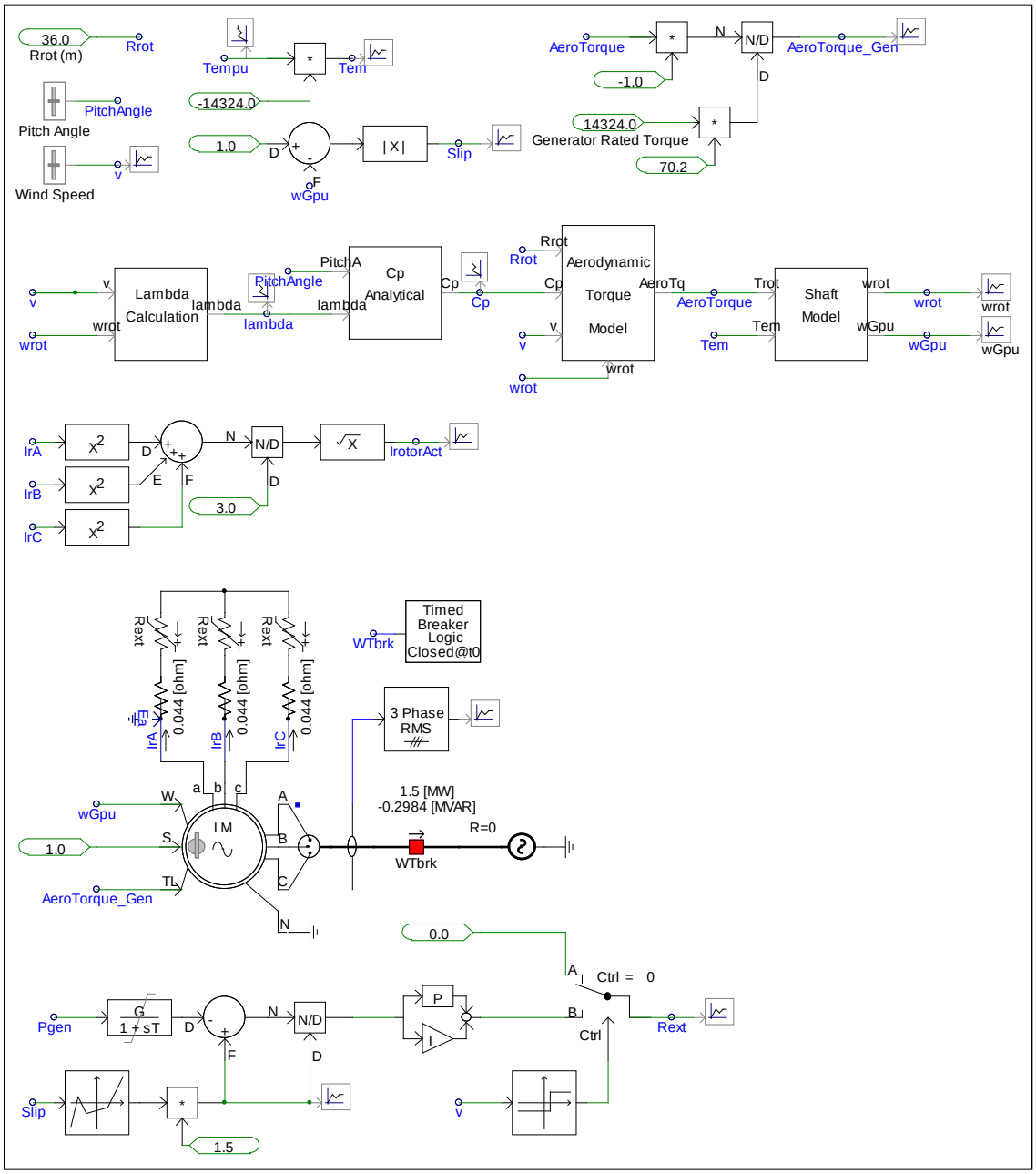

A.2. WIND TURBINE MODEL WITH USER-DEFINED PI CONTROLLER

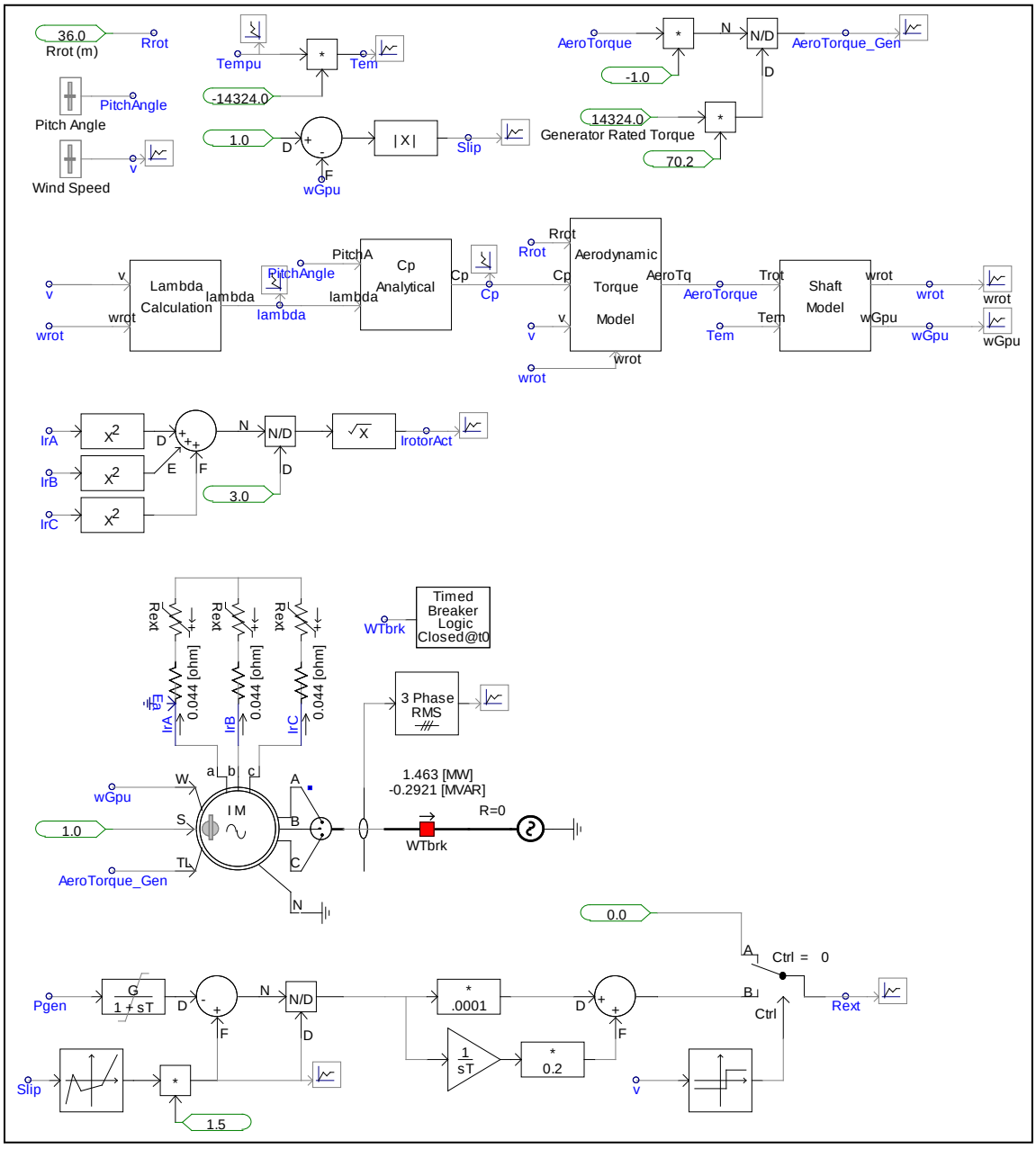

A.3. TIP SPEED RATIO CALCULATION

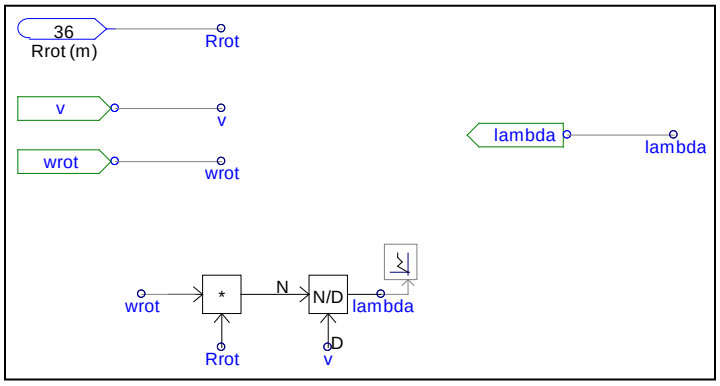

A.4. COEFFICIENT OF PERFORMANCE CALCULATION

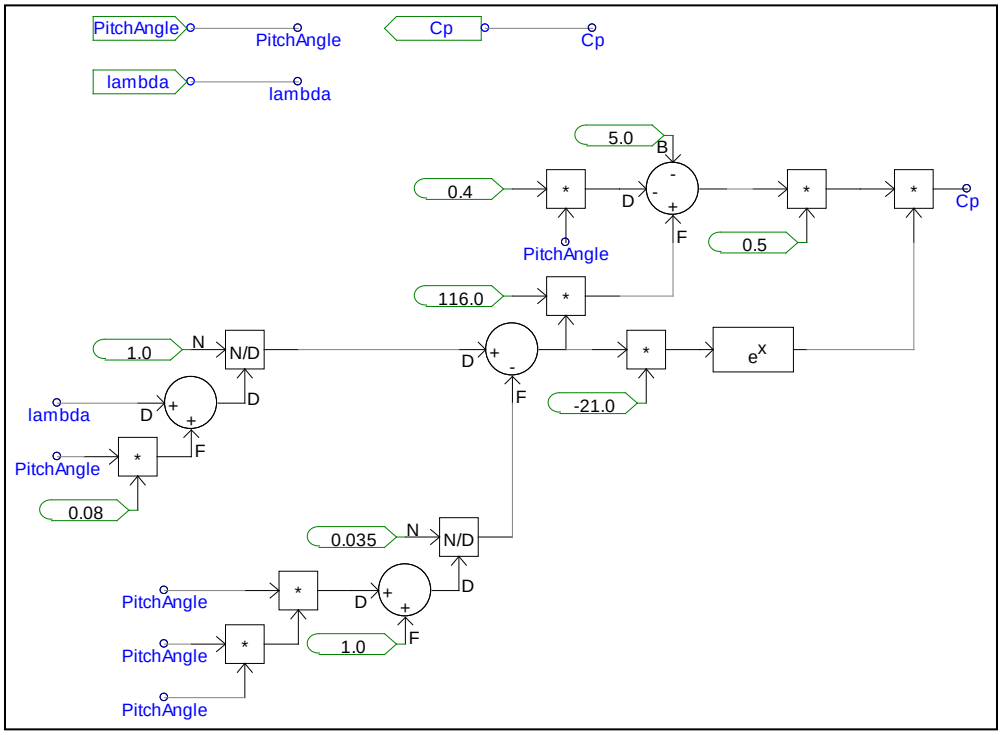

A.5. AERODYNAMIC TORQUE CALCULATION

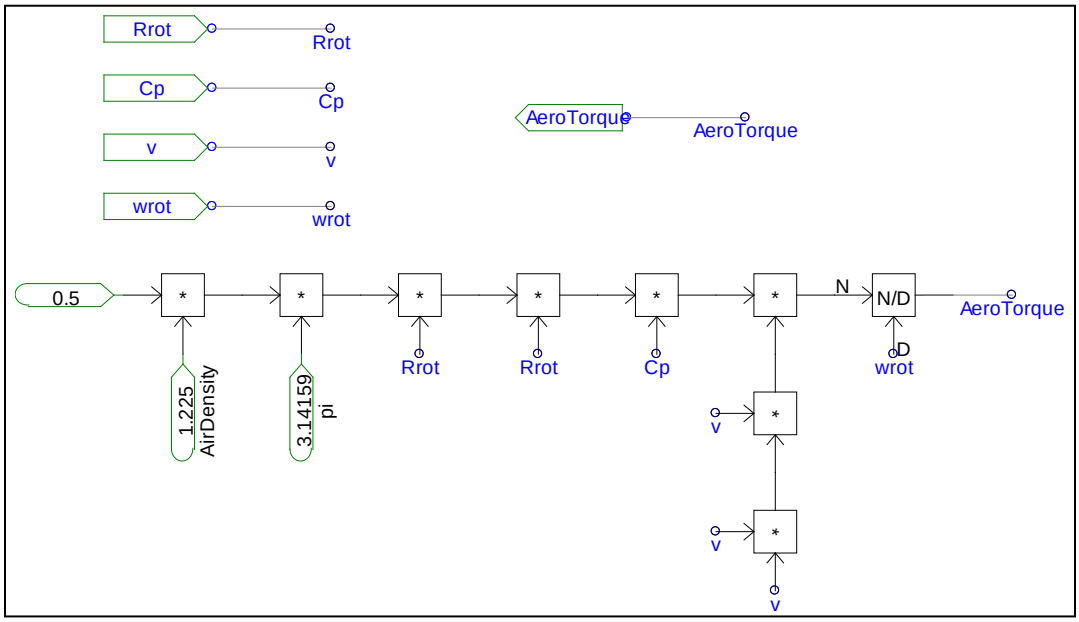

A.6. TWO-MASS SHAFT MODEL

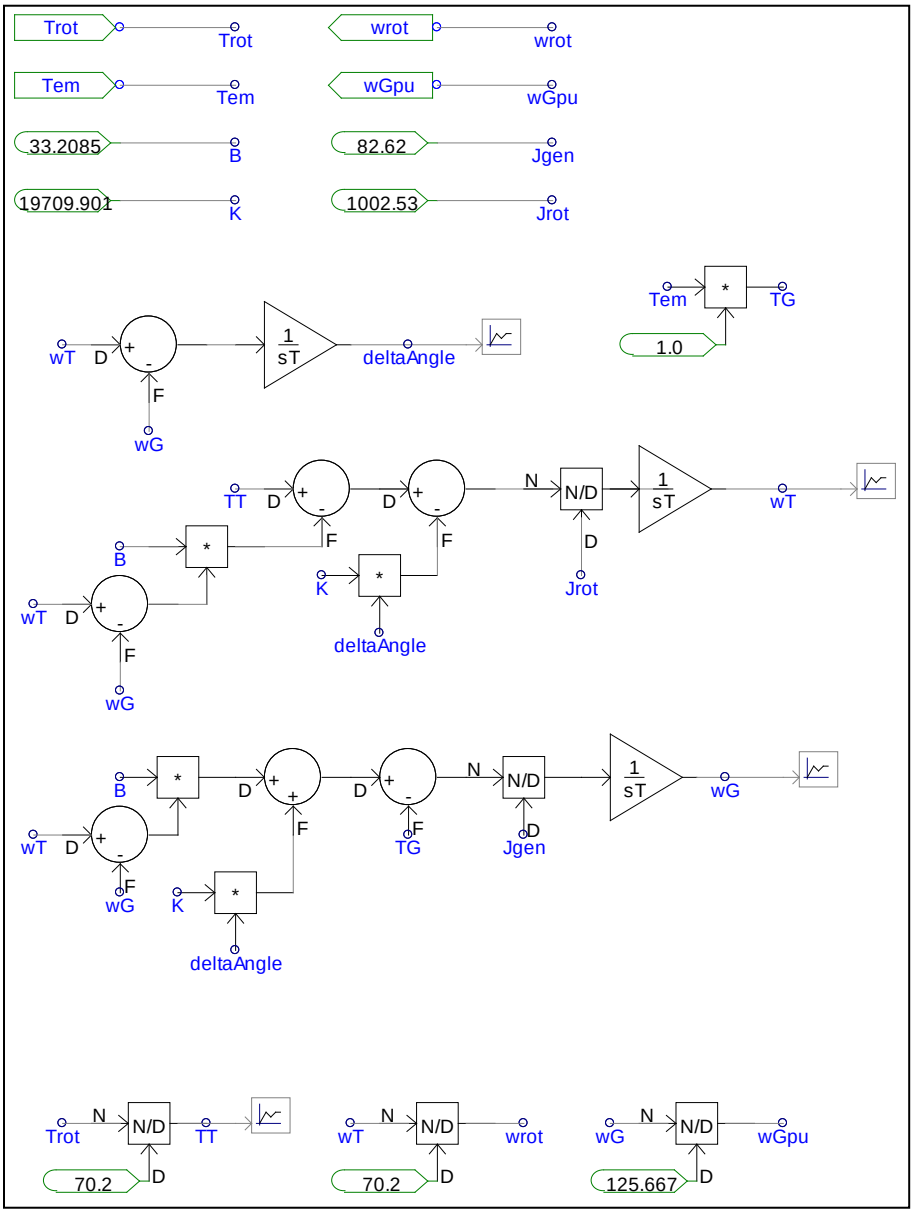

Appendix B:

B.1. AirPropCalcMass.m

```
function[Mmix,R,cp,cv,k,h,u,s,h_,u_,s_]=AirPropCalcMass(yO2,yN2,yCO2,yH
2O,yAr,yHe,P,T)

%{
%input y ----------------------------------------------------------------
yO2=    .2095;
yN2=    .7808;
yCO2=   .0003;
yH2O=   0.0;
yAr=    0.0093;
yHe=    0.0001;
%P & T ------------------------------------------------------------------
P=      4309.2;    %kPa
T=      810.93;        %K
%}

%Molarity input ---------------------------------------------------------
MO2=32.00;                                              %kg/kmol
MN2=28.02;                                              %kg/kmol
MCO2=44.01;                                             %kg/kmol
MH2O=18.02;                                             %kg/kmol
MAr=39.948;                                             %kg/kmol
MHe=4.003;                                              %kg/kmol

%R_ ---------------------------------------------------------------------
R_=8.31441;  %kJ/kmol*K

%reference values-------------------------------------------------------
Tref=273;                                               %K
Pref=101.325;                                           %kPa
TZ=T/1000;
TZref=Tref/1000;                                        %K

%h (kJ/kmol)
hO2_ref=248.80;                                         %kJ/kg
hN2_ref=283.99;                                         %kJ/kg
hCO2_ref=192.15;                                        %kJ/kg
hH2O_ref=503.22;                                        %kJ/kg
```

```
hAr_ref=5/2*R_/MAr*Tref;                                    %kJ/kg
hHe_ref=5/2*R_/MHe*Tref;                                    %kJ/kg

href=[hO2_ref;hN2_ref;hCO2_ref;hH2O_ref;hAr_ref;hHe_ref];  %kJ/kg

%u (kJ/kmol)
uO2_ref=177.78;                                             %kJ/kg
uN2_ref=202.86;                                             %kJ/kg
uCO2_ref=140.51;                                            %kJ/kg
uH2O_ref=377.07;                                            %kJ/kg
uAr_ref=3/2*R_/MAr*Tref;                                    %kJ/kg
uHe_ref=3/2*R_/MHe*Tref;                                    %kJ/kg

uref=[uO2_ref;uN2_ref;uCO2_ref;uH2O_ref;uAr_ref;uHe_ref];  %kJ/kg

%s_not (kJ/kmol.K)
sO2_ref=6.3303;                                             %kJ/kg*K
sN2_ref=6.7494;                                             %kJ/kg*K
sCO2_ref=4.7857;                                            %kJ/kg*K
sH2O_ref=10.310;                                            %kJ/kg*K
sAr_ref=5/2*R_/MAr*log(Tref);                               %kJ/kg*K
sHe_ref=5/2*R_/MHe*log(Tref);                               %kJ/kg*K

sref=[sO2_ref;sN2_ref;sCO2_ref;sH2O_ref;sAr_ref;sHe_ref];  %kJ/kg*K

% Calculate M mix, R, ------------------------------------------------
M=[MO2;MN2;MCO2;MH2O;MAr;MHe];                              %kg/kmol
y=[yO2, yN2, yCO2, yH2O, yAr, yHe];
Mmix=y*M;                                                   %kg/kmol
R=R_/Mmix;                                                  %kJ/kg*K
x=y.*M'/Mmix;

% Coefficients for polynomial function of Cp(mass) based on T ---------
% From 'Gas Turbine Performance' by Philip Walsh and Paul Fletcher ----
%   Dry air    O2         N2         CO2        H2O       Ar
He
A=[ 0.992313,  1.006450,  1.075132,  0.408089,  1.937043, 5/2*R_/MAr,
5/2*R_/MHe;
    0.236688, -1.047869, -0.252297,  2.027201, -0.967916, 0,
0;
   -1.852148,  3.729558,  0.341859, -2.405549,  3.338905, 0,
0;
    6.083152, -4.934172,  0.523944,  2.039166, -3.652122, 0,
0;
```

```
   -8.893933,  3.284147, -0.888984, -1.163088,  2.332470, 0,
0;
    7.097112, -1.095203,  0.442621,  0.381364, -0.819451, 0,
0;
   -3.234725,  0.145737, -0.074788, -0.052763,  0.118783, 0,
0;
    0.794571,  0,         0,         0,         0,        0,
0;
   -0.081873,  0,         0,         0,         0,        0,
0;
    0.422178,  0.369790,  0.443041,  0.366740,  2.860773, 0,
0;
    0.001053,  0.000491,  0.0012622, 0.001736, -0.000219, 0,
0];
cpc=A(1:7,2:7)';

% Calculate Cp mix, Cv mix, k mix (all mass units)---------------------
TZ_=[1; TZ; TZ^2; TZ^3; TZ^4; TZ^5; TZ^6];
%cp kJ/kg*K
cp=x*cpc*TZ_;
%cv kJ/kg*K
cv=cp-R;
%k
k=cp./cv;

% Calculate all mixture properties-------------------------------------

%enthalpy---------------------------------------
Tbar=  [   (TZ-TZref);
           (TZ^2-TZref^2)/2;
           (TZ^3-TZref^3)/3;
           (TZ^4-TZref^4)/4;
           (TZ^5-TZref^5)/5;
           (TZ^6-TZref^6)/6;
           (TZ^7-TZref^7)/7]*1000;
%h kJ/kg (mass)
h=x*href+x*(cpc*Tbar);
%h_ kJ/kmol (molar)
h_=y*(Mmix*href)+y*(Mmix*cpc*Tbar);
h_2=Mmix*h;

%internal energy-------------------------------
%u kJ/kg (mass)
u=x*(uref)+(h-x*href)-R*(T-Tref);
%u_ kJ/kmol (molar)
```

```
u_=y*(Mmix*uref)+(h_2-y*(Mmix*href))-R_*(T-Tref);
u_2=Mmix*u;

%entropy---------------------------------------
Ts=         [   log(TZ/TZref);
                TZ-TZref;
                (TZ^2-TZref^2)/2;
                (TZ^3-TZref^3)/3;
                (TZ^4-TZref^4)/4;
                (TZ^5-TZref^5)/5;
                (TZ^6-TZref^6)/6];
%s_o Term --> kJ/(kg*K)
s_o =(x*(sref))+((x*cpc)*Ts);
%Pressure Term
s_press = R*log(P/Pref);
%Mixing Term
s_mix = 0;
for j = 1:6
    if y(j) == 0;
    else
        s_mix = s_mix + R*y(j)*log(y(j));
    end
end

%s kJ/kg*K (mass)
s = s_o - s_press - s_mix;
%s kJ/kmol*K (molar)
s_=(y*Mmix*sref)+y*(Mmix*cpc*Ts)-R_*log(P/Pref)-Mmix*s_mix;
s_2 = Mmix*s;
```

Appendix C:

C.1. DREEM.M

```
%Jared Garrison - DREEM (Dispatchable Renewable Electrical Energy
Model)
%Master's Thesis work
%
clear all

% User specified data-----------------------------------------------------

%Baseline air inlet conditions in English Units (_e tail on variable)
P0_e = 14.7; % in psi
T0_e = 72 + 459.67; % in degrees Rankine
ALT_e = 2385; % Altitude in feet
%Baseline air inlet conditions in SI Units (_si tail on variable)
P0_si = P0_e*6.8948; % in kPa
T0_si = T0_e/1.8; % in Kelvin
ALT_si = ALT_e/3.2808; % Altitude in Meters

%RH0 = 0; % Relative Humidity Fraction

%Inlet Air Composition Molal Fractions (should sum to 1)
yO2=    .2095;
yN2=    .7808;
yCO2=   .0003;
yH2O=   0.0;
yAr=    0.0093;
yHe=    0.0001;

%Input Design Parameters
rpC1 = 4.16;    % Compressor 1 Pressure Ratio of 4.16
rpC2 = 2.55;    % Compressor 2 Pressure Ratio of 2.55
rpC3 = 2.65;    % Compressor 3 Pressure Ratio of 2.65
rpC4 = 2.33;    % Compressor 4 Pressure Ratio of 2.33
nc1 = 0.80;     % Compressor 1 Efficiency of 0.80
nc2 = 0.80;     % Compressor 2 Efficiency of 0.80
nc3 = 0.80;     % Compressor 3 Efficiency of 0.80
nc4 = 0.80;     % Compressor 4 Efficiency of 0.80
erT1 = 2.48;    % Turbine 1 Expansion Ratio of 2.48
erT2 = 14.57;   % Turbine 2 Expansion Ratio of 14.57
nt1 = 0.891;    % Turbine 1 Efficiency of 0.891
nt2 = 0.8739;   % Turbine 2 Efficiency of 0.8739
ngen = 0.90;    % Generator Efficiency of 0.90
nmotor = 0.90;  % Motor Efficiency of 0.90
ef_Rec = 0.7699;% Recuperator Effectiveness of 0.7699
ef_HX1 = 0.85;  % Heat Exchanger 1 Effectiveness of 0.85
```

```
ef_HX2 = 0.85;  % Heat Exchanger 2 Effectiveness of 0.85
ef_IC = 0.85;   % Inner Cooler Effectiveness of 0.85
ef_AC = 0.85;   % After Cooler Effectiveness of 0.85

%Given Design Parameters
T9_e = 110;         %Fahrenheit - Temperature entering air storage
cavern
T11_e = 100;        %Fahrenheit - Temperature entering Recuperator
T13_e = 1000;       %Fahrenheit - Temperature at inlet to Turbine 1
T15_e = 1600;       %Fahrenheit - Temperature at inlet to Turbine 2
T9 = (T9_e + 459.67)*(5/9);       %Kelvin
T11 = (T11_e + 459.67)*(5/9);     %Kelvin
T13 = (T13_e + 459.67)*(5/9);     %Kelvin
T15 = (T15_e + 459.67)*(5/9);     %Kelvin
Pgen = 100;         %MW - Rated Generator Output
Pcav_max = 1150;    %psia - Maximum Air Storage Cavern Pressure
Pcav_min = 750;     %psia - Minimum Air Storage Cavern Pressure

%Baseline Pressure losses
Ploss_IC = 0.02;    % 2% pressure loss in all Inner Coolers
Ploss_AC = 0.02;    % 2% pressure loss in After Cooler
Ploss_Rec = 0.0265; % 2.65% pressure loss in Recuperator (both sides)
Ploss_HX1 = 0.1265; % 12.65% pressure loss in Heat Exchanger 1
Ploss_HX2 = 0.1265; % 12.65% pressure loss in Heat Exchanger 2

% Time period for power generation
dt_gen = 4;             %hr
% Calculate the corresponding number of 15min intervals
dt_gen_int = 4*dt_gen;  %(4 intervals every hour)
% Time period for compression
dt_comp = 24 - dt_gen;  %hr

% Determine Pressures at every State (1-17)----------------------------
P1 = P0_si;                 %Ambient Pressure
P2 = P1*rpC1;               %Pressure rise in Compressor 1
P3 = P2*(1-Ploss_IC);       %Pressure drop through Inner Cooler 1
P4 = P3*rpC2;               %Pressure rise in Compressor 2
P5 = P4*(1-Ploss_IC);       %Pressure drop through Inner Cooler 2
P6 = P5*rpC3;               %Pressure rise in Compressor 3
P7 = P6*(1-Ploss_IC);       %Pressure drop through Inner Cooler 3
P8 = P7*rpC4;               %Pressure rise in Compressor 4
P9 = P8*(1-Ploss_AC);       %Pressure drop through After Cooler
P17 = P0_si;                %Ambient Pressure
P16 = P17/(1-Ploss_Rec);    %Pressure drop through Recuperator
P15 = P16*erT2;             %Pressure drop in Turbine 1
P14 = P15/(1-Ploss_HX2);    %Pressure drop through Heat Exchanger 2
P13 = P14*erT1;             %Pressure drop in Turbine 1
P12 = P13/(1-Ploss_HX1);    %Pressure drop through Heat Exchanger 1
P11 = P12/(1-Ploss_Rec);    %Pressure drop through Recuperator

%-------------------------------------------------------------------------
%-----------------------------Begin Simulation----------------------------
```

```
%-------------------------------------------------------------------------

% Turbine System---------------------------------------------------------
% -----------------------------------------------------------------------

% Calculate Rated Turbine Output
Pturb_tot = Pgen/ngen;  %MW

% Analyze Turbine 1 to find specific work w_t1
[h13,T14,h14,s13,s14] =
Turbine(T13,P13,P14,nt1,yO2,yN2,yCO2,yH2O,yAr,yHe);
w_t1 = h13-h14;     %kJ/kg

% Analyze Turbine 2 to find specific work w_t2
[h15,T16,h16,s15,s16] =
Turbine(T15,P15,P16,nt2,yO2,yN2,yCO2,yH2O,yAr,yHe);
w_t2 = h15-h16;     %kJ/kg

% Calculate the total specific energy production of the Turbine System
% (kJ/kg)
w_t_tot = w_t1 + w_t2;

% Calculate the air flow rate (kg/s) through turbine section using
% Pturb_tot, w_t1 & w_t2, include comversions: 1MW=1000kW, kW=kJ/s
madot_t = Pturb_tot*1000/w_t_tot;

% Analyze Recuperator to find T12, h12, T17, h17
[T12,h12,T17,h17,h11,s11,s12,s17] =
Recuperator(T11,P11,P12,T16,P16,P17,ef_Rec,yO2,yN2,yCO2,yH2O,yAr,yHe);

% Analyze HX1 to find q1_required (kJ/kg) and inlet enthalpy for CSP
% system (kJ/kg)
[q1_req,hin1_h] = HX(h12,h13,ef_HX1,yO2,yN2,yCO2,yH2O,yAr,yHe);

% Analyze HX2 to find q2_required (kJ/kg) and inlet enthalpy for CSP
% system (kJ/kg)
[q2_req,hin2_h] = HX(h14,h15,ef_HX2,yO2,yN2,yCO2,yH2O,yAr,yHe);


% Compression System ----------------------------------------------------
% -----------------------------------------------------------------------

%Initialize State 1 (needed for s1)
[Mmix,R,cp1,cv1,k1,h1,u1,s1,h_1,u_1,s_1]=AirPropCalcMass(yO2,yN2,yCO2,y
H2O,yAr,yHe,P1,T0_si);

% Analyze Compressor 1 to find specific work w_c1
[h1,T2,h2,s2] = Compressor(T0_si,P1,P2,nc1,yO2,yN2,yCO2,yH2O,yAr,yHe);
w_c1 = h2-h1;       %kJ/kg
```

```
% Analyze Inner Cooler 1 to set state 3
[T3,h3,q1_rem,s3] =
Cooler(h2,P3,T0_si,P0_si,ef_IC,yO2,yN2,yCO2,yH2O,yAr,yHe);  %Change to
reflect water cooling!!

% Analyze Compressor 2 to find specific work w_c2
[h3,T4,h4,s4] = Compressor(T3,P3,P4,nc2,yO2,yN2,yCO2,yH2O,yAr,yHe);
w_c2 = h4-h3;       %kJ/kg

% Analyze Inner Cooler 2 to set state 5
[T5,h5,q2_rem,s5] =
Cooler(h4,P5,T0_si,P0_si,ef_IC,yO2,yN2,yCO2,yH2O,yAr,yHe);  %Change to
reflect water cooling!!

% Analyze Compressor 3 to find specific work w_c3
[h5,T6,h6,s6] = Compressor(T5,P5,P6,nc3,yO2,yN2,yCO2,yH2O,yAr,yHe);
w_c3 = h6-h5;       %kJ/kg

% Analyze Inner Cooler 3 to set state 7
[T7,h7,q3_rem,s7] =
Cooler(h6,P7,T0_si,P0_si,ef_IC,yO2,yN2,yCO2,yH2O,yAr,yHe);  %Change to
reflect water cooling!!

% Analyze Compressor 4 to find specific work w_c4
[h7,T8,h8,s8] = Compressor(T7,P7,P8,nc4,yO2,yN2,yCO2,yH2O,yAr,yHe);
w_c4 = h8-h7;       %kJ/kg

% Analyze After Cooler to set state 9
[T9,h9,q4_rem,s9] =
Cooler(h8,P9,T0_si,P0_si,ef_AC,yO2,yN2,yCO2,yH2O,yAr,yHe);  %Change to
reflect water cooling!!

% Calculate total specific energy requirement for Compression System
% (kJ/kg)
w_c_tot = w_c1 + w_c2 + w_c3 + w_c4;


% Air Storage Cavern ------------------------------------------------
% ------------------------------------------------------------------

% Calculate total air mass for generation (kg) and (short tons)
% (60sec/min, 15 min intervals, 4 intervals/hour, # of hours)
m_air = madot_t*60*15*4*dt_gen;
m_air_e = m_air/907.18474;

% Calculate the total empty volume needed to hold the required air at
the
% specified temp and betweeen the specified pressure range (m^3)
[CavernVol] =
AirCavernSize(T9,P9,Pcav_max,Pcav_min,m_air,yO2,yN2,yCO2,yH2O,yAr,yHe);
```

```
%Calculate the cavern volume in ft^3 (m^3 = 35.315ft^3)
CavernVol_e = CavernVol*35.315;


% Solar Collector and Thermal Storage Sizing -------------------------
% --------------------------------------------------------------------

% Calculate the total specific heat requirement (kJ/kg)
q_req_tot = q1_req + q2_req;

% Calculate heat requirement during steady state operation (MW)
Qdot_req_ss = (madot_t * q_req_tot)/1000;

% Calculate daily heat requirement for CSP/thermal storage system (MWh)
Q_req_day = Qdot_req_ss * dt_gen;

% Determine necessary installed capacity for CSP system


% Calculate the solar field area, receiver area, and land area (m^2)
% for Tower using Sargent & Lundy data (also need MWt installed
capacity)
%SolarFieldArea = 5589*;
%ReceiverArea = 4.5954*;
%LandArea = 57132*;


% Wind Turbine System and Sizing -------------------------------------
% --------------------------------------------------------------------

% Calculate the air flow rate (kg/s) through compressor section using
total
% air mass required and total compression time (60min/hr & 60s/min)
madot_c = m_air/(dt_comp*60*60);

% Calculate the compression power requirement during steady state
operation
% (MW)
Wdot_comp_ss = (madot_c * w_c_tot)/1000;

% Calculation of needed electrical power requirement during steady
state
% operation to run the motor that drives the compressors (MW)
Wdot_req_ss = Wdot_comp_ss/nmotor;

% Calculate daily electricity requirement for Wind Turbine system (MWh)
W_req_day = Wdot_req_ss * dt_comp;
```

```
% Compression Cooling System ---------------------------------------
% -------------------------------------------------------------------

% Calculate the total cooling load (kJ/kg)
qtot_rem = q1_rem + q2_rem + q3_rem + q4_rem;

% Calculate the cooling load for steady state operation (MW)
Qdot_rem_ss = (madot_c * qtot_rem)/1000;


% Performance Parameters --------------------------------------------
% -------------------------------------------------------------------

% Calculate the specific energy requirement of the motor that runs the
% compressors (kJ/kg)
w_motor_tot = w_c_tot / nmotor;

% Calculate the specific energy output of the generator (kJ/kg)
w_gen_tot = w_t_tot * ngen;

% Calculate total specific energy input required (kJ/kg) and percentage
% that is from Wind electricity and from CSP heat
e_in_tot = w_motor_tot + q_req_tot;
e_in_PercentWind = w_motor_tot/e_in_tot;
e_in_PercentSolar = q_req_tot/e_in_tot;

% Calculate thermodynamic efficiency
eff = w_gen_tot / e_in_tot;

% Calculate the amount of energy inputs per unit electricity output
elec_in_per_unit_output = w_motor_tot/w_gen_tot;
heat_in_per_unit_output = q_req_tot/w_gen_tot;


% Calculation of Specific Volume at all States ----------------------
% -------------------------------------------------------------------

% Calculates specific volume (m^3/kg) based on Ideal Gas Law
v1 = SpecificVolumeIG(T0_si,P1,R);
v2 = SpecificVolumeIG(T2,P2,R);
v3 = SpecificVolumeIG(T3,P3,R);
v4 = SpecificVolumeIG(T4,P4,R);
v5 = SpecificVolumeIG(T5,P5,R);
v6 = SpecificVolumeIG(T6,P6,R);
v7 = SpecificVolumeIG(T7,P7,R);
v8 = SpecificVolumeIG(T8,P8,R);
v9 = SpecificVolumeIG(T9,P9,R);
v11 = SpecificVolumeIG(T11,P11,R);
v12 = SpecificVolumeIG(T12,P12,R);
```

```
v13 = SpecificVolumeIG(T13,P13,R);
v14 = SpecificVolumeIG(T14,P14,R);
v15 = SpecificVolumeIG(T15,P15,R);
v16 = SpecificVolumeIG(T16,P16,R);
v17 = SpecificVolumeIG(T17,P17,R);
```

C.2. COMPRESSOR.M

```
function[hin,Tout,hout,s1,s2] =
Turbine(Tin,Pin,Pout,nt,yO2,yN2,yCO2,yH2O,yAr,yHe)

% Get all Thermo Props at Inlet State (1 indicates inlet state)
[Mmix1,R1,cp1,cv1,k1,h1,u1,s1,h_1,u_1,s_1]=AirPropCalcMass(yO2,yN2,yCO2
,yH2O,yAr,yHe,Pin,Tin);

% Loop to determine Isentropic Exit State ----------------------------
% Initialize s_2 (2 indicates outlet state)
s2=s1+s1/2;
% Set bounds on T2
T2l=0;
T2h=3000;
% Set convergence criteria in while loop - Bisection Method
% Want entropy at inlet and exit to be equal (Isentropic condition)
while(abs((s2-s1))>.001)
    % Guess for Tout (middle of lower and upper bound)
    Tout=(T2h+T2l)/2;
    % Thermo Props at Pout and guessed Tout

[Mmix2,R2,cp2,cv2,k2,h2,u2,s2,h_2,u_2,s_2]=AirPropCalcMass(yO2,yN2,yCO2
,yH2O,yAr,yHe,Pout,Tout);
        % Reset bound based on s_2
    if(s2-s1<0)
        T2l=Tout;
    else
        T2h=Tout;
    end
end

% Loop to determine Actual Exit State --------------------------------
% Caclulate actual exit enthalpy
Actual_h2=h1-nt*(h1-h2);
% Set temperature bounds
T2l=0;
T2h=3000;
% Set convergence criteria in while loop - Bisection Method
% Want calculated h2 to equal AirPropCalc h2
```

```
while(abs((h2-Actual_h2))>.001)
    % Guess for Tout (middle of lower and upper bound)
    Tout=(T2l+T2h)/2;
    % Thermo Props at Pout and guessed Tout

[Mmix2,R2,cp2,cv2,k2,h2,u2,s2,h_2,u_2,s_2]=AirPropCalcMass(yO2,yN2,yCO2
,yH2O,yAr,yHe,Pout,Tout);
    % Reset bound based on h2
    if(h2-Actual_h2<0)
        T2l=Tout;
    else
        T2h=Tout;
    end
end

% Specify initial and final exit enthalpy
hin = h1;   %kJ/kg
hout = h2;  %kJ/kg
```

C.3. COOLER.M

```
function[Tout_h,hout_h,q_rem,sout_h] =
Cooler(hin_h,Pout_h,Tin_c,Pin_c,ef_IC,yO2,yN2,yCO2,yH2O,yAr,yHe)

% Find air enthalpy at cooling water inlet temperature
[Mmixin_c,Rin_c,cpin_c,cvin_c,kin_c,hin_c,uin_c,sin_c,h_in_c,u_in_c,s_i
n_c]=AirPropCalcMass(yO2,yN2,yCO2,yH2O,yAr,yHe,Pin_c,Tin_c);
%hin_c = CoolingWaterProp(Tin_c,Pin_c);

% Determine hot side exit state ----------------------------------------

% Calculate the actual hot side exit enthalpy (kJ/kg)
Actual_hout_h = hin_h - ef_IC*(hin_h-hin_c);

% Loop to set hot side exit state
% Set temperature bounds
Tout_h_l=0;
Tout_h_h=3000;
% Initialize an incorrect hout_h
hout_h = 0;
% Set convergence criteria in while loop - Bisection Method
% Want calculated hout_h to equal AirPropCalc Actual_hout_h
while(abs((hout_h-Actual_hout_h))>.1)
    % Guess for Tout_h (middle of lower and upper bound)
    Tout_h=(Tout_h_l+Tout_h_h)/2;
    % Thermo Props at Pout_h and guessed Tout_h
```

```
[Mmixout_h,Rout_h,cpout_h,cvout_h,kout_h,hout_h,uout_h,sout_h,h_out_h,u
_out_h,s_out_h]=AirPropCalcMass(yO2,yN2,yCO2,yH2O,yAr,yHe,Pout_h,Tout_h
);
    % Reset bound based on hout_h
    if(hout_h-Actual_hout_h<0)
        Tout_h_l=Tout_h;
    else
        Tout_h_h=Tout_h;
    end
end

% Calculate Heat Removed (_c indicates cold side, _h indicates hot
side)
% (kJ/kg)
q_rem = hin_h-hout_h;
```

C.4. TURBINE.M

```
function[hin,Tout,hout,s1,s2] =
Turbine(Tin,Pin,Pout,nt,yO2,yN2,yCO2,yH2O,yAr,yHe)

% Get all Thermo Props at Inlet State (1 indicates inlet state)
[Mmix1,R1,cp1,cv1,k1,h1,u1,s1,h_1,u_1,s_1]=AirPropCalcMass(yO2,yN2,yCO2
,yH2O,yAr,yHe,Pin,Tin);

% Loop to determine Isentropic Exit State ----------------------------
% Initialize s_2 (2 indicates outlet state)
s2=s1+s1/2;
% Set bounds on T2
T2l=0;
T2h=3000;
% Set convergence criteria in while loop - Bisection Method
% Want entropy at inlet and exit to be equal (Isentropic condition)
while(abs((s2-s1))>.001)
    % Guess for Tout (middle of lower and upper bound)
    Tout=(T2h+T2l)/2;
    % Thermo Props at Pout and guessed Tout

[Mmix2,R2,cp2,cv2,k2,h2,u2,s2,h_2,u_2,s_2]=AirPropCalcMass(yO2,yN2,yCO2
,yH2O,yAr,yHe,Pout,Tout);
        % Reset bound based on s_2
    if(s2-s1<0)
        T2l=Tout;
    else
        T2h=Tout;
```

```
    end
end

% Loop to determine Actual Exit State --------------------------------
% Caclulate actual exit enthalpy
Actual_h2=h1-nt*(h1-h2);
% Set temperature bounds
T2l=0;
T2h=3000;
% Set convergence criteria in while loop - Bisection Method
% Want calculated h2 to equal AirPropCalc h2
while(abs((h2-Actual_h2))>.001)
    % Guess for Tout (middle of lower and upper bound)
    Tout=(T2l+T2h)/2;
    % Thermo Props at Pout and guessed Tout

[Mmix2,R2,cp2,cv2,k2,h2,u2,s2,h_2,u_2,s_2]=AirPropCalcMass(yO2,yN2,yCO2
,yH2O,yAr,yHe,Pout,Tout);
    % Reset bound based on h2
    if(h2-Actual_h2<0)
        T2l=Tout;
    else
        T2h=Tout;
    end
end

% Specify initial and final exit enthalpy
hin = h1;   %kJ/kg
hout = h2;  %kJ/kg
```

C.5. HX.M

```
function[q_req,hin_h] =
HX(hin_c,hout_c,ef_HX,yO2,yN2,yCO2,yH2O,yAr,yHe)

% Calculate Heat Requirement (_c indicates cold side, _h indicates hot
% side) (kJ/kg)
q_req = hout_c-hin_c;

% Calculate the hot side inlet enthalpy (kJ/kg)
hin_h = (hout_c-hin_c)/ef_HX + hin_c;
```

C.6. RECUPERATOR.M

```
function[T12,h12,T17,h17,h11,s11,s12,s17] =
Recuperator(T11,P11,P12,T16,P16,P17,ef_Rec,yO2,yN2,yCO2,yH2O,yAr,yHe)

% Get all Thermo Props at cold side Inlet State and hot side Inlet
State
% (11 indicates inlet cold side (cavern), 16 indicates inlet hot side
(turbine))
[Mmix11,R11,cp11,cv11,k11,h11,u11,s11,h_11,u_11,s_11]=AirPropCalcMass(y
O2,yN2,yCO2,yH2O,yAr,yHe,P11,T11);
[Mmix16,R16,cp16,cv16,k16,h16,u16,s16,h_16,u_16,s_16]=AirPropCalcMass(y
O2,yN2,yCO2,yH2O,yAr,yHe,P16,T16);


% Determine State 12 ------------------------------------------------
% Calculate actual h12 using Recuperator Effectiveness
Actual_h12 = ef_Rec*(h16-h11)+h11;

% Loop to set State 12
% Set temperature bounds
T12l=0;
T12h=3000;
% Initialize an incorrect h12
h12 = 0;
% Set convergence criteria in while loop - Bisection Method
% Want calculated h12 to equal AirPropCalc h12
while(abs((h12-Actual_h12))>.1)
    % Guess for T12 (middle of lower and upper bound)
    T12=(T12l+T12h)/2;
    % Thermo Props at P12 and guessed T12

[Mmix12,R12,cp12,cv12,k12,h12,u12,s12,h_12,u_12,s_12]=AirPropCalcMass(y
O2,yN2,yCO2,yH2O,yAr,yHe,P12,T12);
    % Reset bound based on h12
    if(h12-Actual_h12<0)
        T12l=T12;
    else
        T12h=T12;
    end
end

% Determine State 17 ------------------------------------------------
% Calculate actual h17 using COE
Actual_h17 = h16+h11-h12;
```

```
% Loop to set State 17
% Set temperature bounds
T17l=0;
T17h=3000;
% Initialize an incorrect h17
h17 = 0;
% Set convergence criteria in while loop - Bisection Method
% Want calculated h17 to equal AirPropCalc h17
while(abs((h17-Actual_h17))>.1)
    % Guess for T17 (middle of lower and upper bound)
    T17=(T17l+T17h)/2;
    % Thermo Props at P17 and guessed T17

[Mmix17,R17,cp17,cv17,k17,h17,u17,s17,h_17,u_17,s_17]=AirPropCalcMass(y
O2,yN2,yCO2,yH2O,yAr,yHe,P17,T17);
    % Reset bound based on h17
    if(h17-Actual_h17<0)
        T17l=T17;
    else
        T17h=T17;
    end
end
```

C.7. AIRCAVERNSIZE.M

```
function[CavernVol] =
AirCavernSize(T9,P9,Pcav_max,Pcav_min,m_air,yO2,yN2,yCO2,yH2O,yAr,yHe)

% Get all Thermo Props at Inlet State (9 indicates inlet state to
cavern)
[Mmix9,R9,cp9,cv9,k9,h9,u9,s9,h_9,u_9,s_9]=AirPropCalcMass(yO2,yN2,yCO2
,yH2O,yAr,yHe,P9,T9);

% Calculate the required empty air volume (cubic meters) for known air
% mass, temp, and between specified pressure range
CavernVol = m_air*R9*T9/(Pcav_max-Pcav_min);

% Calculate the amount of air left in cavern at fully discharged (kg),
and
% the total amount of air at fully charged (kg)
m_air_min = Pcav_min*CavernVol/(R9*T9);
m_air_max = Pcav_max*CavernVol/(R9*T9);
```

C.8. SPECIFICVOLUMEIG.M

```
function[v] = SpecificVolumeIG(T,P,R)

% Calculates the Specific Volume (m^3/kg) based on Ideal Gas Law Pv=RT
% units work out as long as R(kJ/(kg*K)), T(K), P(kPa)
v = R*T/P;
```

References

[1] IPCC, E. Jansen, J. Overpeck, K. R. Briffa, J.-C. Duplessy, F. Joos, V. Masson-Delmotte, D. Olago, B. Otto-Bliesner, W. R. Peltier, S. Rahmstorf, R. Ramesh, D. Raynaud, D. Rind, O. Solomina, R. Villalba, and D. e. Zhang, "Palaeoclimate. In: Climate Change 2007: The Physical Science Basis. Contribution of Working Group I to the Fourth Assessment Report of the Intergovernmental Panel on Climate Change," IPCC, New York, NY 2007.

[2] IPCC, H. L. Treut, R. Somerville, U. Cubasch, Y. Ding, C. Mauritzen, A. Mokssit, T. Peterson, and M. Prather, "Historical Overview of Climate Change. In: Climate Change 2007: The Physical Science Basis. Contribution of Working Group I to the Fourth Assessment Report of the Intergovernmental Panel on Climate Change," IPCC, New York, NY 2007.

[3] IPCC, R. E. H. Sims, R. N. Schock, A. Adegbululgbe, J. Fenhann, I. Konstantinaviciute, W. Moomaw, H. B. Nimir, B. Schlamadinger, J. Torres-Martinez, C. Turner, Y. Uchiyama, S. J. V. Vuori, N. Wamukonya, and X. Zhang, " Energy Supply. In: Climate Change 2007: Mitigation. Contribution of Working Group III to the Fourth Assessment Report of the Intergovernmental Panel on Climate Change," New York, NY 2007.

[4] EIA, "Annual Energy Review 2007," U.S. Department of Energy, Energy Information Administration, Washington D.C. DOE/EIA-0384(2007), 2008.

[5] AWEA, "U.S. Wind Energy Projects - Texas."

[6] Comptroller, "The Energy Report 2008," Office of the Texas Comptroller, , Austin, TX 2008.

[7] ERCOT, "Compliance Report - EECP Step 1 Event, February 24, 2007," 2007.

[8] SECO, "Fact Sheet - Renewable Energy Resources for Texas," 2008.

[9] AEI, "Texas Wind Class Map," Alternative Energy Institute - West Texas A&M University, 2004.

[10] EERE and WindPoweringAmerica, "Installed U.S. Wind Capacity and Wind Project Locations," U. S. DOE, Ed., 2009.

[11] D. M. Wogan, "Assessing the Potential for Algal Biofuels Production in Texas," in *ASME Energy Sustainability 2009* San Francisco, CA, 2009.

[12] M. Kapner, "Dispatchable Hybrid Wind / Solar Power Plant," Austin Energy, Austin.

[13] G. Vliet, "Texas Solar Radiation Database," The University of Texas at Austin.

[14] AEI, "Wind Data for Tall Tower South (Sweetwater)," Alternative Energy Institute - West Texas A&M University, 2007.

[15] PUCT, "Commission Staff's Petition for Selection of Entities Responsible for Transmission Improvements Necessary to Deliver Renewable Energy from Competitive Renewable-Energy Zones," Public Utility Commission of Texas, 2009.

[16] M. Giberson, "Frequent Negative Power Prices in the West Region of ERCOT Result from Wasted Renewable Power Subsidies," in *Knowledge Problem*, 2009.

[17] ERCOT, "2009 Balancing Energy Services (BES) Market Clearing Price of Electricity (MCPE)," ERCOT, 2009.

[18] ESA, "Pumped Hydro," Morgan Hill, CA: Electricity Storage Association.

[19] ConsumersEnergy, "Ludington Pumped Storage Plant," 2006.

[20] NREL, "Survey of Thermal Storage for Parabolic Trough Power Plants," National Renewable Energy Laboratory 2000.

[21] R. Tamme, D. Laing, and W.-D. Steinmann, "Advanced Thermal Energy Storage Technology for Parabolic Trough," *ASME Journal of Solar Energy Engineering,* vol. 126, pp. 794-800, 2004.

[22] EERE, "Concentrating Solar Power: Energy from Mirrors," U.S. Department of Energy 2001.

[23] BINE, "Compressed Air Energy Storage Power Plants," 2007.

[24] R. B. Schainker and M. Nakhamkin, "Compressed Air Energy Storage (CAES): Overview, Performance and Cost Data For 25MW to 220MW Plants," IEEE Power Engineering Society 1985.

[25] Ridge, "The Economic Impact of CAES on Wind in TX, OK, and NM," Texas State Energy Conservation Office, Ridge Energy Storage & Grid Services, Houston, TX June 27 2005.

[26] M. Nakhamkin, L. Andersson, E. Swensen, J. Howard, R. Meyer, R. Schainker, R. Pollak, and B. Mehta, "AEC 110 MW CAES Plant: Status of Project," *Journal of Engineering for Gas Turbines and Power,* vol. 114, pp. 695-700, 1992.

[27] D. Sibley and S. Wolens, "Restructuring of the Electric Utility Industry - S.B.7," in *Texas 76th Legislature*, 1999.

[28] AWEA, "American Recovery and Reinvestment Act Provides Measures to Sustain and Expand Wind Energy Industy Growth," American Wind Energy Association, 2009.

[29] "American Clean Energy and Security Act of 2009," in *H.R. 2454*, 2009.

[30] "Clean Energy Jobs and American Power Act," in *S. 1733*, 2009.

[31] Z. Lubosny, *Wind Turbine Operation in Electric Power Systems: Advanced Modeling*: Springer, 2003.

[32] "Energy Story Chapter 16: Wind Energy," California Energy Commission, 2002.

[33] S. Santoso, "Project 3 - Modeling and Simulation of a Variable Speed Wind Turbine in PSCAD," Course EE 394V - Modeling and Simulation of Wind Power Plants ed, 2009.

[34] M. J. Moran and H. N. Shapiro, *Fundamentals of Engineering Thermodynamics*, 4th ed. New York: John Wiley & Sons, 2000.

[35] P. P. Walsh and P. Fletcher, *Gas Turbine Performance*: Blackwell Science Ltd and ASME, 2004.

[36] P. S. Schmidt, O. A. Ezekoye, J. R. Howell, and D. K. Baker, *Thermodynamics An Integrated Learning System*: John Wiley & Sons, 2006.

[37] Wikipedia, "Brayton Cycle."

[38] Reclamation, "Construction Cost Trends," U.S. Department of the Interior, Bureau of Reclamation, Wahington D.C. 2008.

[39] IEA, "Energy Technology Perspectives 2006," Organisation for Economic Co-operation and Development, International Energy Agency, Paris, France 2008 2007.

[40] IEA and NEA, "Projected Costs of Generating Electricity 2005 Update," Organisation for Economic Co-operation and Development, International Energy Agency, Nuclear Energy Agency, Paris, France 2005 2005.

[41] EERE, "Annual Report on U.S. Wind Power Installation, Cost, and Performance Trends: 2007," U.S. Department of Energy, Washington D.C. 2008.

[42] Navigant, "The Changing Face of Renewable Energy," Navigant Consulting June 2003 2003.

[43] Enermodal, "Cost Reduction Study for Solar Thermal Power Plants," Enermodal Engineering Limited, Kitchnener, ON 1999 1999.

[44] Sargent and Lundy, "Assessment of Parabolic Trough and Power Tower Solar Technology Cost and Performance Forecasts," National Renewable Energy Laboratory, Sargent and Lundy LLC Consulting Group, Chicago, IL NREL/SR-550-34440, 2003.

[45] LCRA, "Study of Electric Transmission in Conjunction with Energy Storage Technology," Texas State Energy Conservation Office, Lower Colorado River Authority, Austin, TX August 21, 2003 2003.

[46] EPRI, "Program on Technology Innovation: Integrated Generation Technology Options," Electric Power Research Institute, Palo Alto, CA 2008.

[47] TIPS, "Texas Interactive Power Simulator." vol. 2008 Austin, TX: The University of Texas at Austin, 2008.

[48] EIA, "Natural Gas Navigator." vol. 2008: U.S. Department of Energy, Energy Information Administration, 2008, p. monthly natural gas prices.

Vita

Jared Brett Garrison was born on October 12, 1983 in Pender, Nebraska to Donald Rex Garrison and Yvonne Miserez Garrison. Mr. Garrison graduated as valedictorian of Lufkin High in 2002, after which he enrolled at the University of Texas at Austin for undergraduate study. While in school as an undergraduate, Mr. Garrison was active in several engineering student organizations, including holding various officers positions in Kappa Theta Epsilon, the engineering coop honors society, and ASME, the American Society of Mechanical Engineers. He also spent a summer working for Lufkin Industries as a student intern design engineer in their transmission department. Mr. Garrison gained further work experience at Halliburton's measuring while drilling research and development department. As a part of Halliburton's cooperative education program, Mr. Garrison spent a total of 13 months over a period of two years working full time as a student design engineer. Additionally, he spent his last two summers working full time and final two semesters working part time at Applied Research Laboratories' Advanced Sonar Division as a student engineering technician. Mr. Garrison graduated with honors from the University of Texas at Austin with a Bachelors of Science in Mechanical Engineering in May of 2007.

He began his graduate study at The University of Texas at Austin in August 2007 in the Thermal Fluids Systems Division of Mechanical Engineering, and will remain enrolled in this program to pursue a Doctor of Philosophy in Mechanical Engineering. While in school as a graduate student, Mr. Garrison has continued his activities in numerous engineering student organizations, including serving as President of the student

chapter of ASME, being a member of the Engineering Leadership Team, and serving on the staff of the Leadershape Texas summer 2008 program.

Permanent address:802 Saint Lo

Lufkin, TX 75901

This thesis was typed by the author.